PEBBLE Nanosensors for Intracellular Imaging and Analysis of Free Calcium and Zinc

by

Di Si

A dissertation submitted in partial fulfillment
of the requirements for the degree of
Doctor of Philosophy
(Chemistry)
in the University of Michigan
2011

Doctoral Committee:

Professor Raoul Kopelman, Chair
Professor Carol A. Fierke
Professor Martin A. Philbert
Associate Professor Kristina I. Hakansson

Acknowledgments

Throughout my entire graduate study, many people have provided me with valuable scientific advice and support. Hereby, I would like to thank those who have made the work presented here possible. First of all, I would like to thank my advisor Dr. Raoul Kopelman for his intellectual guidance both in and out of the lab. Without his scientific ideas and thoughtful guidance, this work would not become a successful contribution to our research.

I would also like to thank my research committee. Dr. Carol Fierke has provided great research directions for our collaborations. Additionally, I am grateful for the assistance provided by Dr. Martin Philbert and Dr. Kristina Hakansson.

There were several individuals instrumental in all my research projects, and they must be acknowledged. Dr. Yoon-Eun Lee Koo has helped me with many valuable scientific ideas and I am very grateful for her assistance throughout my entire study. I have also gained a lot of useful scientific knowledge from Dr. Guochao Nie who has been a great instructor to me. My collaboration with Dr. Tamir Epstein, Dr. Tamiika Hurst, and Carolyn Da Wang was a very successful and great experience, and I would like to express my gratitude to them.

The Kopelman lab has been a very friendly and pleasant environment and I would like to thank many of the past and present group members. When I first joined the Kopelman group, Dr. James Sumner instructed me with my initial studies. I have also received valuable assistance in every aspect of my research from Dr. Gwangseong Kim, Dr. Hao Xu, Dr. Wenzhe Fan, Dr. Hoejin Hah and Dr. Shouyan Wang. Ron Smith, Taeyjuana Curry, and Qin Ming are great friends to me, and it has been a pleasure working with all of them.

Most importantly, this work is dedicated to my family and all my friends. My parents, Lihu and Yuling have always been there to support and encourage me. Their love for me has been the driving force behind every achievement in my life. I must also thank my dear Eric for his support and helping to provide me a happy and relaxing home. This has been an important source of strength for me.

Finally, this work was funded by NIH (F018530) and National Science Foundation (F012801).

Table of Contents

List of Figures

List of Tables

ABSTRACT

PEBBLE Nanosensors for Intracellular Imaging and Analysis of Free Calcium and Zinc

by

Di Si

Chair: Raoul Kopelman

Ca^{2+} is a universal second messenger and plays a major role in intracellular signaling, metabolism and a wide range of cellular processes. To date, the most successful approach for intracellular Ca^{2+} measurement involves the introduction of optically sensitive Ca^{2+} indicators into living cells, combined with digital imaging microscopy. However, the use of free Ca^{2+} indicators for intracellular sensing and imaging has several limitations, such as interference from cellular small ions and biomacromolecules, and unwanted sequestration of the indicator molecules.

Zinc is the second most abundant trace element in the human body. It is an essential component of all six classes of enzymes and several families of regulatory proteins. Zinc deficiencies and excesses were found to be related to a number of health issues. Due to the importance of zinc in the human body, many fluorescent Zn^{2+}

indicators have been developed. Among these indicators, carbonic anhydrase (CA) and its mutants are particularly useful for intracellular Zn^{2+} sensing, because of their outstanding and tunable sensitivity (picomolar level), selectivity and binding kinetics.

In this work, PEBBLE nanosensors have been developed for intracellular measurements of free Ca^{2+} and Zn^{2+}. The general design, matrices and the advantages of PEBBLE nanosensors are briefly reviewed in Chapter 1. Chapter 2 describes the preparation, characterization and intracellular application of PEBBLE nanosensors encapsulated with rhodamine based Ca^{2+} fluorescence indicators. The K_d of Rhod-2 inside PEBBLEs is determined to be 500~600 nM for in-solution calibration and 1 μM for in-cell calibration. Chapter 3 describes the preparation and purification of CA encapsulated PEBBLEs; the active CA encapsulation is about 28%. Chapter 4 describes zinc sensing performed by CA *encapsulated* and *conjugated* PEBBLEs. The Zn^{2+} binding affinity of the CA conjugated on PEBBLE surface is determined to be 9 pM, while the Zn^{2+} sensing by CA encapsulated PEBBLEs is not successful. Chapter 5 summarizes the conclusions and limitations of this work, and proposes future experiments for developing novel PEBBLE nanosensors.

Chapter 1

Introduction

Biological imaging with optical methods, such as fluorescence and Raman scattering, to study the biochemistry and biophysics at a single cell level, has been an active research field for decades. Fluorescence and surface-enhanced Raman scattering (SERS) enable the remote detection or sensing of analytes through a minimally-invasive procedure that can provide spatial and temporal resolution. Fluorescence has been a major technique for intracellular analysis due to its high sensitivity. Recently, SERS has also been developed for intracellular measurements, and it is complementary to luorescence methods [60-62].

Although fluorescence spectroscopy and microscopy do not provide molecular details as traditional vibrational spectroscopy does, their abilities for non-destructive and real time sensing make them particularly useful for imaging biological samples. Due to the tremendous advances in computer based imaging processing technologies and the abundance of commercially available fluorescent molecular probes [1], significant progress has been achieved in the visualization of biological processes by using fluorescence microscopy. These molecular probes are advantageous for real-time cell

imaging because they exhibit fast responses and intense signals, with relatively low background noise, and they require simple instruments for data acquisition, i.e. a simple instrumental setup on a regular epifluorescence microscopy.

However, the use of free indicator dyes for intracellular imaging has several disadvantages [2-4]: 1) Most of the commercially available indicators are not ratiometric; although the equivalent to ratiometric measurements can also be achieved by lifetime and phase-sensitive detection, these two methods are much less commonly used than fluorescence intensity based detection. 2) Some indicators chemically perturb the cells and thus have the potential for subverting pertinent biochemical processes or may exhibit cytotoxicity. 3) Unwanted compartmentalization or sequestration of the dye affects the reliability of their intracellular measurements. 4) Nonspecific binding of the probes to proteins, membranes and other cellular components often induces artifacts to the measurements, by affecting the intensity or binding affinity of the probes. 5) The indicators are often actively pumped by g-glycolproteins or leak out of the cells, since they are small molecules. 6) The proper derivatization is sometimes required for the indicator dyes to become cell-permeable forms and the derivatization of the dye molecule might affect their sensing properties. 7) For in vivo applications, the delivery of the indicator dye is usually not controllable and only a subset of the probes would reach a specific location of interest; and crossing biological barriers, such as the blood-brain barrier is also a problem.

The development of PEBBLEs (Photonic Explorers by Biologically Localized Embedding) has provided a new type of biological imaging method. The physical perturbation to the cells caused by the PEBBLEs is minimal due to their small sizes (~ 20-200 nm spheres) as a 20-nm particle is 8-9 orders of magnitude smaller in volume than a typical mammalian cell [2]. Also, the inert, non-toxic particle matrices cause minimal chemical perturbation to cells [2, 5]. Furthermore, nanoparticles can be delivered into cells by using a variety of methods, as shown in Figure 1.1. Nanoparticles can be engulfed by the cells through nonspecific endocytosis, due to their nanometer size, or through receptor mediated endocytosis by conjugating translocating proteins or peptides such as F3-peptide on the particle surfaces [37-39]. The TAT peptide, from the HIV virus, is able to cross the cell membrane in an energy independent manner and with no discernible cytotoxicity issues [40]. It has been reported that PEBBLEs with TAT peptide conjugated on the particle surfaces can be translocated through the cell membrane and thus enter the cells [13, 41]. PEBBLEs have also been successfully delivered into cells by gene gun and the cell viability after gene gun delivery was found to be around 99% compared to that of the control cells [5]. Pico-injection has been used to inject picoliter volumes of solution containing nanoparticles into single cells. However, since each cell must be individually injected, this method is very time consuming and labor intensive [7]. In the liposome delivery method, PEBBLEs are first incubated with commercially available liposomes and the liposomes are then placed in the cell culture where the liposomes fuse with the cell membrane and release the PEBBLEs into the cells [5]. Among all these methods, the nonspecific or receptor mediated (F3 peptide)

endocytosis and the TAT peptide delivery are the most commonly used methods in our lab due to their biocompatibility to cells and their straightforward preparation. The minimal physical and chemical perturbations to the cells caused by PEBBLEs were demonstrated by cell viability test after the PEBBLEs were delivered by gene gun, and the cell viability was found to be 99% compared to that of control cells [5].

In summary, PEBBLEs have many advantages for intracellular sensing because of their small size, nontoxicity and excellent engineerability: 1) By incorporating both the sensing indicators and the reference dyes in the PEBBLEs, ratiometric measurements can be easily achieved. Ratiometric measurement is probably the best way for fluorescence intensity (rather than lifetime) based methods, because it cancels out variations in dye concentration, path length and optical instabilities. A number of fluorescent probes exhibit small or even no excitation or emission shifts, but only intensity changes upon binding to the analytes. For these probes, co-loading in the PEBBLEs with a reference dye enables ratiomatric measurements. 2) The inert polymer matrix of the PEBBLEs protects the cellular environment from any potential toxicity of the indicators and, vice versa, protects the indicators from cell components. The particle matrix also reduces or eliminates the sequestration of the indicator and nonspecific binding of the indicator to proteins. 3) The high surface-to-volume ratio of the PEBBLEs, and its small size, grant the analytes high and fast accessibility to the indicators, resulting in a fast response time. 4) The excellent engineer-ability enables the conjugation of biomacromolecules, such as proteins or targeting peptides, so that the PEBBLEs can be delivered to specific cell types or specific organelles inside cells [2].

Significant progress has been made in the intracellular sensing and imaging by using free indicators and, more recently, by using PEBBLEs. Both methods have their advantages and limitations. As for PEBBLEs, although encapsulated sensing indicators are protected by the PEBBLE matrix from interference by cellular biomacromolecules, small ions (i.e. H^+) can still diffuse into PEBBLEs and affect the indicators. Another important limitation of PEBBLEs is that most the PEBBLE delivery methods can only deliver PEBBLEs into the cytosol, except that in gene-gun delivery, PEBBLEs are "shot" into cells more homogenously. Although targeted delivery of PEBBLEs into cellular organelles, such as mitochondria, has become part of our ongoing research, free indicators are currently more useful for sensing and imaging inside organelles.

A variety of particle matrices have been developed and utilized for intracellular optical sensing and these matrices exhibit excellent chemical stability and biocompatibility. These matrices include polyacrylamide, silica, etc. Among these, PAA has been the most commonly used matrix for intracellular sensing in our lab's work and it has been extensively studied and reviewed [2-9]. The typical size distribution of the PAA PEBBLEs prepared by the traditional preparation procedure is usually between 20-80 nm, as characterized by SEM, TEM or Dynamic Light Scattering (DLS) [2-9]. We note that a PEBBLE showing a 20 nm size by electron microscopy may show a size of 50 nm by DLS, due to swelling in solution. By adjusting the reaction conditions during the particle synthesis, i.e. the type and the amount of surfactants, the amount of initiators and reaction time, the size of PAA PEBBLEs can be fine-tuned between 20-200 nm (examples will be shown in Chapter 3 of this work). PAA PEBBLEs were prepared by a reverse

micelle microemulsion polymerization technique established by Candau et al. [10], with some modifications. This reverse micelle microemulsion, also referred to as water-in-oil (W/O) microemulsion, is a thermodynamically stable liquid media with an aqueous phase homogenously compartmentalized by surfactants as nanometer-sized micelles in a continuous oil phase such as hexane. These micelles act as nano-reactors for the polymerization reaction of acrylamide monomers and crosslinkers [7]. It has been reported that the PAA nanoparticles can also be synthesized with different functional groups such as amino or carboxyl groups, depending on the functionalized monomers added to the polymerization mixture [11]. These functionalized PEBBLEs can be used for covalently conjugating peptides and biomacromolecules, such as proteins or enzymes. For instance, amine-functionalized PAA nanoparticles can be prepared by using a mixture of monomers, acrylamide monomer, amine-functionalized monomer APMA (N-(3-aminopropyl) methacrylamide hydrochloride), and crosslinker GDMA (glycerol dimethacrylate) that forms the aqueous cores of the micellar droplets. The polymerization occurs after the addition of polymerization initiators, TEMED (N,N,N',N'-tetraethylmethylenediamine) and ammonium persulfate, and thus forms particles. The sensing indicators can be immobilized into the PEBBLEs by encapsulation, covalent linkage, physical absorption, etc.

Fluorescence indicator dyes have been encapsulated in PAA PEBBLEs for sensing pH [8, 12], Ca^{2+} [12-13], Mg^{2+} [14-15], Zn^{2+} [16], Fe^{3+} [17], $Cu^{+/2+}$ [18], OH radicals [19], oxygen, and glucose [20]. In these PEBBLE nanosensors, a reference dye that is not sensitive to the

analyte, is also incorporated into the PEBBLEs so as to achieve ratiometric measurements.

Silica nanoparticles have been produced by the sol-gel process which was first established by Stober et al. [31]. In a basic environment, the precursor, usually TMOS (tetramethyl orthosilicate) or TEOS (tetraethyl orthosilicate), undergoes a hydrolysis and condensation reaction to form the silica network, and therefore produces silica nanoparticles. Silica-based PEBBLEs have been developed for the determination of intracellular molecular oxygen [32] and pH [52]. Additionally, silica matrix has been utilized for immobilizing enzymes, such as protease, glucose oxidase, horse radish peroxide (HRP), catalase, lysozyme and phosphatase, for the purposes of biosensing and biocatalysis [53-59].

Other matrices, such as organically modified silicates (ormosil) particles have been utilized for sensing dissolved oxygen [33], singlet oxygen [34], hydrogen peroxide [35] and intracellular electric field [36]. Poly(decylmethacrylate) PEBBLEs have been developed and utilized for sensing K^+ [21], Na^+ [22], Cl^- [23], and dissolved oxygen [24]. Poly(ethylene glycol) hydrogel spheres containing horseradish peroxidase have been fabricated for sensing hydrogen peroxide [25]. Poly(methacrylate) particles have been utilized for the determination of metronidazole [26]. Poly(n-butylacrylate) nanospheres have been developed for sensing K^+ [27]. Polystyrene nanobeads have been utilized for monitoring intracellular oxygen [28-29] and pH [30].

In this work, PEBBLE nanosensors were fabricated and applied for the intracellular sensing of free Ca^{2+} and Zn^{2+}. Ca^{2+} plays an important role in the physiology and biochemistry of mammalian organisms and cells. It acts as a second messenger in signal transduction pathways where it is the key to many cellular processes and functions such as neurotransmitter release from neurons, muscle contractions, cell metabolism and fertilization, gene expression, and many enzymes require Ca^{2+} as a cofactor [42-43]. Free Ca^{2+} levels in cells are tightly regulated by varieties of Ca^{2+} "buffering pools" such as mitochondria, the smooth sarcoplasmic reticulum, Ca^{2+}-binding membrane components and proteins, while the internal free Ca^{2+} is controlled by the cells at the optimal 100-200 nM level [43]. In Chapter 2, the development and intracellular application of polyacrylamide PEBBLEs encapsulating rhodamine-based Ca^{2+} indicators will be discussed.

Zinc is the second most prevalent trace element found in the human body after iron. It is an essential component of all six classes of enzymes and several families of regulatory proteins [44-46]. In most of these enzymes, zinc is directly involved in the catalysis of substrates; for other enzymes and proteins, zinc is a purely structural component that preserves the integrity of subcellular organelles. These zinc containing enzymes and proteins are involved in virtually all aspects of the metabolism. Additionally, zinc plays a key role in gene expression; 46 genes have been identified to have transcriptional level changes in response to variations in the extracellular zinc concentration [47]. Zinc deficiencies and excesses were found to be related to a number of health issues. Zinc deficiency plays a key role in the pathogenesis of acrodermatitis

enteropathica in infants, which is fatal without treatment but can be treated by dietary zinc supplementation [48]. Zinc deficiency also causes growth retardation, gastrointestinal disorders, defects in reproductive organs, dysfunction of the immune system and dermatological lesions [49]. Zinc excess may cause nausea, drowsiness and symptoms of copper deficiency due to the decreased absorption of copper in the presence of large amounts of zinc [50]. Zinc is also important in the development of chronic diseases such as Alzheimer's disease, diabetes and asthma [51]. Although zinc is found to be implicated with a number of diseases, its full purpose in the human body still remains unclear.

Chapter 3 will be focusing on the method development of immobilizing a zinc-sensing enzyme, carbonic anhydrase in PAA nanoparticles. In the traditional PAA PEBBLE preparation method, a mixture of an anionic surfactant, AOT (Sodium dioctyl sulfosuccinate) and a nonionic surfactant, Brij 30 was used to stabilize the microemulsion and keep the initial monomer micelles at the nanometer size, which controls the size of the produced particles also at the nanometer level. Additionally, the size of the resulting particles can be fine-tuned by varying the amount of surfactants, initiators, the water/oil ratio or the temperature of the reaction [9-10]. While the traditional synthetic method of PAA nanoparticles have been successful for encapsulating not only molecular dyes but also enzymes like glucose oxidase, it did deactivate the encapsulated carbonic anhydrase, which is probably due to current surfactants, AOT (Sodium dioctyl sulfosuccinate) and Brij30. Therefore we have expanded the choices of surfactant systems to a wide range of nonionic surfactants,

which make the resulting nanoparticles more hydrophilic and more biocompatible. In Chapter 4, the application of the carbonic anhydrase immobilized PEBBLEs for zinc sensing will be discussed.

At last, Chapter 5 will summarize the conclusions and the limitations of this work as well as propose some future experiments for developing novel PEBBLE nanosensors.

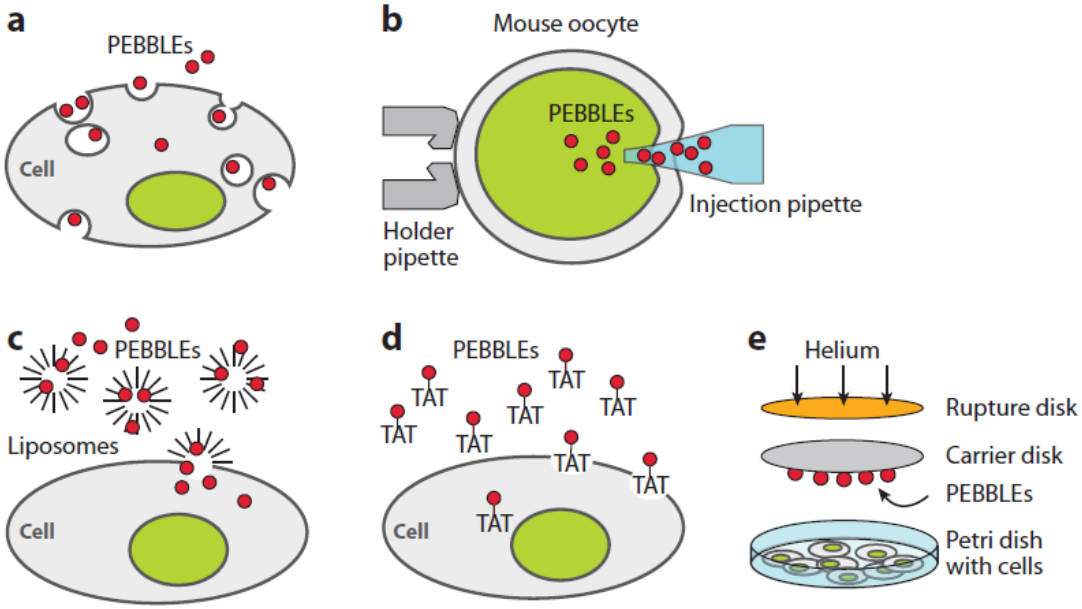

Figure 1.1 The delivery of nanoparticles into single cells [2]. (a) Endocytosis (nonspecific or receptor mediated). (b) Picoinjection. (c) Liposomal delivery. (d) Cell penetrating peptide (TAT). (e) Gene gun.

References

[1] R. P. Haugland, " The Handbook: A Guide to Fluorescent Probes and Labeling Technologies ", 10th Edition, *Molecular Probes, Inc.*, 2005

[2] Y. Koo Lee, R. Smith, and R. Kopelman, "Nanoparticle PEBBLE Sensors in Live Cells and In Vivo", *Annual Review of Analytical Chemistry*, (2)1: 57-76, 2009

[3] Y. Koo Lee, and R. Kopelman, "Optical Nanoparticle Sensors for Quantitative Intracellular Imaging", *Wiley Interdisciplinary Reviews: Nanomedicine and Nanobiotechnology*, (1)1: 98-110, 2009

[4] S. M. Buck, Y. Koo Lee, E. Park, H. Xu, M. A. Philbert, M. A. Brasuel, and R. Kopelman, "Optochemical Nanosensor PEBBLEs: Photonic Explorers for Bioanalysis with Biologically Localized Embedding", *Current Opinion in Chemical Biology*, (8):540-546, 2004

[5] H. A. Clark, M. Hoyer, S. Parus, M. A. Philbert, and R. Kopelman, "Optochemical Nanosensors and Subcellular Applications in Living Cells", *Microchimica Acta*, (131)1: 121-128, 1999

[6] M. Brasuel, R. Kopelman, M.A. Philbert, J.W. Aylott, H. Clark, I. Kasman, M. King, E. Monson, J. Sumner, H. Xu, M. Hoover, T.J. Miller, and R. Tjalkens, F. Ligler and C. Rowe-Taitt, Eds., "PEBBLE Nanosensors for Real Time Intracellular Chemical Imaging", in *Optical Biosensors: Present and Future*, Elsevier (Amsterdam), 497-536, 2002

[7] S. M. Buck, H. Xu, M. Brasuel, M. A. Philbert, and R. Kopelman, "Nanoscale Probes Encapsulated By Biologically Localized Embedding (PEBBLEs) for Ion Sensing and Imaging in Live Cells", *Talanta*, (63)1: 41-59, 2004

[8] H. A. Clark, S. L. Barker, M. Brasuel, M. T. Miller, E. Monson, S. Parus, Z. Shi, A. Song, B. Thorsrud, R. Kopelman, A. Ade, W. Meixner, B. Athey, M. Hoyer, D. Hill, R. Lightle, and M. A. Philbert, "Subcellular optochemical nanobiosensors: probes encapsulated by biologically localised embedding (PEBBLEs)", *Sensors and Actuators B: Chemical*, (51): 12-16, 1998

[9] H. A. Clark, M. Hoyer, M. A. Philbert, and R. Kopelman, "Optical Nanosensors for Chemical Analysis inside Single Living Cells. 1. Fabrication, Characterization, and Methods for Intracellular Delivery of PEBBLE Sensors", *Analytical Chemistry*, (71)21: 4831-4836, 1999

[10] Y. S. Leong, and F. Candau, "Inverse microemulsion polymerization", *The Journal of Physical Chemistry*, (86)13: 2269-2271, 1982

[11] A. Vakurov, N. A. Pchelintsev, J. Forde, C. O'Fagain, T. Gobson, and P. Millner, "The preparation of size-controlled functionalized polymeric nanoparticles in micelles", *Nanotechnology*, (20): 295605 (7pp), 2009

[12] H. A. Clark, R. Kopelman, R. Tjalkens, and M. A. Philbert, "Optical Nanosensors for Chemical Analysis inside Single Living Cells. 2. Sensors for pH and Calcium and the Intracellular Application of PEBBLE Sensors", *Analytical Chemistry*, (71)21: 4837-4843, 1999

[13] A. Webster, S. J. Compton, and J. W. Aylott, "Optical calcium sensors: development of a generic method for their introduction to the cell using conjugated cell penetrating peptides", *Analyst*, (130)2: 163-170, 2005

[14] E. J. Park, M. Brasuel, C. Behrend, M. A. Philbert, and R. Kopelman, "Ratiometric Optical PEBBLE Nanosensors for Real-Time Magnesium Ion Concentrations Inside Viable Cells", *Analytical Chemistry*, (75)15: 3784-3791, 2003

[15] N.M. Orozco, N. Touret, M. Zaharik, E. Park, R. Kopelman, S. Miller, B. Finlay, P. Gros, and S. Grinstein, " Visualization of Vacuolar Acidification-Induced Pathogen Gene Transcription Inside Macrophages", *Molecular Biology of the Cell*, (17): 498-510, 2005

[16] J. P. Sumner, J. W. Aylott, E. Monson, and R. Kopelman, "A fluorescent PEBBLE nanosensor for intracellular free zinc", *Analyst*, (127)1: 11-16, 2002

[17] J. P. Sumner, and R. Kopelman, "Alexa Fluor 488 as an iron sensing molecule and its application in PEBBLE nanosensors", *Analyst*, (130)4: 528-533, 2005

[18] J. P. Sumner, N. M. Westerberg, A. K. Stoddard, C. A. Fierke, and R. Kopelman, "Cu^{+}- and Cu^{2+}-sensitive PEBBLE fluorescent nanosensors using DsRed as the recognition element", *Sensors and Actuators B: Chemical*, (113)2: 760-767, 2006

[19] M. King, and R. Kopelman, "Development of a hydroxyl radical ratiometric nanoprobe", *Sensors and Actuators B: Chemical*, (90)1-3: 76-81, 2003

[20] H. Xu, J. W. Aylott, and R. Kopelman, "Fluorescent nano-PEBBLE sensors designed for intracellular glucose imaging", *Analyst*, (127)11: 1471-1477, 2002

[21] M. Brasuel, R. Kopelman, T. J. Miller, R. Tjalkens, and M. A. Philbert, "Fluorescent Nanosensors for Intracellular Chemical Analysis: Decyl Methacrylate Liquid Polymer Matrix and Ion-Exchange-Based Potassium PEBBLE Sensors with Real-Time Application to Viable Rat C6 Glioma Cells", *Analytical Chemistry*, (73)10: 2221-2228, 2001

[22] M. Brasuel, R. Kopelman, I. Kasman, T. J. Miller, and M. A. Philbert, "Ion concentration in live cells from highly selective ion correlation fluorescent nano-sensors for sodium", *Proceedings of IEEE*, (1): 288-292, 2002

[23] M. G. Brasuel, T. J. Miller, R. Kopelman, and M. A. Philbert, "Liquid polymer nano-PEBBLEs for Cl^- analysis and biological applications", *Analyst*, (128): 1262-1267, 2003

[24] Y. Cao, Y. Lee Koo, and R. Kopelman, "Poly(decyl methacrylate)-based fluorescent PEBBLE swarm nanosensors for measuring dissolved oxygen in biosamples", *Analyst*, (129)8: 745-750, 2004

[25] S. Kim, B. Kim, V. K. Yadavalli, and M. V. Pishko, "Encapsulation of Enzymes within Polymer Spheres To Create Optical Nanosensors for Oxidative Stress", *Analytical Chemistry*, (77)21: 6828-6833, 2005

[26] S. Tan, J. Jiang, B. Yan, G. Shen, and R. Yu, "Preparation of a novel fluorescence probe based on covalent immobilization by emulsion polymerization and its application to the determination of metronidazole", *Analytica Chimica Acta*, (560): 191-196, 2006

[27] M. J. Ruedas-Rama, and E. A. H. Hall, "K^+-selective nanospheres: maximising response range and minimising response time", *Analyst*, (131)12: 1282-1291, 2006

[28] Y. Kuang, and D. R. Walt, "Detecting oxygen consumption in the proximity of *Saccharomyces cerevisiae* cells using self-assembled fluorescent nanosensors", *Biotechnology and Bioengineering*, (96)2: 318-325, 2007

[29] E. Schmalzlin, J. T. van Dongen, I. Klimant, B. Marmodee, M. Steup, J. Fisahn, P. Geigenberger, and H. Lohmannsroben, "An Optical Multifrequency Phase-Modulation Method Using Microbeads for Measuring Intracellular Oxygen Concentrations in Plants", *Biophysical Journal*, (89)2: 1339-1345, 2005

[30] E. Pringsheim, D. Zimin, and O. S. Wolfbeis, "Fluorescent Beads Coated with Polyaniline: A Novel Nanomaterial for Optical Sensing of pH", *Advanced Materials*, (13)11: 819-822, 2001

[31] W. Stober, A. Fink, and E. Bohn, "Controlled growth of monodisperse silica spheres in the micron size range", *Journal of Colloid and Interface Science*, (26)1: 62-69, 1968

[32] H. Xu, J. W. Aylott, R. Kopelman, T. J. Miller, and M. A. Philbert, "A Real-Time Ratiometric Method for the Determination of Molecular Oxygen Inside Living Cells Using Sol−Gel-Based Spherical Optical Nanosensors with Applications to Rat C6 Glioma", *Analytical Chemistry*, (73)17: 4124-4133, 2001

[33] Y. L. Koo, Y. Cao, R. Kopelman, S. M. Koo, M. Brasuel, and M. A. Philbert, "Real-Time Measurements of Dissolved Oxygen Inside Live Cells by Organically Modified Silicate Fluorescent Nanosensors", *Analytical Chemistry*, (76)9: 2498-2505, 2004

[34] Y. Cao, Y. Lee Koo, S. Koo, and R. Kopelman, "Ratiometric Singlet Oxygen Nano-optodes and Their Use for Monitoring Photodynamic Therapy Nanoplatforms", *Photochemistry and Photobiology*, (81)6: 1489-1498, 2005

[35] G. Kim, Y. K. Lee, H. Xu, M. A. Philbert, and R. Kopelman, "Nanoencapsulation Method for High Selectivity Sensing of Hydrogen Peroxide inside Live Cells", *Analytical Chemistry*, (82)6: 2165-2169, 2010

[36] K. M. Tyner, R. Kopelman, and M. A. Philbert, ""Nanosized Voltmeter" Enables Cellular-Wide Electric Field Mapping", *Biophysical Journal*, (93)4: 1163-1174, 2007

[37] W. C. W. Chan, and S. Nie, "Quantum Dot Bioconjugates for Ultrasensitive Nonisotopic Detection", *Science*, (281)5385: 2016 -2018, 1998

[38] M. E. Akerman, W. C. W. Chan, P. Laakkonen, S. N. Bhatia, and E. Ruoslahti, "Nanocrystal targeting in vivo", *Proceedings of the National Academy of Sciences*, (99)20: 12617 -12621, 2002

[39] G. R. Reddy, M. S. Bhojani, P. McConville, J. Moody, B. A. Moffat, D. E. Hall, G. Kim, Y. Lee Koo, M. J. Woolliscroft, J. V. Sugai, T. D. Johnson, M. A. Philbert, R. Kopelman, A. Rehemtulla, and B. Ross, "Vascular Targeted Nanoparticles for Imaging and Treatment of Brain Tumors", *Clinical Cancer Research*, (12)22: 6677-6686, 2006

[40] P. Lundberg, and U. Langel, "A brief introduction to cell-penetrating peptides", *Journal of Molecular Recognition*, (16)5: 227-233, 2003

[41] S. Kumar, N. Harrison, R. Richards-Kortum, and K. Sokolov, "Plasmonic Nanosensors for Imaging Intracellular Biomarkers in Live Cells", *Nano Letters*, (7)5: 1338-1343, 2007

[42] D. E. Clapham, "Calcium signaling", *Cell*, (80)2: 259-268, 1995

[43] L. Fedrizzi, D. Lim, and E. Carafoli, "Calcium and signal transduction", *Biochemistry and Molecular Biology Education*, (36)3: 175-180, 2008

[44] B. L. Vallee, and D. S. Auld, "Zinc coordination, function, and structure of zinc enzymes and other proteins", *Biochemistry*, (29)24: 5647-5659, 1990

[45] J. M. Berg, and Y. Shi, "The Galvanization of Biology: A Growing Appreciation for the Roles of Zinc", *Science*, (271)5252: 1081 -1085, 1996

[46] T. V. O'Halloran, "Transition metals in control of gene expression", *Science*, (261)5122: 715 -725, 1993

[47] T. J. Lyons, A. P. Gasch, L. A. Gaither, D. Botstein, P. O. Brown, and D. J. Eide, "Genome-wide characterization of the Zap1p zinc-responsive regulon in yeast", *Proceedings of the National Academy of Sciences*, (97)14: 7957-7962, 2000

[48] S. Küry, M. Devilder, H. Avet-Loiseau, B. Dreno, and J. Moisan, "Expression pattern, genomic structure and evaluation of the human *SLC30A4* gene as a candidate for acrodermatitis enteropathica", *Human Genetics*, (109)2: 178-185, 2001

[49] B. Vallee, and K. Falchuk, "The biochemical basis of zinc physiology", *Physiological Reviews*, (73)1: 79-118, 1993

[50] A. Taylor, "Detection and monitoring of disorders of essential trace elements", *Annals of Clinical Biochemistry*, (33): 486-510, 1996

[51] C. Devirgiliis, P. D. Zalewski, G. Perozzi, and C. Murgia, "Zinc fluxes and zinc transporter genes in chronic diseases", *Mutation Research: Fundamental and Molecular Mechanisms of Mutagenesis*, (622): 84-93, 2007

[52] J. Peng, X. He, K. Wang, W. Tan, Y. Wang, and Y. Liu, "Noninvasive monitoring of intracellular pH change induced by drug stimulation using silica nanopartilces sensors", *Analytical and Bioanalytical Chemistry*, (388)3: 645-654, 2007

[53] K. Ramanathan, B. R. Jonsson, and B. Danielsson, "Sol-gel based thermal biosensor for glucose", *Analytica Chimica Acta*, (427)1: 1-10, 2001

[54] Y. Wang, and F. Caruso, "Mesoporous Silica Spheres as Supports for Enzyme Immobilization and Encapsulation", *Chemistry of Materials*, (17)5: 953-961, 2005

[55] S. A. Grant, C. Weilbaecher, and D. Lichlyter, "Development of a protease biosensor utilizing silica nanobeads", *Sensors and Actuators B: Chemical*, (121)2: 482-489, 2007

[56] D. Avnir, S. Braun, O. Lev, and M. Ottolenghi, "Enzymes and Other Proteins Entrapped in Sol-Gel Materials", *Chemistry of Materials*, (6)10: 1605-1614, 1994

[57] U. Narang, P. N. Prasad, F. V. Bright, K. Ramanathan, N. D. Kumar, B. D. Malhotra, M. N. Kamalasanan, and S. Chandra, "Glucose Biosensor Based on a Sol-Gel-Derived Platform", *Analytical Chemistry*, (66)19: 3139-3144, 1994

[58] T. K. Jain, I. Roy, T. K. De, and A. Maitra, "Nanometer Silica Particles Encapsulating Active Compounds: A Novel Ceramic Drug Carrier", *Journal of the American Chemical Society*, (120)43: 11092-11095, 1998

[59] K. Smith, N. J. Silvernail, K. R. Rodgers, T. E. Elgren, M. Castro, and R. M. Parker, "Sol−Gel Encapsulated Horseradish Peroxidase: A Catalytic Material for Peroxidation", *Journal of the American Chemical Society*, (124)16: 4247-4252, 2002

[60] E. A. Vitol, Z. Orynbayeva, M. J. Bouchard, J. Azizkhan-Clifford, G. Friedman, and Y. Gogotsi, "*In situ* intracellular spectroscopy with surface enhanced Raman spectroscopy (SERS)-enabled nanopipettes", *ACS Nano*, (3)11: 3529-3536, 2009

[61] J. Kneipp, H. Kneipp, M. McLaughlin, D. Brown, and K. Kneipp, "In vivo molecular probing of cellular compartments with gold nanoparticles and nanoaggregates", *Nano Letter*, (6)10: 2225-2231, 2006

[62] K. Kneipp, H. Kneipp, I. Itzkan, R. R. Dasari, and M. S. Feld, "Surface-enhanced Raman scattering and biophysics", *Journal of Physics: Condensed Matter*, (14)18: R597-R624, 2002

Chapter 2

Calcium Sensing and Imaging Using Polyacrylamide Nanoparticles Encapsulated with Rhodamine Based Calcium Indicators

Introduction

As a universal second messenger that transmits and processes information inside a variety of cells, Ca^{2+} plays a major role in intracellular signaling, muscle contraction, metabolism and a wide range of cellular processes such as fertilization, apoptosis, gene expression and neurotransmitter release. The Ca^{2+} ion was chosen by evolution as a ligand because of its unique properties. The charge and size (2 Å in diameter) of Ca^{2+} allows it to accept binding sites in scores of complex biological molecules such as proteins. These cellular proteins bind to Ca^{2+} tightly to maintain the free Ca^{2+} at low levels, since Ca^{2+} precipitates phosphate which is the established cellular energy currency; or in other cases so as to trigger second messenger pathways. The well-known basic concepts of calcium signaling have been extensively reviewed [1-5].

The total calcium content in resting cells is typically 1-7 mM [3], but almost all of the total cellular calcium (>99.9%) is stored in organelles, for instance in mitochondria and the smooth sarcoplasmic reticulum. Mitochondria can transiently take up Ca^{2+} for later release, contributing to calcium homeostasis. Additionally, cellular Ca^{2+} buffering is

also facilitated by Ca^{2+} binding to membrane components, cytosolic metabolites and cytosolic Ca^{2+}-binding proteins. Through these means, cells regulate the internal free Ca^{2+} at the optimal 100-200 nM level [2], which is 20,000 fold lower than extracellular Ca^{2+} level.

The Ca^{2+} signal is evanescent in its nature as increases in cytosolic Ca^{2+} dissipate rapidly due to diffusion. Also various "buffering pools" help to maintain a low Ca^{2+} level. Because changes in cytosolic Ca^{2+} concentration are transitory, the monitoring of the intracellular Ca^{2+} signals necessitates direct measurements in intact living cells. To date, the most successful approach for intracellular Ca^{2+} measurement is by the introduction of optically sensitive Ca^{2+} probes into living cells, combined with digital imaging microscopy.

The development of chemical fluorescence probes has been a breakthrough for monitoring Ca^{2+} inside living cells [6-9]. These probes were synthesized by adding a chromophore onto the molecule BAPTA (1,2-bis(o-aminophenoxy)ethane-N,N,N',N'-tetraacetic acid). Ca^{2+} binds to the carboxylic cage of BATPA and induces a fluorescence change. A variety of chemical fluorescence probes are commercially available. These probes are available in ratiometric or non-ratiometric forms, with a wide range of excitation and emission wavelengths, as well as Ca^{2+} binding affinity, and are available in various forms such as cell impermeable salts, as well as cell permeable AM (acetoxymethyl) ester and dextran conjugates. Of these Indo-1 and Fura-2 are the most commonly used ratiometric probes [8]. However, the use of these two dyes requires UV

excitation which causes much cell or tissue autofluorescence in many situations. It also has been reported that both dyes degenerate into Ca^{2+}-insensitive fluorescent compounds due to the UV illumination [4]. This can lead to inaccurate measurements. Visible wavelength excitation is more favorable since it causes less cellular autofluorescence and less damage to the cells or tissues. To that end, indicators with visible excitation such as Fluo-3, calcium green and Rhod-2 have also been widely used for intracellular Ca^{2+} measurements.

Rhod-2 is a rhodamine-based Ca^{2+} indicator developed by Tsien and co-workers [9]. Rhod-2 is often used for *in situ* measurement of Ca^{2+} level in brain cells, cardiac cells or in organs, such as perfused mouse or rabbit heart [8, 10-14] because the long excitation wavelength gives better tissue penetration and induces less background autofluorescence. Additionally, Rhod-2 has been used for measurements of mitochondrial Ca^{2+} levels because the AM (acetoxymethyl) ester form of Rhod-2, which is positively charged, tends to be accumulated and trapped in mitochondria [15, 16].

The major limitation of Rhod-2 is the lack of shift of absorbance, excitation or emission wavelength upon Ca^{2+} binding [9]; therefore the dye by itself is not ratiometric. Ratiometric measurement is probably the best way for fluorescence intensity (rather than lifetime) based methods, for achieving accurate monitoring of calcium levels in living cells, because it cancels out variations in dye concentration, path length and optical instabilities. Although the dye is highly sensitive by itself, the fluorescence intensity cannot be accurately converted to Ca^{2+} levels without retiometric

measurements, unless the dye concentration, path length, and instrumental sensitivity are precisely known. For solution tests in cuvettes, these conditions can be easily achieved; but it is almost impossible to reproduce them in single cell test without lysing the cells and titrating the dye in the supernatant. An alternative route, [9, 12, 13, 15] is to monitor the fluorescence change over time during cell stimulation or other manipulation. Such a method at least cancels out variations in dye concentration and path length, and enables accurate measurements of the change in Ca^{2+} concentration. But, of course, the intracellular Ca^{2+} is not calculated as absolute levels but only relative to the pre-treatment values.

Ratiometric measurements can also be achieved effectively through the use of fluorescence lifetime imaging (FLIM), as reported by Lakowicz and co-workers [17-19]. The local decay times can be resolved into a composition of free and bound form of the dye molecule and therefore reveal the free Ca^{2+}. The FLIM method allows images to be generated by the local lifetime, which is independent of dye concentration, rather than by local fluorescence intensity. For this reason, the need for ratiometric probes can be bypassed. Unfortunately, for dyes like Rhod-2 or Fluo-3, their lifetimes are in the picosecond range for the free and bound form [9]. Consequently, for this method, an instrument with picosecond resolution is required, which is not what is available with standard confocal microscopes.

Other problems encountered when measuring intracellular Ca^{2+} using the above fluorescent molecular probes are: 1). Cytotoxicity; some probes may be toxic to some

type of cells. For example, it has been reported that sea urchin eggs loaded with Fluo-3 do not develop normally [4, 20]. 2). Unwanted compartmentalization due to sequestration; one of the most important issues in the use of chemical fluorescence probes is that the indicators are not homogeneously distributed throughout the whole cell but are trapped or sequestered within some organelles [4, 9, 13]. The level of Ca^{2+} in a given compartment is usually not the same as in the cytosol, therefore compartmentalization would result in inaccurate measurements of cytosolic Ca^{2+}. 3). Binding to other ions and proteins; many of the probes bind with intracellular proteins and thus undergo changes in their diffusion constant, emission spectra, reaction kinetics, and their K_d for Ca^{2+} [4, 11, 21]. Additionally, all of these indicators are affected by pH, to various degrees [4, 10, 22], or by other divalent cations, such as Mg^{2+}, Mn^{2+}, Co^{2+}, Zn^{2+}, etc [4, 9, 11, 23]. 4). Indicator dye leakage from the cytosol to the extracellular medium. This leakage is regulated by anion transport systems, and the leaking rate is dependent on temperature, the cell type and the dye itself [4].

By loading these probes into a particle's matrix, most of these issues are minimized or totally eliminated. First of all, although some of the probes are not ratiometric by themselves, the PEBBLE nanosensors can be constructed to be ratiometric by encapsulating or conjugating a reference dye. Other issues, like cytotoxicity, non-specific binding with intracellular proteins, and dye leakage to the extracellular medium are prevented since the dye molecule is trapped in the particle matrix and is not in direct contact with the cellular contents (except those diffusing in, e.g. small ions). Therefore, both the dye and the cellular environment are largely

protected from each other [24, 25]. Also, the PEBBLE matrix is a well defined environment, with a well defined K_d that can be calibrated in a test-tube and still be valid anywhere inside the cell. Furthermore, the PEBBLE nanosensors can be targeted to specific cell compartments, avoiding the problem of sequestration [30-31].

Confocal microscopy has been one of the most successful methods for intracellular Ca^{2+} sensing and imaging [4, 5, 12, 14]. As discussed previously, Ca^{2+} almost never distributes homogeneously across the cell; the local Ca^{2+} events may occur on a very fast time scale; and Ca^{2+} cannot be preserved in cell or tissue extracts. Therefore, a reliable Ca^{2+} imaging method for live specimens with high temporal and spatial resolution is necessitated. Confocal microscopy meets the requirement, and is fully synergistic with PEBBLE nanosensors. A basic optical setup is illustrated in Figure 2.1; a confocal aperture with a pinhole is placed directly in front of the light detector, usually a photomultiplier tube (PMT). This confocal aperture blocks out-of-focus light generated from areas of no interest, and only allows in-focus signal into the PMT [26]. Unlike regular epifluorescence microscopy, which captures light along the entire Z-axis, confocal microscopy provides measurements on optical sections with thickness of a few microns.

In the work described in this chapter, Ca^{2+}-sensitive ratiometric PEBBLE nanosensors loaded with rhodamine based Ca^{2+} indicators were developed and characterized. The PEBBLEs were introduced into the living cells by either endocytosis or TAT peptide delivery. Intracellular calcium imaging was performed on a Leica laser scanning confocal microscope.

Experimental and Methods

Reagents. Acrylamide, glycerol dimethacrylate (GDMA), polyoxyethylene (4) lauryl ether (Brij 30), polysorbate 80 (Tween 80), sorbitan monooleate (Span 80), N,N,N',N'-tetraethylmethylenediamine (TEMED), ammonium persulfate, 4-morpholinepropanesulfonic acid (MOPS), Dimethyl sulfoxide (DMSO), ethylene glycol-bis(2-aminoethylether)-N,N,N',N'-tetraacetic acid (EGTA) and all metal salts were purchased from Sigma-Aldrich (St. Louis, MO, USA). N-(3-aminopropyl)methacrylamide hydrochloride (APMA) was purchased from Polyscience (Warrington, PA, USA). Hexanes and ethanol were purchased from Fisher (Fair Lawn, NJ, USA). Chelex 100 resin was purchased from Bio-Rad (Hercules, CA, USA). Rhod-2, Rhod-dextran and Rhod-5N were purchased from Invitrogen (Eugene, OR, USA). HiLyte Fluor^{TM} 647 was purchased from AnaSpec (Fremont, CA, USA). Sulfosuccinimidyl-4-[N-maleimidomethyl]cyclohexane-1-carboxylate (Sulfo-SMCC) was purchased from Soltec Ventures (Beverly, MA). TAT peptide was purchased from RS synthesis, LLC. (Louisville, KY). All buffer solutions were prepared from 18MΩ Milli-Q water purified by a Millipore Advantage A10 system and passed through a Chelex 100 column.

PC-3 human prostate carcinoma cells and 9L gliosarcoma cells were purchased from ATCC (Rockville, MA, USA). All cell media, fetal bovine serum (FBS), penicillin, streptomycin, HEPES buffer and Hank's Balanced Salt Solution (HBSS) were purchased from Invitrogen (Eugene, OR, USA).

PEBBLE preparation. The polymerization procedure was as described previously with minor changes [24]. The monomer solution was prepared by first dissolving 711 mg acrylamide in 1.2 ml MOPS buffer (pH=7.2), then dissolving 55 mg APMA and adding 480 µl GDMA at last. Calcium indicators were added into the monomer solution for preparing the calcium sensing PEBBLEs. This monomer solution was added to an argon deoxygenated solution that contained 45 ml of hexanes, 2.6 g Brij 30, 1.6 g Tween 80 and 1.3 g Span 80. The solution was stirred under argon throughout the duration of the preparation. To initiate the polymerization, 100 µl of 20% (w/w) ammonium persulfate solution and 100 µl TEMED were added. The solution was stirred at room temperature for two hours to assure complete polymerization. The hexanes were removed by rotary evaporation and the remaining solution was mixed with 100 ml ethanol and then transferred to an Amicon ultra-filtration cell (Millipore Corp., Bedford, MA). The surfactant, unreacted monomers and dye molecules were separated from the PEBBLEs using a 300 kDa filter under 10 psi of pressure. The PEBBLEs were washed with 500 mL ethanol and 500 ml Milli-Q water. The PEBBLEs were freeze dried on a Thermo ModulyoD Freeze Dryer and then collected.

Conjugation of the reference dye. 100 mg PEBBLEs were suspended in 5 ml MOPS buffer yielding a 20 mg/ml particle solution, into which 10 ~ 20 µl of Hylite 647 solution (0.1 mg/ml in DMSO) was added. The mixture was stirred for 2 hours at room temperature, then transferred to an Amicon ultra-filtration cell and washed with 60 ml Milli-Q water. The PEBBLEs were freeze dried and collected.

Conjugation of TAT peptide. 50 mg PEBBLEs were firstly suspended in 2.5 ml 10 mM MOPS pH 7.22, into which 3 mg Sulfo-SMCC was added. The mixture was kept stirring at 600 rpm for 2 hours at room temperature, then transferred to an Amicon cell and washed with 60 ml MOPS buffer. 3 mg TAT peptide was added into the resulting mixture under constant stirring at 600 rpm and the mixture was kept stirring overnight at room temperature. 1.736 mg L-cysteine was added afterwards and the mixture was kept stirring for 2 more hours. Finally PEBBLEs were washed in Amicon cells with 60 ml MOPS to eliminate unreacted peptides.

Dissociation constants for free Rhod-2 and encapsulated Rhod-2 inside PEBBLEs binding with Ca^{2+}. To determine the K_d for free Rhod-2 and encapsulated Rhod-2, solutions with various Ca^{2+} concentrations were prepared from a stock solution of known Ca^{2+} concentration. This method was established by Tsien and Pozzan [27], based on the principle that most Ca^{2+} ions bind with EGTA when the Ca^{2+} concentration and EGTA concentration are very close to each other. Therefore, in the equilibrium of Ca^{2+} and EGTA, the effective free Ca^{2+} is a function of K_d(Ca^{2+}EGTA), the dissociation constant of Ca^{2+}EGTA (which is dependent on pH, the temperature and the ionic strength). The actual free Ca^{2+} concentrations in the calibration solutions, at a given pH, temperature and ionic strength, were computed using a web-based computer program, Webmaxclite v1.15 (Stanford University, http://www.stanford.edu/~cpatton/webmaxc/webmaxclite115.htm). According to the equation below, the free Ca^{2+} concentrations were obtained.

$$[Ca^{2+}]_{free} = K_d(Ca^{2+}EGTA) \times ([Ca^{2+}EGTA]/[K_2EGTA])$$

Once the effective free Ca^{2+} concentrations were acquired, the K_d for free Rhod-2 or encapsulated Rhod-2 and Ca^{2+} was derived, based on the free Ca^{2+} concentrations and the resulting fluorescence of Rhod-2 or the fluorescence ratio of the Rhod-2 PEBBLEs:

$$K_d(Ca^{2+}Rhod\text{-}2\text{-}free) = [Ca^{2+}]_{free} \times (F_{max} - F)/(F - F_{min})$$

Or

$$K_d(Ca^{2+}Rhod\text{-}2\text{-}encapsulated) = [Ca^{2+}]_{free} \times (R_{max} - R)/(R - R_{min})$$

Here F_{max}, F_{min} and R_{max}, R_{min} refer to the fluorescence (F) or fluorescence ratio (R) of the Ca^{2+} saturated state (max) and the Ca^{2+} depleted state (min), respectively. In principle, the K_d for free Rhod-2 or encapsulated Rhod-2 and Ca^{2+} was computed by plotting the log of $[Ca^{2+}]_{free}$ (the x-axis) versus the log of $(F - F_{min})/(F_{max} - F)$ or $(R - R_{min})/(R_{max} - R)$ (the y-axis). This log-log plot yields an x-intercept which is the log of K_d for free Rhod-2, or encapsulated Rhod-2, and Ca^{2+} at a given condition.

PEBBLE calibration. To calibrate the calcium sensitive PEBBLEs, a 2 mg/ml PEBBLE solution was prepared by suspending PEBBLEs in 10 mM MOPS buffer pH 7.22 containing 0.1 mM EGTA. The free Ca^{2+} concentrations in the calibration solutions were computed by Webmaxclite v1.15. Spectra were collected on a Horiba FluoroMax-3 fluorometer by exciting the sample at 540 nm and recording the resulting emission from 565 nm to 700 nm in 1 nm increments with an integration time of 0.5 second. An aliquot

of calcium chloride was added after each successive spectrum was collected. The samples were prepared and continuously stirred by a magnetic stir bar in a 4.5 ml quartz cuvette which was kept at 37°C by a water-jacketed temperature controlled cuvette holder. All experiments were repeated in triplicate.

PEBBLE calibrations were also performed in the presence of background ions in the calibration solutions. Samples with 2 mg/ml PEBBLEs in 0.1 mM EGTA 10 mM MOPS buffer pH 7.22 containing (i) 20 mM Mg^{2+}; (ii) 20 mM Mg^{2+}, 20 mM Na^{+} and 120 mM K^{+} were prepared. An aliquot of calcium chloride was added after each successive spectrum was collected. All experiments were performed at 37°C.

PEBBLE interference. An assay was conducted on Rhod-2, and on Rhod-2 PEBBLEs, to monitor the interference due to non-specific binding of proteins to the sensors. Samples containing 0.1 µM Rhod-2, or 2 mg/ml Rhod-2 PEBBLEs, 1% w/v Bovine Serum Albumin (BSA), 0.1 mM EGTA in 10 mM MOPS buffer, pH 7.22 were prepared. An aliquot of calcium chloride was added after each successive spectrum was collected. The experiments were performed at 37°C.

pH dependence test. A series of 10 mM MOPS buffers with pH range 4-9 were prepared. PEBBLEs were suspended in these buffers at a final concentration of 2 mg/ml. $CaCl_2$ concentrated solution (10 mM) was added into the PEBBLE suspension at a final concentration of 10 µM Ca^{2+}. No EGTA was added, because the binding of EGTA and Ca^{2+} changes with pH.

PEBBLE Leaching. First a suspension containing 2mg/ml Rhod-2 PEBBLEs and MOPS (10 mM pH 7.2) was prepared. The initial fluorescence was measured and the dye concentration was calculated, based on a calibration curve of free dye in solution. After that, BSA was added into the suspension to make the final BSA concentration 1% w/v and the suspension was kept stirring. At different time intervals, a 3 ml aliquot was filtered and the filtrate was analyzed. The dye concentration in the filtrate was calculated based on another calibration curve of free dye in solution at the presence of 1% BSA. Previous studies show that the leaching behavior of the dye encapsulated PEBBLEs are different in the presence or absence of proteins, or in solution vs. in cellular environment. Therefore, the function of the 1% BSA in this case is to mimic the cellular environment so that the leaching test results would better represent the PEBBLE leaching behavior in cell work.

PEBBLE ratiometric validation. The PEBBLEs' ability to be ratiometric was also examined. Samples containing 0.1, 0.2, 0.5, 1, 2 and 5 mg/ml PEBBLE 0.1 mM EGTA in 10 mM MOPS buffer pH 7.22 were prepared. Spectra were collected by exciting the sample at 540 nm and recording the resulting emission from 565 nm to 700 nm. The fluorescence ratio $F_{Rhod\text{-}2}/F_{Hilyte}$ was calculated.

Zeta potential. PEBBLEs were first suspended in Milli-Q water at a concentration of 2-5 mg/ml and sonicated for 30 minutes to one hour to reduce aggregation. Samples were then filtered through a 2.7 µM glass fiber syringe filter (13 mm diameter, Whatman). The Zeta potential of the PEBBLEs was measured on Delsa™Nano Submicron

Particle Size and Zeta potential instrument (Beckman Coulter, Inc., Fullerton, CA) by electrophoretic light scattering.

Confocal microscopy. Fluorescence images were obtained on a laser scanning confocal microscope. Scanner and detector were mounted on an inverted microscope (Leica sp5) equipped with oil-immersion, 1.4-numerical aperture, ×40 and ×60 objective (Leica). A white light laser (540 nm) served as a primary light source and fluorescence light (560-620 nm, 660-720 nm) from the calcium sensing dye and the reference dye was detected with a high efficiency photomultiplier tube. Confocal pinhole aperture settings were kept at 2 μm throughout the entire experiments.

Cell culture. PC-3 human prostate carcinoma cells were cultured in DMEM medium containing 10% fetal bovine serum (FBS) and penicillin (10 IU/ml). 9L gliosarcoma cells were cultured in RPMI medium containing 10% fetal bovine serum (FBS) and penicillin (10 IU/ml). All cells were maintained at 37°C in a humidified incubator containing 5% CO_2. Cells were plated on 1.0 Borosilicate chambered coverglass one day prior to experiments.

Cell imaging and the manipulation of free intracellular Ca^{2+}. Cells were incubated with PEBBLEs (0.1~0.5 mg/ml) for 30 minutes to 3 hours in the culture media at 37°C. Rhod-2 was loaded into cells by adding Rhod-2 AM 5 μM from a 1 mM stock in dry DMSO to the culture media and incubating at 37°C for 30 minutes. After loading, cells were washed 3 times with PEBBLE free dye free HHBSS (20 mM HEPES, 1× Hanks

Balanced Salt Solution, 2 g/l D-glucose, pH 7.4) and incubated at 37^0C for about 30 minutes prior to mounting on the microscope.

To reduce cell calcium, cells were first washed 3 times with Ca^{2+}-free HHBSS then incubated in Ca^{2+}-free HHBSS containing 1 mM EGTA and 5 µM A23187 for 30 minutes, for Ca^{2+} to be depleted from the cytoplasm. An aliquot of $CaCl_2$ was added into HHBSS to alter the extracellular Ca^{2+} level, and the cells were incubated for 10~30 minutes before the images were taken. Finally, the indicator was saturated by adding $CaCl_2$ to a final concentration of 5 mM. Images at maximum Ca^{2+} level were taken before cell death occurs, which is indicated by membrane blebbing and change in size. For each image acquired at different Ca^{2+} levels, peak intensity ratios of $F_{Rhod\text{-}2}/F_{Hilyte}$ were calculated on computer software ImageJ.

Results and Discussion

The focus of this chapter is on the calcium nanosensors developed using rhodamine-based calcium sensitive dyes, Rhod-2 and Rhod-5N (Figure 2.2). The reported calcium sensing range (Molecular Probes Inc.) of Rhod-2 is at the nanomolar level and the sensing range of Rhod-5N is at the micromolar level. Hilyte Fluor 647 was conjugated onto the PEBBLEs as a reference dye for ratiometric sensing. The majority of the work focuses on Rhod-2/Hilyte PEBBLEs.

In Table 2.1, the calcium affinities of encapsulated Rhod-2 in PEBBLEs with different dye loadings were tested and compared with that of the free dye. Four samples, with a certain amount of dye (0.1, 0.2, 0.5 and 1 mg Rhod-2) initially added in the preparation, were calibrated. For all four samples, the K_d values are between 500~600 nM, which is somewhat higher than that of the free Rhod-2 dye. This result can be explained by the positive charge of the PEBBLEs matrix, which is considered to be caused by the amine functional groups on APMA. However, comparing the PEBBLEs with 0.5% APMA to the PEBBLEs with 2.5% APMA, a 2% increase of APMA is not high enough to dramatically affect the zeta potential of the whole particle matrix and consequently affect the affinity (see Table 2.2). The function of APMA is to provide amine functional groups for conjugating targeting peptide and reference dyes. For that purpose, 2.5% APMA would suffice.

Figure 2.3 shows typical spectra of Rhod-2/Hilyte PEBBLEs with Rhod-2 emission increases as the free Ca^{2+} concentration increases while the emission of Hilyte is

independent of the free Ca^{2+} concentration. Calibrations of the PEBBLEs without background ions or in the presence of 20 mM Mg^{2+}, 20 mM Na^{+} and 120 mM K^{+} were also performed, as shown in Figure 2.4. The peak intensities of Rhod-2 and Hilyte were ratioed and plotted against the free Ca^{2+} concentration. Without background ions, K_d is determined to be 429±38 nM. In the presence of 20 mM Mg^{2+}, the K_d rises to 786±65 nM, indicating a decreasing affinity of Rhod-2 for Ca^{2+}. Although the addition of Na^{+} and K^{+} changes the ionic strength of the solution, thereby influencing the equilibrium of EGTA and Ca^{2+}, it does not significantly affect K_d, which remains at 830±87 nM in this case.

As a divalent cation, Mg^{2+} also binds with EGTA and changes the free Ca^{2+} level in solution, although Mg^{2+} binds with EGTA much weaker than Ca^{2+}. At pH 7.22, ionic strength of 0.15 M, and 37°C, $K_d(Ca^{2+}EGTA)$ is found to be 0.115 μM while $K_d(Mg^{2+}EGTA)$ is 9.4 mM. As expected, Mg^{2+} also binds with the BAPTA moiety on Rhod-2, as it binds with other BAPTA-based calcium indicators such as Fluo-3 [9]. Therefore the binding of Mg^{2+} slightly weakens the affinity of Rhod-2 for Ca^{2+}. However, the Mg^{2+} binding has relatively little effect on the Rhod-2 fluorescence, compared to the 100-fold enhancement from Ca^{2+} binding, because Mg^{2+} binds mostly to the half of Rhod-2 which is remote from the xanthene chromophore. Besides, although the intracellular free Mg^{2+} concentration fluctuates, intracellular free Mg^{2+} is estimated to be much less than 20 mM and its fluctuation is usually within 1 mM range [36]. As long as the interference caused by Mg^{2+} is taken into consideration in the calibration, intracellular free Mg^{2+} should pose no serious problem for intracellular Ca^{2+} measurements.

It has also been found that Rhod-2 binds with some transition metal ions and its emission increases, such as by binding with Mn^{2+}, Zn^{2+}, Cd^{2+} and Hg^{2+}; other transition metal ions, such as Fe^{3+}, Co^{2+}, Ni^{2+} and Pb^{2+} also bind to Rhod-2 and quench its fluorescence. Therefore, binding with these transition metal ions is a potential interference to Ca^{2+} sensing. Fortunately, Rhod-2 binds to Ca^{2+} much tighter than to most of the transition metal ions and also the intracellular concentrations of these transition metal ions are much lower than those of calcium in most cases [33]. When interference occurs, it can be identified and controlled by using the selective heavy metal ion chelator TPEN (N, N, N', N'-tetrakis (2-pyridylmethyl)-ethylenediamine) [34, 35].

An interference test, with 1% w/v BSA, was conducted on the Rhod-2 dye and Rhod-2/Hilyte PEBBLEs (see Figure 2.5). The K_d of the free dye in the presence of BSA is about 200 nM higher than the K_d of the free dye in the absence of BSA. On the other hand, the PEBBLEs containing Rhod-2 are unaffected by the addition of BSA. This suggests that BSA is unable to enter the PEBBLEs due to its large size and thus unable to come in contact with the dye so as to affect its fluorescence or Ca^{2+} affinity. Non-specific binding of interferents occurs for many small molecule Ca^{2+} indicators, as reported [4, 11, 21], by enhancing or weakening their fluorescence. As shown in Figure 2.6, in the presence of 1% w/v BSA, the fluorescence of Rhod-2 free dye decreases. This concept demonstrates a major drawback for the intracellular measurements using free dyes, as well as a key advantage of PEBBLE nanosensors. In the complicated cellular environment, in the presence of numerous proteins and enzymes, free dyes show at least some change in their binding affinity, if they still remain fluorescent. Evidently, the use of

PEBBLEs eliminates this issue, by protecting the sensing elements in a polymer matrix. For that reason, a calibration in solution would remain valid for measurements in the cellular environment. In addition, the cellular environment is also protected by the PEBBLE matrix from potential toxicity of the dye.

The leaching of Rhod-2 from the PEBBLEs was also monitored. The leaching behavior of the PEBBLEs could be different in solution and in the cellular environment, since dye molecules can be pulled out from the particle matrix by proteins or enzymes, due to non-specific binding. Two particle samples with 0.5 and 1 mg dye loading were monitored over a 3-day time period. A 1% w/v BSA solution was used to mimic the cellular environment. As illustrated in Figure 2.7, leaching mostly occurred at the initial 6 hours, with totally 18% dye having leached out from the 1 mg dye loaded sample but less than 3% from the 0.5 mg dye loaded sample.

The pH dependence tests shown in Figure 2.8 suggest that the PEBBLEs are stable at neutral pH (pH 6-9). At low pH, the fluorescence of Rhod-2 was quenched due to the protonation of the dye molecule. Previous studies also indicate that the $K_d(Ca^{2+}$Rhod-2) value rises when the pH drops below 6.6 [10]. Note that the PEBBLE matrix pores easily allow passage of the small hydroxyl and hydronium ions [24].

Figure 2.9 demonstrates the ratiometric property of the Rhod-2/Hilyte PEBBLEs. The peak ratio of $F_{Rhod\text{-}2}/F_{Hilyte}$ does not change as the PEBBLE concentration increases from 0.1 to 5 mg/ml. Among all the commercially available calcium probes, few are ratiometric by themselves. This feature limits the use of these non-ratiometric

indicators since ratiometric measurement is the best and most accurate method, unless a fluorescence lifetime measurement is used. On the other hand, encapsulating the indicator probes inside the matrix of the PEBBLEs can solve this issue, because a reference dye can easily be encapsulated inside or conjugated onto the nanoparticles.

A prevalent method used for almost all calcium indicators involves adding a Ca^{2+} ionophore A23187 or Br-A23187 to the cell medium as to manipulate the intracellular free Ca^{2+} levels [7]. Calcium ionophores A23187 and Br-A23187 are mobile ion carriers that form stable complexes with divalent cations and carry these ions cross cell membranes. In this method, the Ca^{2+} depleted state (F_{min}) and the Ca^{2+} saturated state (F_{max}) are determined, and then the free Ca^{2+} level is calculated using the equation:

$$[Ca^{2+}]_{free} = K_d(Ca^{2+}\text{Rhod-2}) \times (F - F_{min})/ (F_{max} - F)$$

However, as discussed previously, if free dye is used for the measurement, extra efforts have to be made to measure the precise $K_d(Ca^{2+}\text{Rhod-2})$ in the intracellular environment, due to the weakening of the Ca^{2+} affinity by proteins and enzymes [11].

Figure 2.10 is a demonstration of this method. The AM form of Rhod-2 enters the cells, except for the nucleus, through incubation. A Ca^{2+} depleted state and a saturated state were imaged. Rhod-2 AM has shown signs of compartmentalized loading into mitochondria. The uneven distribution of Rhod-2 may lead to over- or under-estimation of the Ca^{2+} level at a certain spot. However, with ratiometric measurements by PEBBLEs, this issue is resolved (see Figure 2.11). The Rhod-2/Hylite PEBBLEs were delivered into 9L cells by nonspecific endocytosis. In the presence of A23187, the

intracellular free Ca^{2+} level changes with the extracellular free Ca^{2+} level which was manually manipulated by controlling the concentration of EGTA and total calcium in cell medium. The emission of Rhod-2 (as shown in green color) increases with the free Ca^{2+} concentration while the emission of Hilyte (as shown in red color) is independent of the free Ca^{2+} concentration. Therefore, in the overlaid images of green and red, one would see a color change from red to green as the free Ca^{2+} level changes from low (0.32 nM) to high (5 mM). The fluorescence confocal images were processed by an image-processing software ImageJ, and the intensity ratios of Rhod-2 (green)/Hilyte (red) at each free Ca^{2+} level were calculated. The intensity ratio was plotted against extracellular free Ca^{2+} concentration in Figure 2.12. We name it an "in-cell calibration". The K_d of the encapsulated Rhod-2 binding to Ca^{2+} in the in-cell calibration was determined to be 1003±975 nM. An in-solution calibration of PEBBLEs was also performed on a Leica confocal microscope, in the same cell media, Ca^{2+}, Mg^{2+}-free HEPES buffered Hanks Balanced Salt Solution (pH 7.4) containing 10 mM EGTA, without adding A23187. The K_d was determined to be 478±32 nM.

The other two rhodamine-based Ca^{2+} indicators, Rhod-dextran and Rhod-5N were also encapsulated in PEBBLEs with the reference dye Hilyte Fluor 647. Calibrations of these two PEBBLEs were shown in Figure 2.13. The Ca^{2+} binding affinities of these encapsulated dyes were determined to be at micromolar levels, as 698±179 μM for encapsulated Rhod-dextran and 1.25±0.06 mM for encapsulated Rhod-5N. Note that the actual K_d of encapsulated Rhod-dextran may be higher than the calculated value 698±179 μM, because it did not reach the Ca^{2+} saturated state at the end point (Ca^{2+}

level at 0.01 M), as shown in Figure 2.12 (c). Because of their high calcium binding affinity, these PEBBLEs are not sufficiently sensitive for intracellular measurements. Figure 2.14 shows the fluorescence confocal images of 9L cells loaded with Rhod-dextran and Rhod-5N PEBBLEs. As shown in the images, PEBBLEs were delivered into 9L cells by surface-conjugated HIV-1 TAT peptide.

It has been reported that free Rhod-2 tends to be trapped in mitochondria due to its large negative membrane potential [9, 13]. Therefore, dye leaching from the PEBBLEs became a concern. However, cell imaging using Rhod-dextran/Hilyte PEBBLEs, which contain the much larger molecules of Rhod-2 dextran conjugates (10 kDa), also show a similar distribution pattern, indicating that leaching is not a serious concern (Figure 2.13). Although leaching is not at all an issue for the Rhod-dextran PEBBLEs, its weaker Ca^{2+} binding affinity (353±45 μM) makes it less effective for intracellular measurement, compared to the Rhod-2 PEBBLEs.

Conclusions

This chapter details the preparation and characterization of Ca^{2+}-sensitive PEBBLEs loaded with rhodamine based probes as the Ca^{2+} sensing dye and conjugated with Hilye Fluor 647 as the reference dye. The advantages in the use of PEBBLEs are well demonstrated by this work. 1) Ratiometric measurements can be achieved by co-loading a reference dye, allowing the changes in fluorescence ratio to be converted to Ca^{2+} levels. 2) The polymer matrix protects the dye from non-specific binding caused by intracellular proteins, because the proteins are simply too big to enter the particle and interact with the dye molecules. 3) The dye molecules are trapped in nanoparticles, and therefore some other issues one may have when using the free dye, such as the dye sequestration and leakage out of the cells, are reduced or eliminated. 4) The K_d of the encapsulated dye in PEBBLEs is well defined so that calibrations in a test tube still remains valid for intracellular measurements.

There are several limitations of this work that are important to discuss. Although the particle matrix protects the dye from the cellular protein, small ions such as H^+ and Mg^{2+} can still enter the matrix freely and interact with the dye, which would interfere with the Ca^{2+} measurements, similarly as for the free molecular probes. Fortunately, these interferences do not significantly affect the binding of Rhod-2 and Ca^{2+}, and corrections can be made by taking these factors into consideration when calibration is conducted.

Another limitation is that the Rhod-2 PEBBLEs were delivered into cells by nonspecific endocytosis. It is argued that after cell entry by endocytosis, particles may stay in endosomes which contain different Ca^{2+} levels and pH than the cytosol, resulting in inaccurate Ca^{2+} measurements [28]. Other delivery methods, such as receptor mediated endocytosis or cell-penetrating TAT peptide, lead to less PEBBLE sequestration and more PEBBLEs can be delivered directly into the cytosol. It has been reported that the translocation of TAT peptide into the cells is unaffected by endocytosis inhibitors, indicating a non-endocytotic pathway [32]. In a matter of fact, targeted delivery is another advantage of PEBBLEs. Targeting peptides or proteins can be surface-conjugated on PEBBLEs, so that the PEBBLEs can be delivered to specific cell types or to specific organelles inside cells [30]. Therefore, these methods will be introduced in our future work.

The calcium levels in cellular organelles are also of great interest due to the function of calcium as a second messenger. However, as demonstrated in our work, without targeting, nano PEBBLEs cannot be internalized by cellular organelles, such as nucleus, mitochondria, etc. Although targeted delivery of PEBBLEs into cellular organelles has become part of our ongoing research, currently for the calcium sensing inside organelles, free calcium indicators may be more useful than PEBBLEs. For example, free Rhod-2 was utilized to monitor calcium levels in mitochondria [4, 13-16], while the emergence of mithochondrial calcium into the cytosol was easily observed by PEBBLEs [24].

	K_d (nM)
Rhod-2	317±16
0.1 mg loading Rhod-2 PEBBLE	554±44
0.2 mg loading Rhod-2 PEBBLE	587±64
0.5 mg loading Rhod-2 PEBBLE	523±22
1 mg loading Rhod-2 PEBBLE	526±33

Table 2.1 Dissociation constant K_d of free Rhod-2 or encapsulated Rhod-2 in PEBBLEs with different dye loading and Ca^{2+}. The K_d values were computed from experiments performed in 10 mM MOPS buffer pH 7.22 containing 0.1 mM EGTA at 37°C.

	Zeta potential (mV)	K_d (nM)
PEBBLE with 0.5% APMA	15.34	593±31
PEBBLE with 1% APMA	15.36	588±21
PEBBLE with 2.5% APMA	20.46	564±40

Table 2.2 Zeta potential and dissociation constant K_d of encapsulated Rhod-2 in PEBBLEs with different percentages of APMA in the polymer matrix. PEBBLEs were suspended in Milli-Q water for zeta potential measurements. The K_d values were computed from experiments performed in 10 mM MOPS buffer, pH 7.22, containing 0.1 mM EGTA at 37°C.

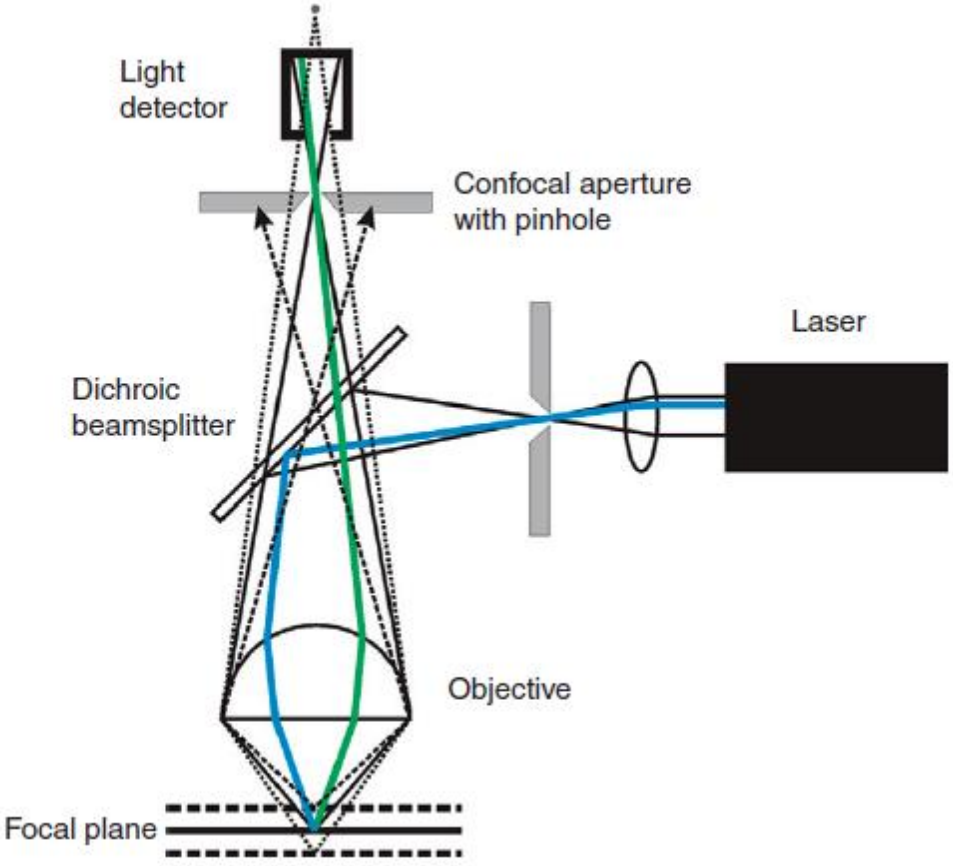

Figure 2.1 Illustration of the optical pathway of a confocal microscope [26].

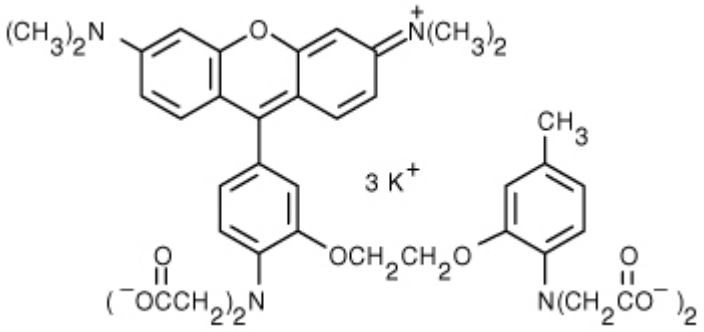

(a)

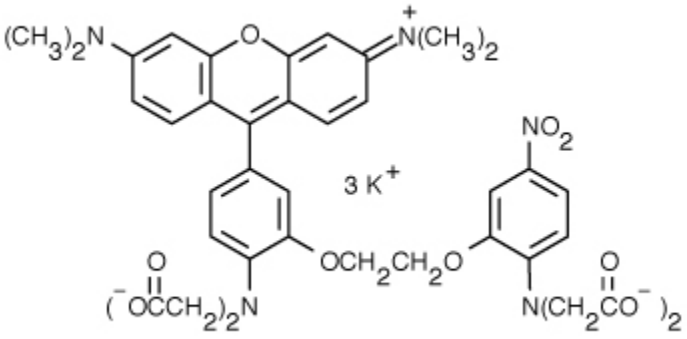

(b)

Figure 2.2 Structures of commercially available rhodamine-based calcium indicators: (a) Rhod-2 and (b) Rhod-5N.

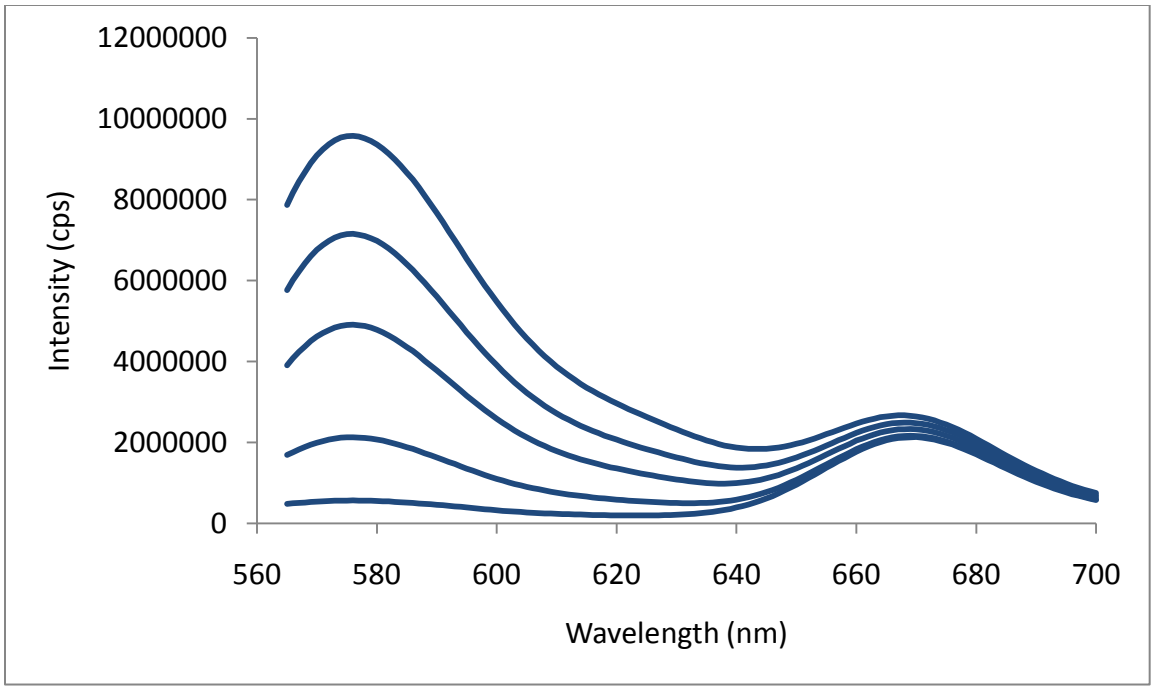

Figure 2.3 Fluorescence emission spectra of Rhod-2/Hilyte PEBBLEs (excitation 550 nm). Samples were buffered at pH 7.22 in 10 mM MOPS and 0.1 mM EGTA. An aliquot of $CaCl_2$ solution was added to the sample, successively. From bottom to top, free Ca^{2+} was at 10, 130, 350, 775 nM and 3.4 µM. An increase in the Rhod-2 peak (575 nm) was observed while the Hilyte peak (668 nm) intensity is independent of the free Ca^{2+} level.

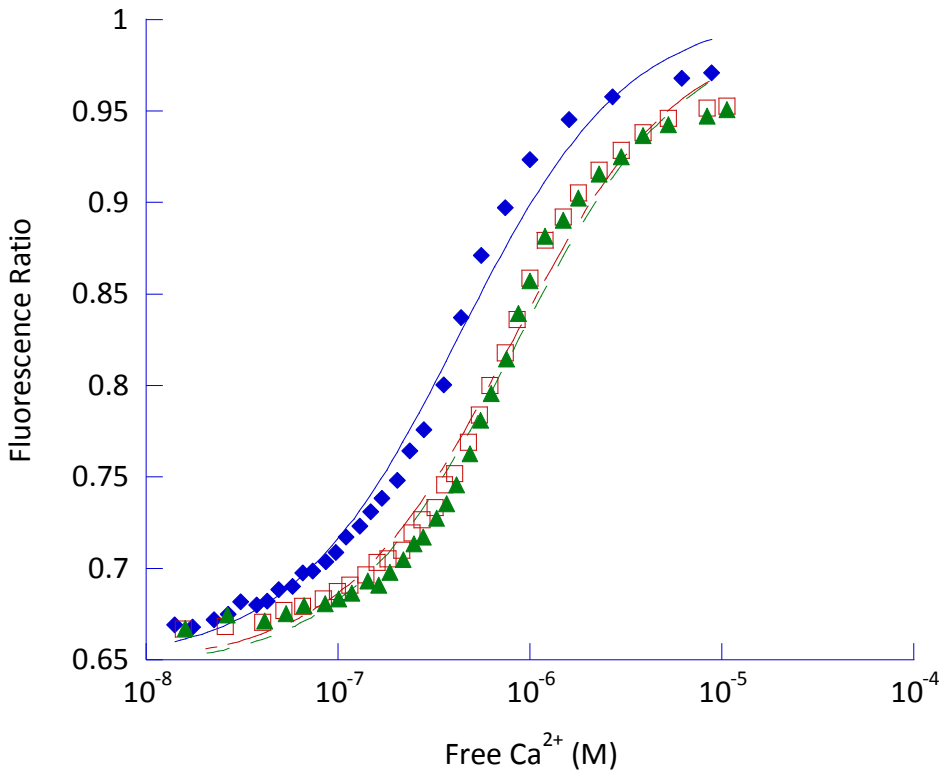

Figure 2.4 Calibration of Rhod-2/Hilyte PEBBLEs in the presence of different background ions concentrations: zero background ions (blue diamonds), 20 mM Mg^{2+} (red squares), 20 mM Mg^{2+}, 20 mM Na^{+} and 120 mM K^{+} mimicking intracellular environment (green triangles). The samples were excited at 550 nm on the fluorometer and the emission spectra were collected. The peak ratio (F_{Rhod-2}/F_{Hilyte}) is plotted against free Ca^{2+} concentration. Without background ions, the K_d is determined to be 429±38 nM. In the presence of 20 mM Mg^{2+}, the K_d rises to 786±65 nM, indicating a decreasing affinity of Rhod-2 for Ca^{2+}. In the presence of 20 mM Mg^{2+}, 20 mM Na^{+} and 120 mM K^{+}, the K_d is determined to be 830±87 nM.

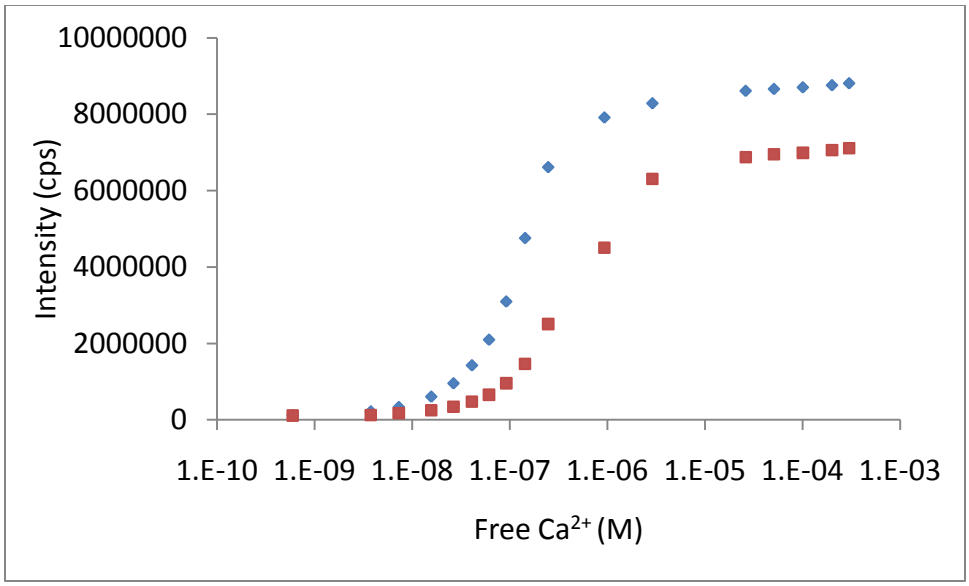

(a)

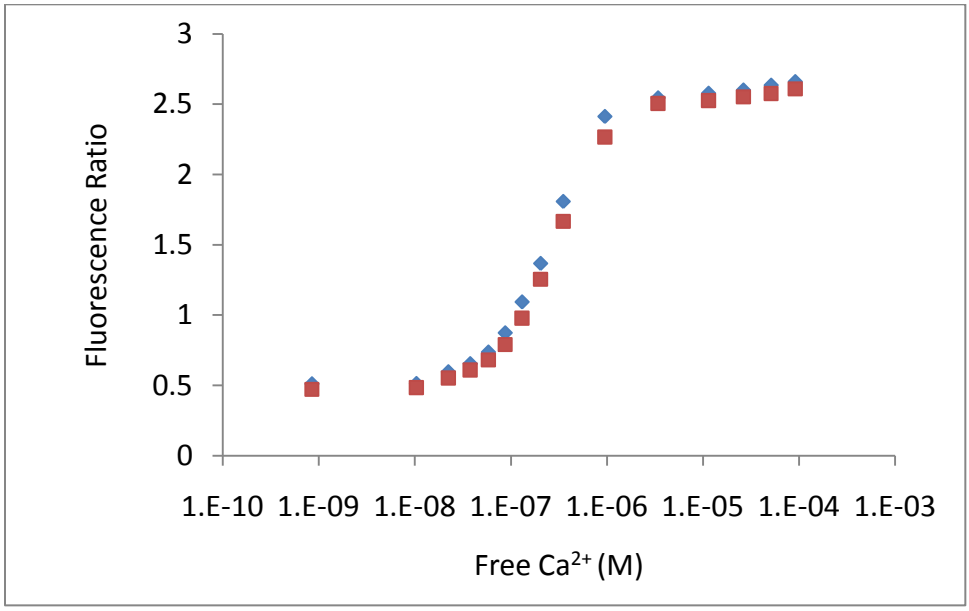

(b)

Figure 2.5 Interference of 1% w/v BSA on Rhod-2 dye (a) and Rhod-2/Hilyte PEBBLE (b). In the absence (blue diamonds) and presence (red squares) of BSA, calibration curves were constructed. The K_d value of the free dye is affected by BSA, while the encapsulated dye is protected by the polyacrylamide matrix.

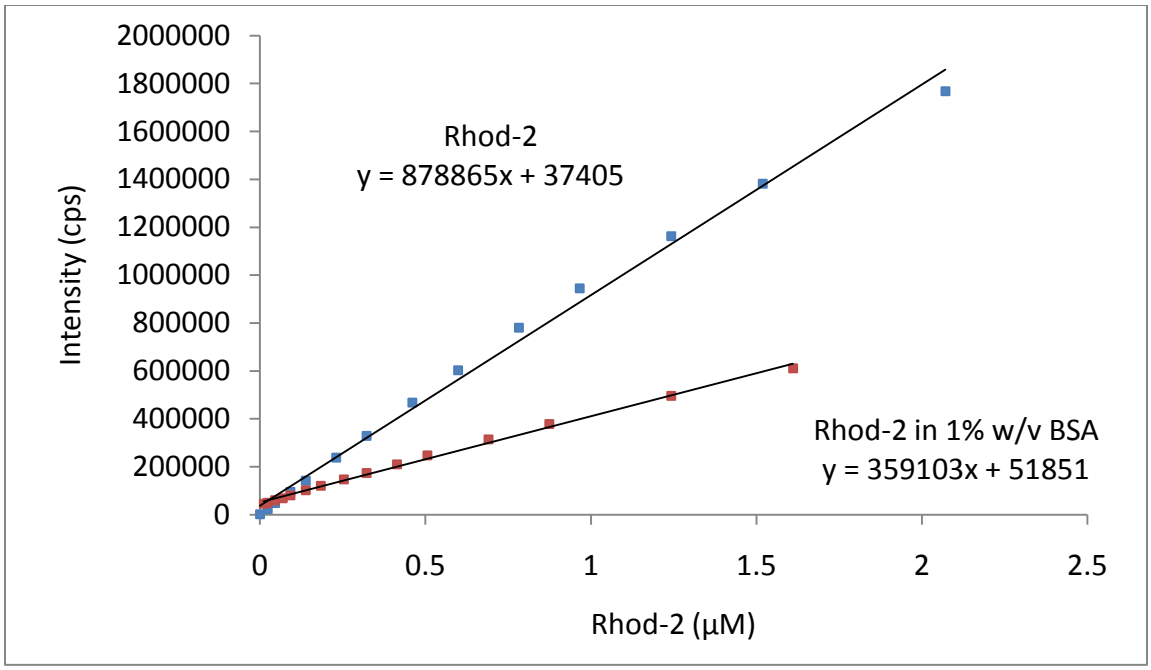

Figure 2.6 Plot of Rhod-2 fluorescence versus dye concentration. A linear fit to the data was constructed. Based on this graph, the amount of dye loading in PEBBLEs was calculated. In addition, the fluorescence increases observed in the dye leaching test with PEBBLEs in 1% w/v BSA were quantified.

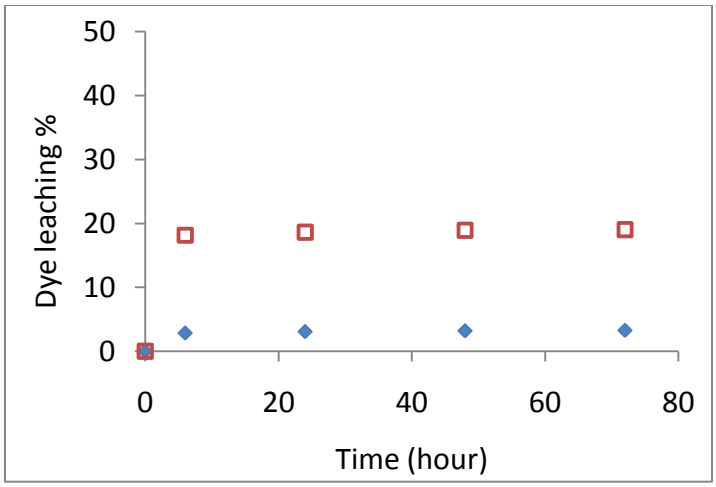

Figure 2.7 Leaching test of the Rhod-2 PEBBLE. PEBBLEs with 0.5 mg Rhod-2 dye loading (blue diamonds) and 1mg Rhod-2 dye loading (red squares) were tested. A total dye leaching of 3% and 18% for these two PEBBLEs was observed. Leaching mainly occurred during the first 6 hours.

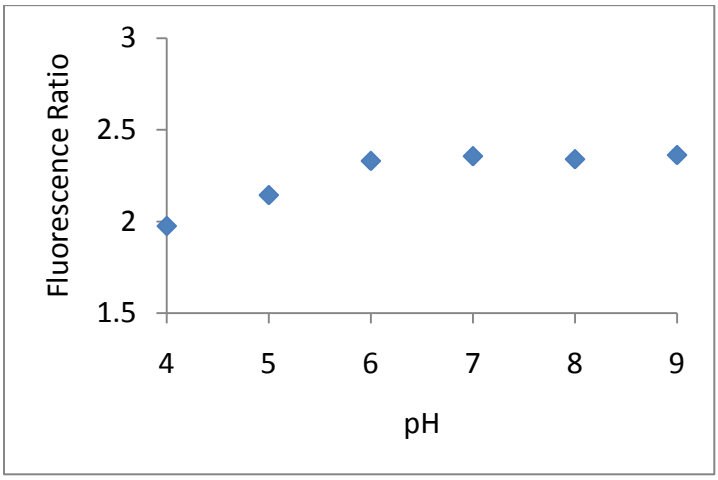

Figure 2.8 Peak ratio of Rhod-2/Hylite PEBBLE versus pH. Calcium concentration was kept at 1 µM without adding EGTA. The fluorescence ratio was affected by low pH, due to the interference of H^+.

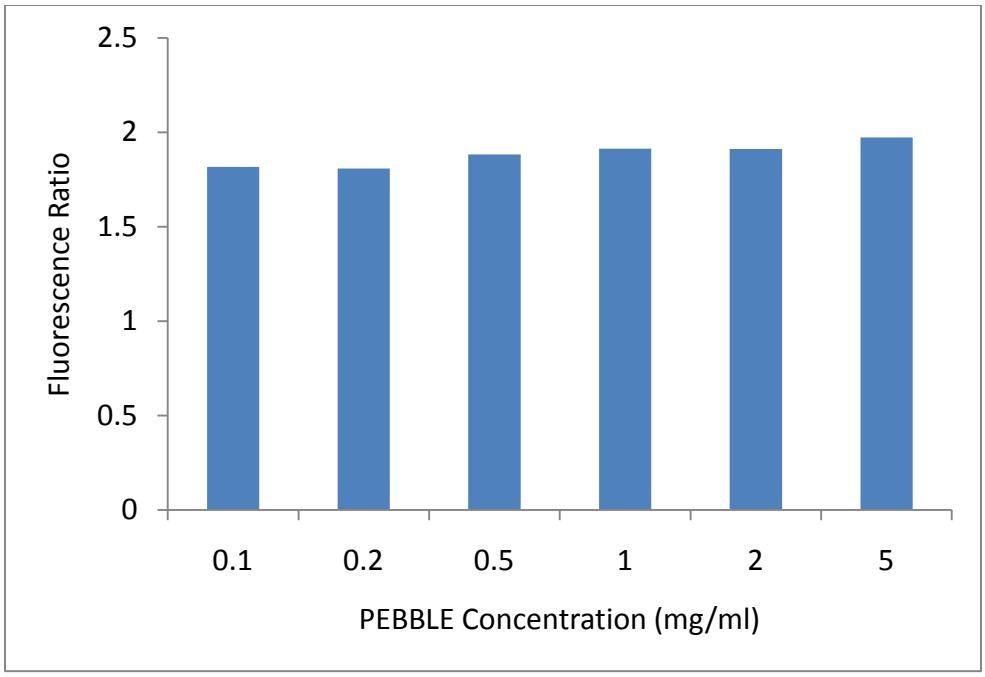

Figure 2.9 Peak ratio versus Rhod-2/Hilyte PEBBLE concentration. Peak ratio does not change as the PEBBLE concentration increases from 0.1 to 5 mg/ml. All samples were buffered at pH 7.22 with 10 mM MOPS and 0.1 mM EGTA. Free calcium level was controlled at below 1 nM.

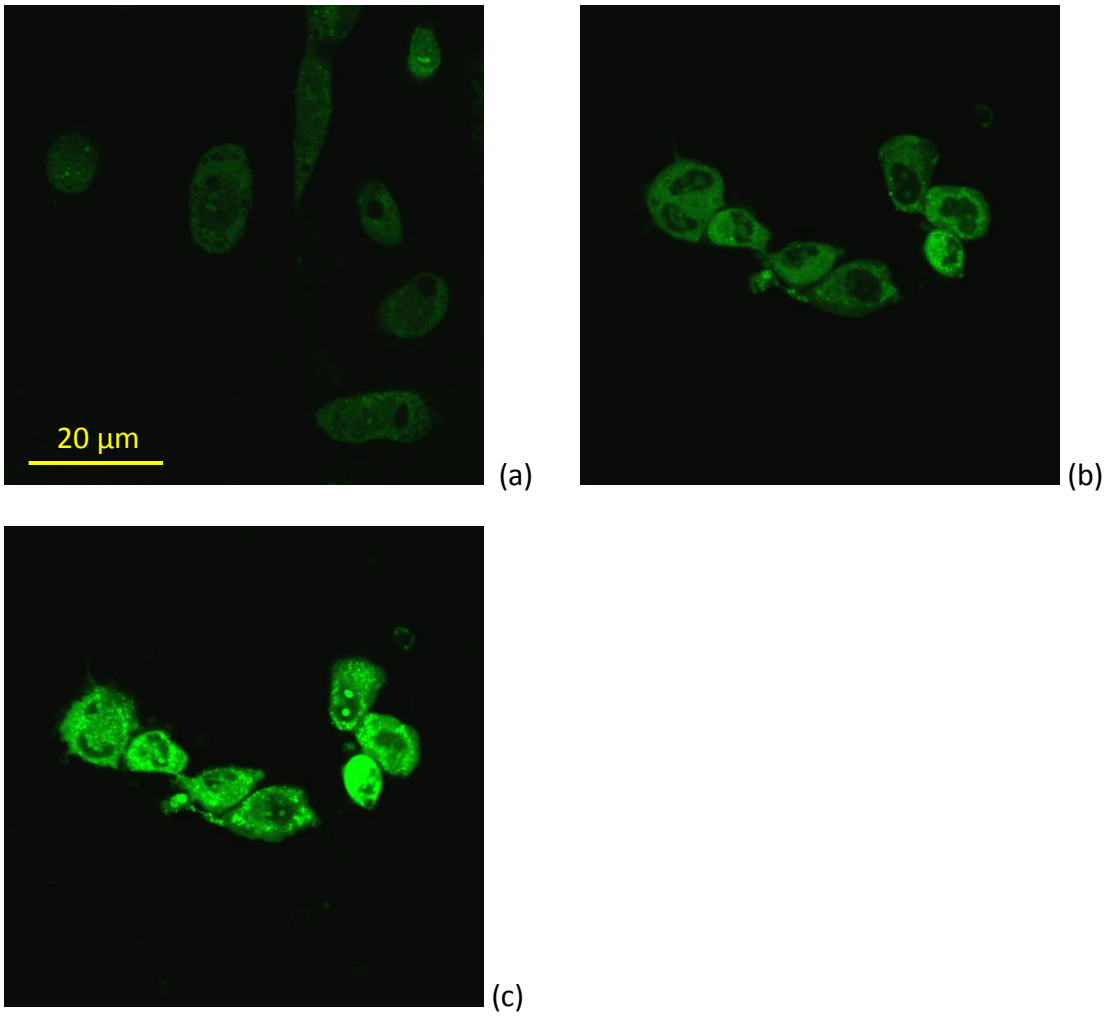

Figure 2.10 Fluorescence confocal images of PC-3 cells loaded with Rhod-2 AM. Free extracellular Ca^{2+} levels were controlled at (a) < 1 nM, (b) 1 µM, and (c) 5 mM. Here calcium ionophore A23187 (5 µM) was added into the medium transporting the Ca^{2+} through the cell membrane. The sample was excited at 540 nm using a white light laser, and the emission of Rhod-2 (560-600 nm) was collected by a PMT and is shown in false color (green). A scale bar is shown in the images.

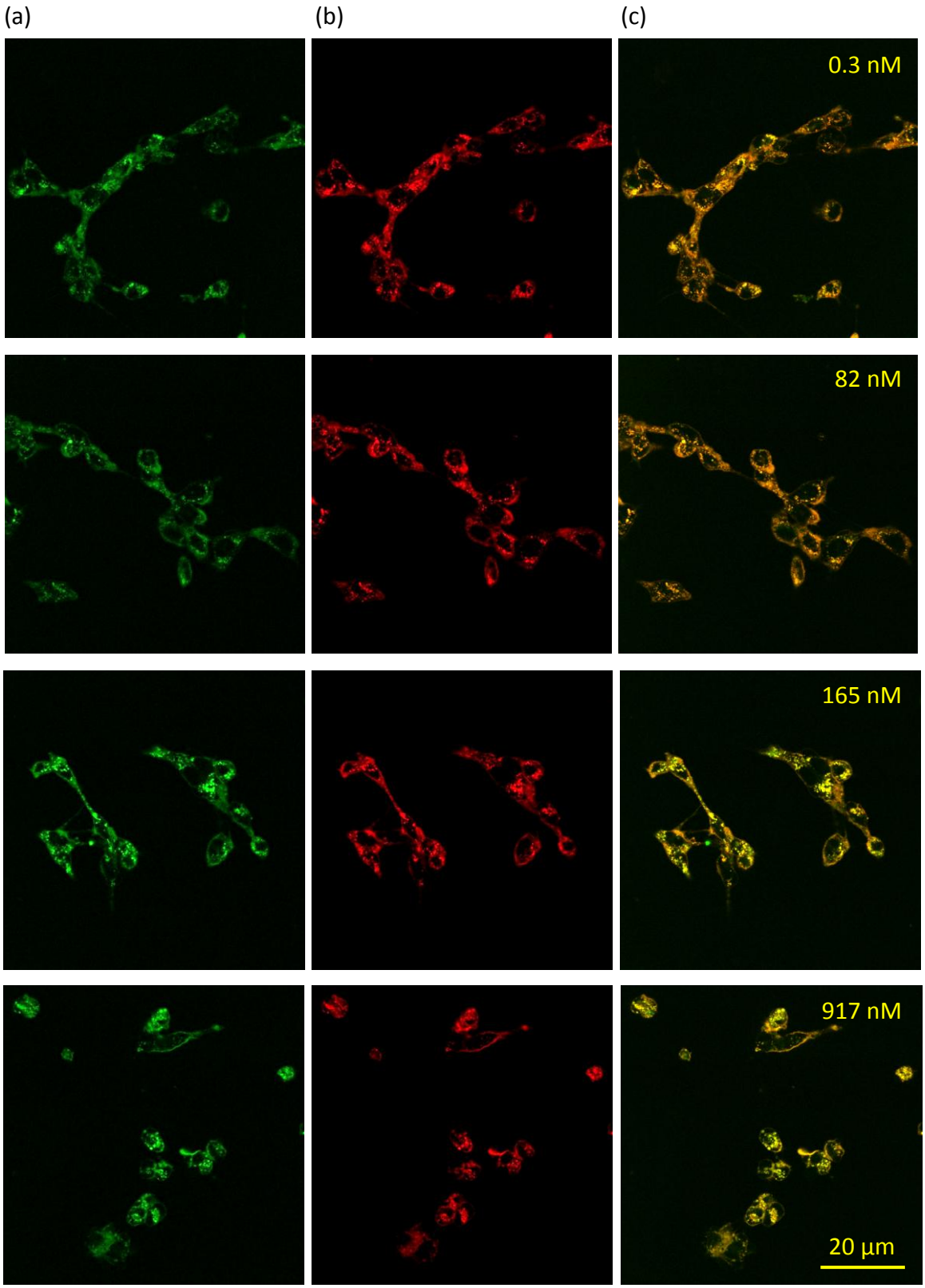
(a)
(b)
(c)
0.3 nM
82 nM
165 nM
917 nM
20 µm

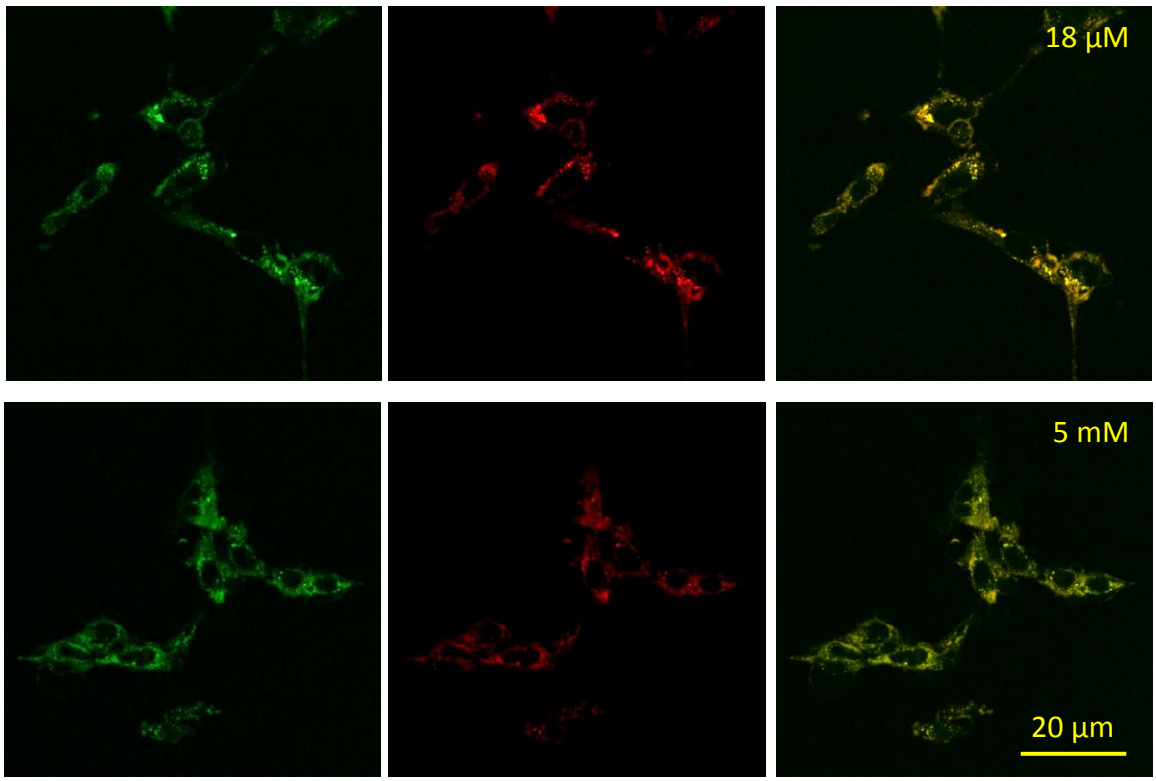

Figure 2.11 Fluorescence confocal images of 9L cells loaded with Rhod-2/Hilyte PEBBLEs. PEBBLEs were delivered by nonspecific endocytosis. Free extracellular Ca^{2+} levels were controlled at 0.3 nM, 82 nM, 165 nM, 917 nM, 18 µM and 5 mM as shown in images. Calcium ionophore A23187 (5 µM) was added into the medium transporting the Ca^{2+} through the cell membrane. The samples were excited at 540 nm by a white light laser, and the emissions of Rhod-2 (560-600 nm) and Hilyte (660-700 nm) were collected by PMTs. Images are shown in false colors as (a) Rhod-2 in green, (b) Hilyte in red and (c) overlaid images of Rhod-2 and Hilyte. A scale bar is shown in the images. The ratio of green (Rhod-2)/red (Hilyte) increases as the free Ca^{2+} level increase.

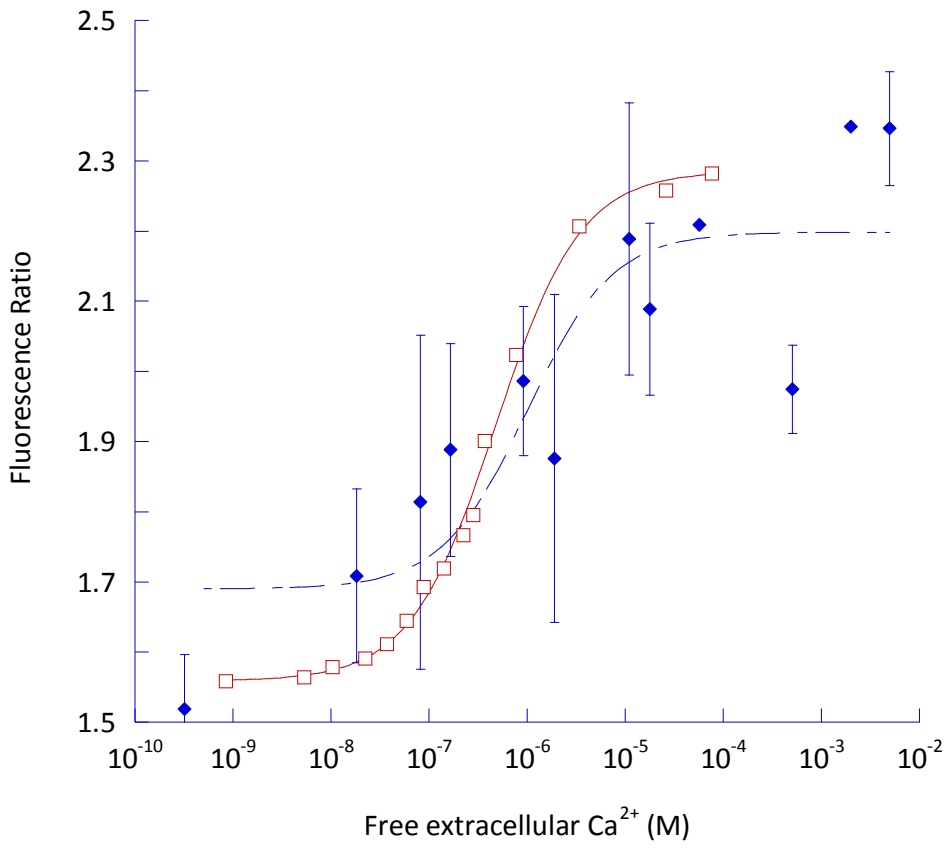

Figure 2.12 An in-cell calibration (blue diamonds) of Rhod-2/Hilyte PEBBLEs conducted on Leica confocal microscope. Intensity ratio of Rhod-2/Hilyte was plotted against free extracellular Ca^{2+} concentration. All data were processed by ImageJ based on fluorescence confocal images of 9L cells loaded with PEBBLEs. The ionophore A23187 transport Ca^{2+} in and out of the cells, therefore the intracellular Ca^{2+} level changes with extracellular Ca^{2+} level. The K_d was determined to be 1003±975 nM. An in-solution calibration of PEBBLEs (red squares) was also performed on Leica confocal microscope in the same cell media (Ca^{2+}, Mg^{2+}-free HEPES buffered Hanks Balanced Salt Solution containing 10 mM EGTA, pH 7.4) without adding A23187. The K_d was determined to be 478±32 nM.

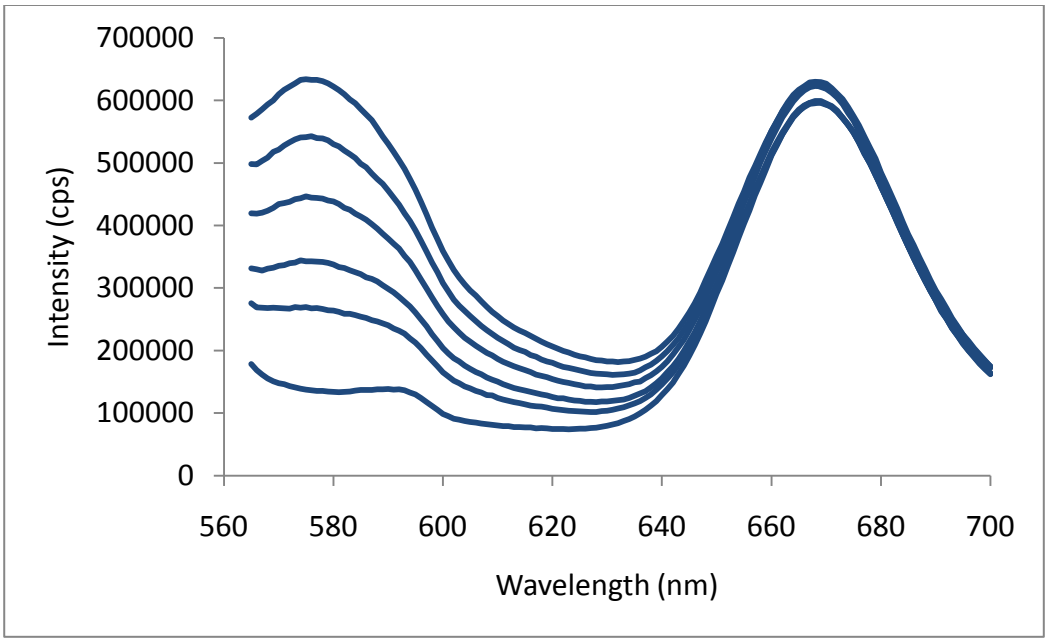
700000
600000
500000
400000
300000
200000
100000
0
Intensity (cps)
560
580
600
620
640
660
680
700
Wavelength (nm)

(a)

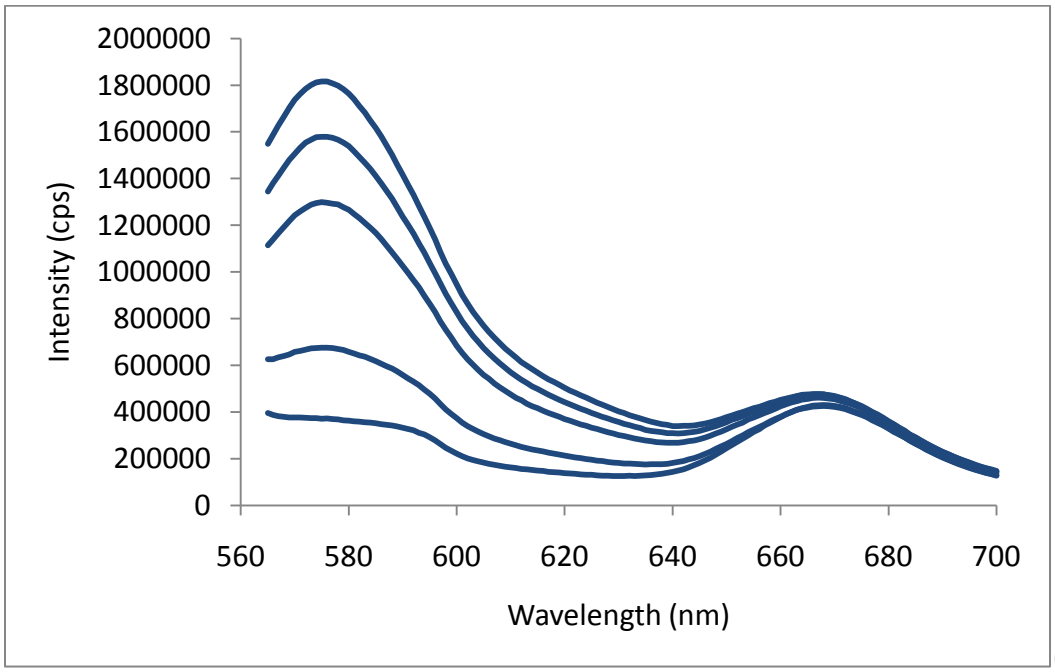
2000000
1800000
1600000
1400000
1200000
1000000
800000
600000
400000
200000
0
Intensity (cps)
560
580
600
620
640
660
680
700
Wavelength (nm)

(b)

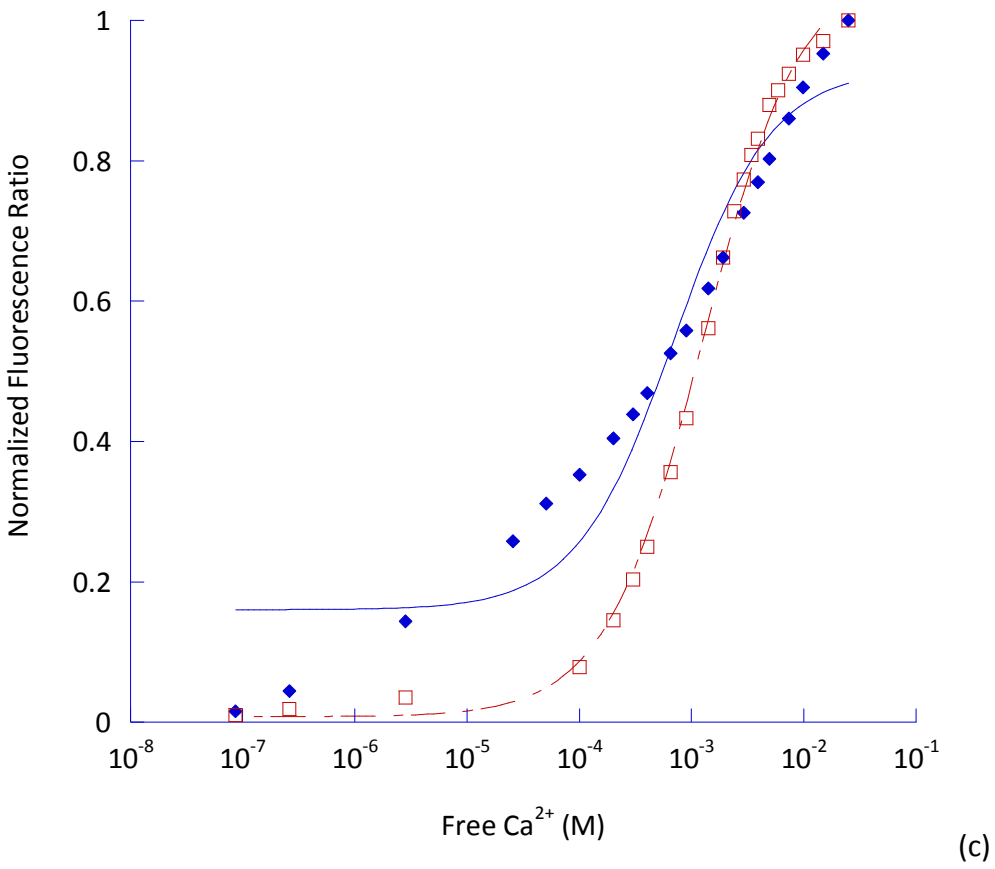

Figure 2.13 Fluorescence emission spectra of the Rhod-dextran/Hilyte PEBBLEs (a) and Rhod-5N/Hilyte PEBBLEs (b) with excitation at 550 nm. From bottom to top, the free Ca^{2+} levels are: (a) 37 nM, 26 µM, 0.3, 1.4, 4.9 and 24.9 mM; (b) 0.26 µM, 0.4, 1.9, 3.9, 24.9 mM. The emissions of Rhod-dextran and Rhod-5N (both at 575 nm) increase with the increase of free Ca^{2+} concentration, while the emission of Hilyte (668 nm) is independent of the free Ca^{2+} level. (c) Calibration of Rhod-dextran/Hilyte PEBBLE (blue diamonds) and Rhod-5N/Hilyte PEBBLE (red squares) shown in a normalized y-axis. The K_d of encapsulated Rhod-dextran binding to Ca^{2+} was determined to be 698±179 µM and the K_d of encapsulated Rhod-5N was determined to be 1.25±0.06 mM.

Rhod-dextran/Hilyte PEBBLEs

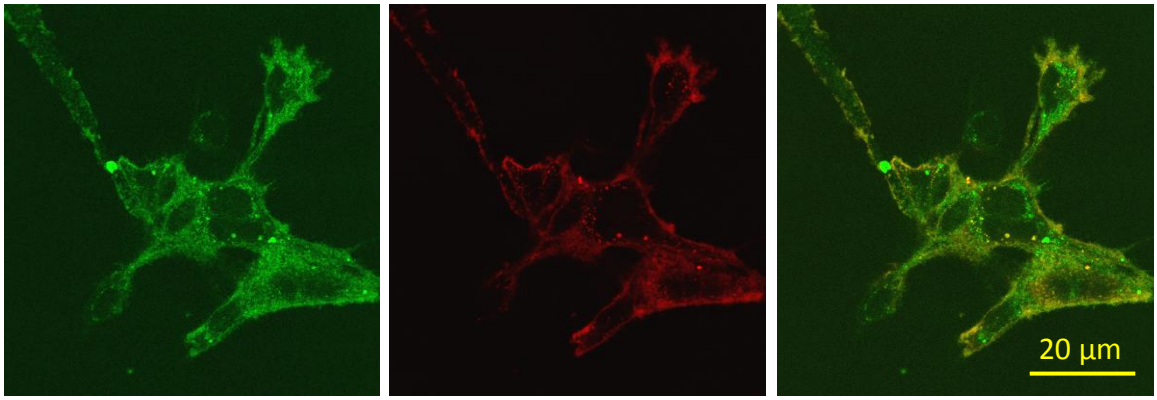

(a) (b) (c)

Rhod-5N/Hilyte PEBBLEs

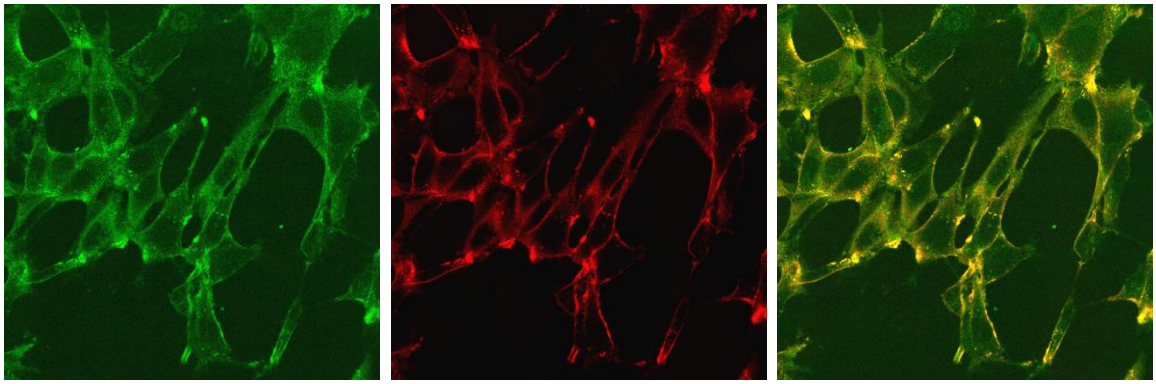

(a) (b) (c)

Figure 2.14 Fluorescence confocal images of 9L cells loaded with Rhod-dextran/Hilyte PEBBLEs and Rhod-5N/Hilyte PEBBLEs. PEBBLEs were delivered by surface-conjugated TAT peptide. The samples were excited at 540 nm, and the emissions of Rhod-dextran or Rhod-5N (560-600 nm) and Hilyte (660-700 nm) were collected by PMTs. Images are shown in false colors as (a) Rhod-dextran or Rhod-5N in green, (b) Hilyte in red and (c) overlaid images. A scale bar is shown in the images.

References

[1] D. E. Clapham, "Calcium signaling", *Cell*, (80)2: 259-268, 1995

[2] L.Fedrizzi, D. Lim, and E. Carafoli, "Calcium and signal transduction", *Biochemistry and Molecular Biology Education*, (36)3: 175-180, 2008

[3] Scharff, and B. Foder, "Regulation of cytosolic calcium in blood cells", *Physiological Reviews*, (73)3: 547-582, 1993

[4] Takahashi, P. Camacho, J. D. Lechleiter, and B. Herman, "Measurement of Intracellular Calcium", *Physiological Reviews*, (79)4: 1089-1125, 1999

[5] Brownlee, "Cellular calcium imaging: so, what's new?", *Trends in Cell Biology*, (10)10: 451-457, 2000

[6] R. Y. Tsien, "New calcium indicators and buffers with high selectivity against magnesium and protons: design, synthesis, and properties of prototype structures", *Biochemistry*, (19)11: 2396-2404, 1980

[7] R. Y. Tsien, "A non-disruptive technique for loading calcium buffers and indicators into cells", *Nature*, (290)9: 527-528, 1981

[8] G. Grynkiewicz, M. Poenie, and R. Y. Tsien, "A new generation of Ca^{2+} indicators with greatly improved fluorescence properties", *Journal of Biological Chemistry*, (260)6 : 3440-3450, 1985

[9] Minta, J. P. Y. Kao, and R. Y. Tsien, "Fluorescent indicators for cytosolic calcium based on rhodamine and fluorescein chromophores", *Journal of Biological Chemistry*, (264)14: 8171 -8178, 1989

[10] Stamm, I. Friehs, Y. H. Choi, D. Zurakowski, F. X. McGowan, and P. J. del Nido, "Cytosolic calcium in the ischemic rabbit heart: assessment by pH- and temperature-adjusted rhod-2 spectrofluorometry", *Cardiovascular Research*, (59)3: 695-704, 2003

[11] C. Du, G. A. MacGowan, D. L. Farkas, and A. P. Koretsky, "Calibration of the calcium dissociation constant of $Rhod_2$ in the perfused mouse heart using manganese quenching", *Cell Calcium*, (29)4: 217-227, 2001

[12] N. Melamed, P. J. Helm, and R. Rahamimoff, "Confocal microscopy reveals coordinated calcium fluctuations and oscillations in synaptic boutons", *The Journal of Neuroscience*, (13)2 : 632-649, 1993

[13] D. R. Trollinger, W. E. Cascio, and J. J. Lemasters, "Selective Loading of Rhod 2 into Mitochondria Shows Mitochondrial Ca^{2+}Transients during the Contractile

Cycle in Adult Rabbit Cardiac Myocytes", *Biochemical and Biophysical Research Communications*, (236)3: 738-742, 1997

[14] D. N. Bowser, T. Minamikawa, P. Nagley, and D. A. Williams, "Role of Mitochondria in Calcium Regulation of Spontaneously Contracting Cardiac Muscle Cells", *Biophysical Journal*, (75)4: 2004-2014, 1998

[15] G. R. Monteith, and M. P. Blaustein, "Heterogeneity of mitochondrial matrix free Ca^{2+}: resolution of Ca^{2+} dynamics in individual mitochondria in situ", *American Journal of Physiology - Cell Physiology*, (276)5: C1193-C1204, 1999

[16] M. P. Muriel, N. Lambeng, F. Darios, P. P. Michel, E. C. Hirsch, Y. Agid, and M. Ruberg, "Mitochondrial free calcium levels (Rhod-2 fluorescence) and ultrastructural alterations in neuronally differentiated PC12 cells during ceramide-dependent cell death", *The Journal of Comparative Neurology*, (426)2: 297-315, 2000

[17] J. Lakowicz, H. Szmacinski, K. Nowaczyk, and M. Johnson, "Fluorescence lifetime imaging of calcium using Quin-2", *Cell Calcium*, (13)3: 131-147, 1992

[18] H. Szmacinski, I. Gryczynski, and J. Lakowicz "Calcium-dependent fluorescence lifetimes of Indo-1 for one- and two-photon excitation of fluorescence", *Photochemistry and Photobiology*, (58)3: 341-345, 1993

[19] J. Lakowicz, H. Szmacinski, K. Nowaczyk, W. Lederer, M. Kirby, and M. Johnson, "Fluorescence lifetime imaging of intracellular calcium in COS cells using Quin-2", *Cell Calcium*, (15)1: 7-27, 1994

[20] S. A. Stricker, V. E. Centonze, S. W. Paddock, and G. Schatten, "Confocal microscopy of fertilization-induced calcium dynamics in sea urchin eggs", *Developmental Biology*, (149)2: 370-380, 1992

[21] L. Blatter, and W. Wier, "Intracellular diffusion, binding, and compartmentalization of the fluorescent calcium indicators indo-1 and fura-2", *Biophysical Journal*, (58)6: 1491-1499, 1990

[22] F. A. Lattanzio, and D. K. Bartschat, "The effect of pH on rate constants, ion selectivity and thermodynamic properties of fluorescent calcium and magnesium indicators", *Biochemical and Biophysical Research Communications*, (177)1: 184-191, 1991

[23] P. Arslan, F. D. Virgilio, M. Beltrame, R. Y. Tsien, and T. Pozzan, "Cytosolic Ca^{2+} homeostasis in Ehrlich and Yoshida carcinomas. A new, membrane-permeant chelator of heavy metals reveals that these ascites tumor cell lines have normal cytosolic free Ca^{2+}", *Journal of Biological Chemistry*, (260)5: 2719-2727, 1985

[24] H. A. Clark, R. Kopelman, R. Tjalkens, and M. A. Philbert, "Optical Nanosensors for Chemical Analysis inside Single Living Cells. 2. Sensors for pH and Calcium and the Intracellular Application of PEBBLE Sensors", *Analytical Chemistry*, (71)21: 4837-4843, 1999

[25] A. Webster, S. J. Compton, and J. W. Aylott, "Optical calcium sensors: development of a generic method for their introduction to the cell using conjugated cell penetrating peptides", *Analyst*, (130)2: 163-170, 2005

[26] G. Smith, M. Reynolds, F. Burton, and O. J. Kemi, "Confocal and multiphoton imaging of intracellular Ca^{2+}", *Methods in Cell Biology*, (99) 225-261, 2010

[27] R. Tsien, and T. Pozzan, "Measurement of cytosolic free Ca^{2+} with quin2", *Methods in Enzymology*, (172) 230-262, 1989

[28] T. Iversen, T. Skotland, and K. Sandvig, "Endocytosis and intracellular transport of nanoparticles: Present knowledge and need for future studies", *Nano Today*, (6)2: 176-185, 2011

[29] C. C. Berry, "Intracellular delivery of nanoparticles via the HIV-1 tat peptide", *Nanomedicine*, (3)3: 357-365, 2008

[30] Y. Koo Lee, R. Smith, and R. Kopelman, "Nanoparticle PEBBLE Sensors in Live Cells and In Vivo", *Annual Review of Analytical Chemistry*, (2)1: 57-76, 2009

[31] Y. Koo Lee, and R. Kopelman, "Optical Nanoparticle Sensors for Quantitative Intracellular Imaging", *Wiley Interdisciplinary Reviews: Nanomedicine and Nanobiotechnology*, (1)1: 98-110, 2009

[32] P. Lundberg, and U. Langel, "A brief introduction to cell-penetrating peptides", *Journal of Molecular Recognition*, (16)5: 227-233, 2003

[33] R. P. Haugland, "The Handbook: A Guide to Fluorescent Probes and Labeling Technologies", 10^{th} Edition, *Molecular Probes, Inc.*, 2005

[34] V. A. Snitsarev, T. J. McNulty, and C. W. Taylor, "Endogenous heavy metal ions perturb fura-2 measurements of basal and hormone-evoked Ca^{2+} signals", *Biophysics Journal*, (71)2: 1048-1056, 1996

[35] H. Hasse, S. Hebel, G. Engelhardt, and L. Rink, "Zinc ions cause the thimerosal-induced signal of fluorescent calcium probes in lymphocytes", *Cell Calcium*, (45)2: 185-191, 2009

[36] G. Szanda, A. Rajki, S. Gallego-Sandín, J. Garcia-Sancho, and A. Spät, "Effect of cytosolic Mg^{2+} on mitochondrial Ca^{2+} signaling", *Pflügers Archiv-European Journal of Physiology*, (457)4: 941-954, 2009

Chapter 3

The Immobilization of Wild Type Bovine Carbonic Anhydrase inside Nanoparticles

Introduction

Protein and enzyme immobilization on nanoparticles has received significant attention due to its potential use in biocatalysis, drug or gene delivery, and biomedical and biosensing devices. Many methods have been developed to incorporate enzymes into nanostructures while maintaining their activity: Surface attachment and conjugation of enzymes have been used on a variety of nanoparticles, such as gold nanoparticles, paramagnetic nanoparticles, carbon nanotubes, silica nanoparticles and polymeric nanoparticles [1-7]. Another route is to entrap enzymes within the nanopores of mesoporous silica gels simply by physical absorption [8-9]. By carefully designing the synthetic process, enzymes can also be encapsulated into silica [7-13] and polymeric particles [17-25].

A few enzymes have been reported attached to or encapsulated in silica nanoparticles and used as biosensors or biocatalysts, such as protease, glucose oxidase, horse radish peroxide (HRP), catalase, lysozyme, phosphatase, etc [7-13]. However, the compatibility of the nanoparticle matrix and the enzymes depends on the

physicochemical properties of the matrix and the intrinsic properties of the enzymes [15]. For example, studies have revealed that upon binding onto silica matrix, human carbonic anhydrase II (CA) and its variants undergo successive conformational rearrangements in a stepwise manner. The active site of the enzymes unfolds and the enzymes lose their tertiary structure and consequently their activities [14-16]. Therefore, specifically for CA, silica might not be a suitable matrix.

Polyacrylamide (PAA) was chosen as a carrier for CA encapsulation because of its hydrophilicity and its biocompatibility for many proteins and enzymes which has been established by extensive previous studies [17-19]. It has been reported that biosensors based on PAA nanoparticles or nanogels encapsulating glucose oxidase [25], phosphate sensing protein [20], lipoamide dehydrogenase and glutathione reductase [21] have been developed. These nanoparticles and hydrogels are very promising tools for intracellular applications such as intracellular sensing or drug and gene delivery [22-24]. Encapsulating the fluorescent sensing probes in PEBBLEs for intracellular measurements has several advantages over directly loading the probes into cells. The inert polymer matrix protects the cellular environment from any potential toxicity of the probes and also protects the probes, in this case CA, from protease attack, interfacial shearing and solvent denaturation [17, 25-27]. The nanometer sized sensors have minimal physical perturbations to the cells and fast response time [26-27]. To this end, encapsulating a fluorescent enzyme probe in PAA PEBBLEs is of great interest to us.

PAA nanoparticles are synthesized in w/o microemulsions and the use of surfactants to stabilize the microemulsion is indispensable. The traditional PEBBLE preparation method requires an anionic surfactant, AOT and a nonionic surfactant, Brij 30. Our studies showed that the use of AOT resulted in the deactivation of carbonic anhydrase, possibly due to the high surface charge density on the micelles. On the other hand, nonionic surfactants affect the enzyme activity much less than AOT. It has been reported that lipase shows improved activity by using tween surfactant stabilized micelles than AOT micelles due to the reduced surface charge density [29]. Additionally, lipase activity has improved up to ~200% in micelles stabilized by nonionic surfactants like Brij 30, Brij 92, Tween 20 and Tween 80 [28]. Moreover, nonionic surfactants like polyethylene glycol, triton X-100, n-hexanol and glycerol have been used as artificial chaperons for assisting refolding and renaturation of enzymes like CA and rabbit muscle creation kinase [30-32]. Therefore, using nonionic surfactants to stabilize the w/o microemulsion during PEBBLE synthesis is the key to enhance the active CA encapsulation.

In the preparation of a w/o microemulsion, the most important step is to choose appropriate surfactants that will effectively stabilize the water-in-oil micelles. For that purpose, the use of HLB (Hydrophile-Lipophile Balance) system enabled us to predict some behavior of a certain surfactant and reduce the amount of work involved in the selection of surfactants. The concept of “HLB” system was first introduced by W. C. Griffin in 1949; surfactants are molecules consisting of both hydrophilic and lipophilic groups (polar and nonpolar groups). HLB is the balance of the size and strength of these

two opposing groups and the HLB value expresses the relative simultaneous attraction of an emulsifier for water and for oil [33-35]. In this work, the HLB system was used to identify suitable multi-surfactant systems and to calculate the composition of each surfactant used in the system.

In this chapter, bovine, rather than human, carbonic anhydrase was chosen as a substrate to encapsulate in PEBBLEs because of its robust nature and its relatively cheaper price. The CA was encapsulated in both silica and polyacrylamide matrices and the results showed that the polyacrylamide matrix was more suitable. The factors that affect CA activity during PEBBLE synthesis are also discussed. New PEBBLE fabrication and purification methods were developed, and the results show that the encapsulation of active CA by the new methods was improved almost 4 times more than that by the traditional method.

Experimental and Methods

Reagents. Carbonic Anhydrase from bovine erythrocytes, triton X-100 (4-(1,1,3,3-tetramethylbutyl)phenyl-polyethylene glycol), 1-hexanol, cyclohexane, TMOS (tetramethyl orthosilicate), acrylamide, GDMA (glycerol dimethacrylate), AOT (Sodium dioctyl sulfosuccinate), Brij (30polyoxyethylene (4) lauryl ether), Tween 80 (polysorbate 80), Span 80 (sorbitan monooleate), PEG 400 (Polyethylene glycol 400), tergitol^{TM} NP-9 (Nonylphenol Ethoxylates), TEMED (N,N,N',N'-tetraethylmethylenediamine), ammonium persulfate, MOPS (4-morpholinepropanesulfonic acid), p-nitrophennyl acetate, Diamox (actazolamide), Sephadex G-25, aluminum oxide (neutral), bicine (N,N-Bis(2-hydroxyethyl) glycine) were purchased from Sigma-Aldrich (St. Louis, MO, USA). APMA (N-(3-aminopropyl) methacrylamide hydrochloride) was purchased from Polyscience (Warrington, PA, USA). Hexanes and ethanol were purchased from Fisher (Fair Lawn, NJ, USA). Chelex 100 resin was purchased from Bio-Rad (Hercules, CA, USA). Coomassie Plus (Bradford) Assay Reagent was purchased from Thermo Fisher Scientific (Pierce) (Rockford, IL, USA). All buffer solutions were prepared from 18MΩ Milli-Q water purified by a Millipore Advantage A10 system and passed through a Chelex 100 column.

Preparation of silica nanoparticles. The procedure described in the literature [12] was used with minor modifications. Briefly, a mixture of triton X-100 and 1-hexanol in a molar ratio of 1:5 was first prepared; this mixture was then mixed with cyclohexane at a concentration of 10% w/w. In 18.4 ml triton X-100/1-hexanol/cyclohexane mixture, 18 µl 50 mg/ml CA solution and 212 µl 1.05 M ammonia solution were added (for blank

particles without CA, 230 µl ammonia solution was added). 290 µl TMOS was added to the final clear microemulsion and the mixture was stirred at room temperature for 3 hours. After reaction, cyclohexane was removed by rotary evaporation. The viscous mixture of nanoparticles and surfactants was extracted with NH_3/NH_4Cl buffer solution (pH ~ 9), and transferred to an Amicon ultra-filtration cell (Millipore Corp., Bedford, MA) with a 100 kDa filter under 10 psi of pressure. The particles were washed with 500 ml Milli-Q water and dried by vacuum filtration.

Preparation of polyacrylamide nanoparticles. Polyacrylamide (PAA) nanoparticles were prepared in microemulsion stabilized by a variety of surfactant systems. Take the AOT/Brij 30 system for example. The monomer solution was prepared by first dissolving CA in 1.2 ml MOPS buffer (pH=7.2), then 711 mg acrylamide and 55 mg APMA and adding 240 µl GDMA at last. This monomer solution was added to an argon deoxygenated solution that contained 45 ml of hexanes, 1.6 g AOT and 3.08 g Brij 30. The solution was stirred under argon throughout the duration of the preparation. To initiate the polymerization, 20 µl 10% (w/w) ammonium persulfate solution and 20 µl TEMED were added. The solution was stirred at room temperature for two hours so as to assure complete polymerization.

Particle separation. In the traditional method, hexane was removed by rotary evaporation and the viscous particle/surfactant mixture was suspended in 100 ml ethanol then transferred into an Amicon stir cell. The particles were washed with 500 ml ethanol and 500 ml Milli-Q water and then freeze dried to obtain dry powder. However,

as ethanol greatly affects the CA activity, this method does not serve our purpose of preserving the enzyme inside the nanoparticles.

A more biofriendly separation method was performed. First, 50 g Al_2O_3 was immersed in water-saturated hexane for 30 minutes to stabilize. This is because upon mixing Al_2O_3 with water, it generates heat which may affect the enzyme. The w/o microemulsion was mixed with the stabilized Al_2O_3 and the mixture was stirred for 30 minutes as the particles in aqueous phase were absorbed onto Al_2O_3 surface leaving most of the surfactants in hexane phase. The mixture was then vacuum-filtered and Al_2O_3 was washed with hexane for eight times, each time with 50 ml. After the washing step, hexane was completely evaporated by vacuum filtration or by rotary evaporation to yield dry Al_2O_3 with particles absorbed on the surface. Particles were then extracted from Al_2O_3 with water for eight times, each time with 50 ml. The resulting particle suspension was centrifuged at 5000 rpm for 10 minutes, and the precipitate and floating mass were discarded. The clear supernatant was transferred into an Amicon stir cell, and the particles were washed with 800-1000 ml water and freeze dried.

SEM imaging. PEBBLEs were dispersed in water at a concentration of 0.1 mg/ml, and the sample was sonicated for 30 minutes to one hour to prevent aggregation of the particles. A drop of the PEBBLE suspension was placed on a metal grid coated with carbon film and then dried gradually at room temperature. The sample was sputter coated with gold and visualized with a Philips XL30FEG scanning electron microscope.

Particle sizing. PEBBLEs were first suspended in Milli-Q water at a concentration of 2-5 mg/ml and sonicated for 30 minutes to one hour to reduce aggregation. Samples were then filtered through a 2.7 µM glass fiber syringe filter (13 mm diameter, Whatman). The particle size of the PEBBLEs was measured on Delsa™Nano Submicron Particle Sizer and Zeta potential instrument (Beckman Coulter, Inc., Fullerton, CA) by dynamic light scattering.

Enzyme activity assay (*p*NPA assay). The activity of CA in PEBBLEs was quantified by this method. The principle is based on the hydrolysis reaction of p-nitrophenyl acetate (pNPA) catalyzed by CA:

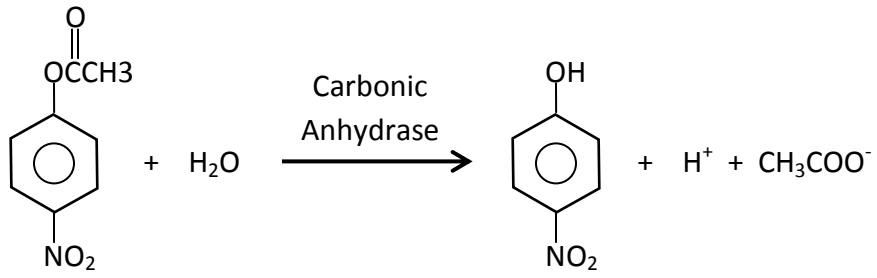

A 10 mM pNPA solution was prepared by dissolving pNPA in acetone/water (40% v/v) mixture, and a 10 mM diamox solution was prepared by dissolving diamox in DMSO/water (10% v/v) mixture. In a 3 ml cuvette, 1.9 ml 10 mM Bicine buffer (pH 8.0), 50 µl pNPA solution and 50 µl CA solution or PEBBLE suspension were mixed quickly and thoroughly. The reaction rate was monitored by recording the sample absorbance at wavelength 400 nm over time. After recording for 100~150 seconds, a background rate was monitored by adding 50 µl diamox solution into the cuvette to inhibit CA's activity then recording the sample absorbance over time for another 100~150 seconds. The

adjusted slope was derived by subtracting the slope of the background rate from that of the reaction rate. As shown in the equation:

$$k_{cat}/K_m = \frac{\text{Adjusted slope}}{\varepsilon_{pNPA} \times C_{pNPA} \times C_{CA}}$$

Where k_{cat}/K_m is the catalytic efficiency of CA for catalyzing this reaction, ε_{pNPA} and C_{pNPA} are the extinction coefficient and concentration of pNPA. Therefore, the adjusted slope is proportional to the concentration of active CA. A calibration curve was constructed by plotting the adjusted slope against CA concentration, and this curve was used for calculating the amount of active CA in PEBBLEs. All experiments were repeated in triplicate and performed on a Shimadzu UV-1601 UV-VIS spectrometer.

Coomassie blue protein assay. The total amount of CA (active and denatured) was measured by this method. The procedure was described in the instruction of the Coomassie Plus Assay Kit provided by the vendor. Briefly, the sample was prepared by mixing 1.5 ml Coomassie Plus Reagent and 50 µl CA solution of PEBBLE suspension. The sample was then incubated at room temperature for 10 minutes to obtain the most consistent results. The absorbance at 595 nm was recorded. A calibration curve was constructed by plotting the absorbance against CA concentration and the total CA in PEBBLEs was quantified based on the calibration curve. All experiments were repeated in triplicate and performed on a Shimadzu UV-1601 UV-VIS spectrometer.

Results and Discussion

The work in this chapter focused on developing PEBBLEs with CA encapsulation and retaining enzymatic activity. Therefore the goal was to best preserve CA during particle fabrication and purification. To achieve that goal, studies were conducted on three aspects: choosing a suitable matrix, a biofriendly surfactant system and a biofriendly particle separation method. Wild type bovine CA was chosen as the substrate in this work for two reasons, its robust nature and its affordable price.

Protein and enzyme encapsulation in silica particles has been studied extensively [7-13]. Conventional sol-gel preparation is not suitable for enzyme encapsulation because it involves low pH (1-2) which leads to protein denaturation. A new method was reported to successfully encapsulate horse radish peroxidase [12] in silica nanoparticles fabricated in w/o microemulsion. Cyclohexane was used as the oil phase, and the microemulsion was stabilized by triton X-100 and 1-hexanol. The reaction was carried out in a basic pH (9-9.5) in which CA remains active as it catalyzes the pNPA hydrolysis [36]. The average size of particles synthesized by this method was determined to be 48 nm, by dynamic light scattering (see Figure 3.2). However, the result of the enzyme activity assay showed that little CA remained active. It also has been reported that human CA II undergoes conformational rearrangement upon binding to silica matrix and changes to a molten-globule-like state. The conformational change of human CA II leads to the loss of activity and the loss of tertiary structure [14-16]. Although silica matrix has

being utilized as a carrier for many proteins and enzymes such as horse radish peroxide, glucose oxidase and lipase [7-13], it appears that it is not a suitable matrix for CA.

The polyacrylamide matrix is considered a better choice, due to its biocompatibility. In the traditional PAA PEBBLE preparation procedure, AOT and brij 30 were used to stabilize the w/o microemulsion, and the particles were washed by 95% ethanol. The CA encapsulated PEBBLEs fabricated by this method show an average size of 50 nm, by SEM imaging, see Figure 3.3. The active CA in the PEBBLEs was quantified by the enzyme activity assay, as shown in Figure 3.4. Comparing with the blank PAA PEBBLEs, the CA encapsulated PEBBLEs did catalyze the hydrolysis of pNPA, thus indicating the presence of active CA. The amount of the active CA in the PEBBLEs was determined to be 0.0031 mg CA per mg PEBBLEs. As 43 mg CA was added into the reaction during PEBBLE preparation and the yield of the PEBBLEs was about 1 g, 7.2% CA was encapsulated in the PEBBLEs and remained active.

The total enzyme in PEBBLEs was quantified by a coomassie blue protein assay, since both active and deactivated CA bind with coomassie blue and increase its absorbance at 595 nm. AOT and brij 30 also increase the absorbance of coomassie blue at 595 nm, therefore blank PEBBLEs prepared at the same condition as CA encapsulated PEBBLEs were tested and used as a background (see Figure 3.5). By subtracting the background, the quantification of the total enzyme in PEBBLEs became more accurate. By this method it was estimated that 40% of CA was encapsulated in the PEBBLEs. In summary, out of 43 mg CA added into the reaction, about 60% was not encapsulated

and therefore separated out from the PEBBLEs during PEBBLE purification and 40% was encapsulated. Of the 40% encapsulated CA, 7.2% remained active while 32.8% became deactivated; or in other words, the overall deactivation of encapsulated CA is 82%.

A 7.2% CA survival rate is low. Therefore, experiments were performed to uncover the factors that caused the CA deactivation. The following solutions were prepared: 0.08 M AOT, 0.19 M Brij 30, Initiator (mixture of 0.1% w/w Ammonium persulfate and 1% v/v). The concentrations of AOT, Brij 30 and initiator were the same as the concentrations used in PEBBLE preparation. The 95% ethanol was also tested since it was used to wash the PEBBLEs. An aliquot of CA solution was mixed with the surfactants and initiator solution. For control an aliquot of CA solution was mixed with 10 mM MOPS pH 7.22. The enzyme activity in each mixture was measured immediately after the mixtures were prepared and after 2 hours of incubation at room temperature. As shown in Figure 3.6, almost no CA showed activity upon mixing with the anionic surfactant AOT and only 20% CA remained active after incubation in 95% ethanol for 2 hours at room temperature. Meanwhile, 70% and 80% of CA remained active after incubating with brij 30 and initiator solution, indicating that most of the CA was not affected by the nonionic surfactant brij 30 or by the free radicals generated by the initiator. Additionally it has been reported that nonionic surfactants such as triton X-100, polyethylene glycol and n-hexanol have been used for assisting the renaturation of CA and other enzymes [30-32]; enzyme activity was enhanced in micelles stabilized by nonionic surfactants such as brij 30 and tween 80 [28]. Therefore, the nonionic surfactants would be more useful in PEBBLE preparation, in order to preserve CA activity.

The structures and HLB (Hydrophile-Lipophile Balance) value of the nonionic surfactants used in this chapter are shown in Figure 3.1. Table 3.1 lists all the recipes used to prepare blank and CA encapsulated PEBBLEs. The amount of initiator was increased to 100 µl 10% (w/w) ammonium persulfate and 100 µl TEMED since the surfactants may lead to chain transfer reactions which would stop the polymerization and limit the particle size or yield [37]. The amount of monomer, water and hexane remained unchanged from the traditional recipe. The HLB value of each surfactant system was calculated by the equation:

$$HLB_{system} = \Sigma\ (Mol\ \% \times HLB_{surfactant})$$

According to the literature [34], and based on our experience, the w/o microemulsion is most stable when its HLB value is between 8 to 10. An illustration of the water droplets stabilized by a multi-nonionic surfactant system is shown in Figure 3.7. The particle size in Table 3.1 was determined by dynamic light scattering (DSL). It was discovered that the size of CA encapsulated PEBBLEs measured by DSL is always bigger than that of the blank PEBBLEs synthesized in the same surfactant systems. And in most of the recipes, more surfactants were needed to be added for preparing the CA encapsulated PEBBLEs. This is possibly because the presence of CA in the water droplets increases the density of the aqueous phase, therefore it requires more surfactants to provide enough surface tension so that the micelles would be stable. As shown in Table 3.1, recipe #5 and #6 produced much bigger particles and the CA encapsulated particles were likely to form aggregates and were not suspended in water very well. The size of

the PEBBLEs prepared by recipe #1 and #2 was favorable; the SEM images are shown in Figure 3.8. The CA encapsulated PEBBLEs produced by recipe #2 (span 80/tween 80/brij 30 system) were used in further experiments for zinc sensing in Chapter 4.

The particle separation method is also essential for preserving CA activity in PEBBLEs. The traditional method involves washing the particles with large amounts of ethanol, which causes the deactivation of CA. Therefore, a new but more complicated separation method was developed, as described in the experimental section. In the new method, particles were maintained in the aqueous phase throughout the entire separation process so that the CA activity would be best preserved.

Figure 3.9 shows the amount of active CA encapsulated in PEBBLEs prepared by the traditional A/B (AOT/Brij 30) system or S/T/B (span 80/tween 80/brij 30) system, separated by Al_2O_3 absorptive filtration or by ethanol washing. By combining the biofriendly surfactant system and the biofriendly separation process, the amount of active CA encapsulated in PEBBLEs was increased almost 4 times compared to the traditional PEBBLE preparation procedure. In other words, as 40% of the total CA was encapsulated, 28% CA remained active and 12% was deactivated; or the overall deactivation of encapsulated CA is 30%. On the other hand, just adding more enzymes during the PEBBLE preparation does not necessarily result in a higher active CA loading. As a matter of fact, a higher enzyme concentration in the PEBBLE synthesis usually yields a lower enzyme loading efficiency, therefore 43 mg CA was enough.

There are two ways to interpret the 28% active and 12% deactivated CA encapsulation in PEBBLEs. One may consider that each enzyme molecule is either 100% active or completely deactivated. Under this assumption, it is estimated that there are 7 active and 3 deactivated CA molecules in every 100 PEBBLEs. Another expression, which might be more accurate, is that all the CA molecules encapsulated inside the PEBBLEs maintain at only 70% of their activity and an overall deactivation is 30%.

The 28% active CA loading is an observed value. We speculate that the true active CA loading is higher than 28% because of the following reasons. 1) The diffusion rates of the substrate, *p*-nitrophenyl acetate is possibly slower in PEBBLEs than in solution. 2) The active site in some CA molecules is possibly blocked by the PEBBLE matrix; therefore it is more difficult for the substrate to reach the active site in the enzymes. 3) Due to the catalysis of the enzyme and the slower diffusion rates of the products, the local concentrations of reaction products (*p*-nitrophenol, H^+ and CH_3COO^-) inside the PEBBLEs may be higher than their concentrations in solution. This leads to a lower local pH in PEBBLEs, at which the absorbance of *p*-nitrophenol is also lower. All these factors may result in an under-estimation of the active CA loading percentage.

Conclusions

This chapter details the development of CA encapsulated PEBBLEs. Since CA has a delicate structure, as do almost all proteins and enzymes, it is not an easy task to encapsulate CA in PEBBLEs while maintaining its activity. The polyacrylamide matrix was chosen because of its well-known biocompatibility, as denoted by previous studies [25-27]. Meanwhile, although many literature articles indicate that proteins and enzymes can be successfully encapsulated in silica particles, apparently it is not a suitable matrix for CA.

Surfactants also play a key role in preserving the enzyme. We have discovered that a wide variety of nonionic surfactants can be used to stabilize the w/o microemulsion and produce nanoparticles. The HLB criterion is a very useful tool for choosing a suitable nonionic surfactant system and calculating its composition. It has been shown that the encapsulation of active CA was enhanced by using a biofriendly nonionic surfactant system, presumably due to the reduced surface charge on the micelles [28], compared with the anionic surfactant AOT.

The biofriendly particle separation method also greatly contributed to the preservation of CA. By combining all these methods, the encapsulation of active CA was increased almost 4 times compared to the traditional PEBBLE preparation process. As demonstrated by the *p*NPA assay, the CA encapsulated PEBBLEs might be a promising tool for biocatalysis.

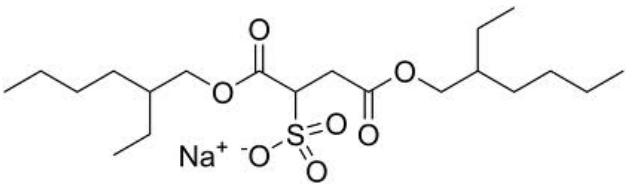

Sodium dioctyl sulfosuccinate (AOT)

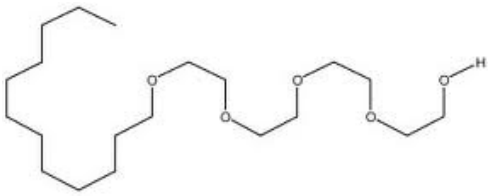

Polyethylene glycol dodecyl ether, FW 362 (Brij 30)

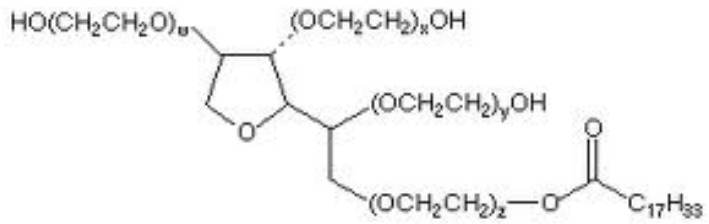

w+x+y+z=20

Polyoxyethylenesorbitan monooleate, or Polysorbate 80, FW 1310 (Tween 80)

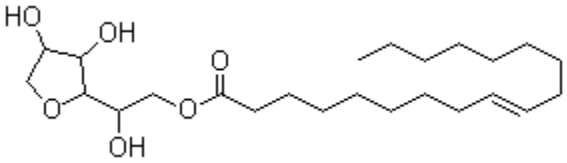

Sorbitane monooleate, FW 428.6 (Span 80)

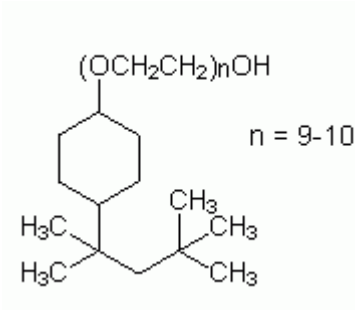

4-(1,1,3,3-Tetramethylbutyl)phenyl-polyethylene glycol (Triton X-100)

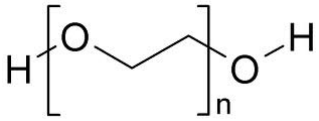

Polyethylene glycol 400, FW 380-420 (PEG 400)

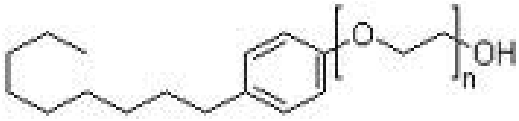

n = 9

Nonylphenol Ethoxylates, FW 606 (Tergitol NP-9)

	Brij 30	Tween 80	Span 80	Triton X-100	PEG 400	Tergitol
HLB value	9.8	15	4.3	13.5	13	12.9

Figure 3.1 Chemical structure and HLB value of surfactants used in the PAA nanoparticle synthesis. HLB values were obtained from the literature [33-35] and vendor website (Sigma-Aldrich).

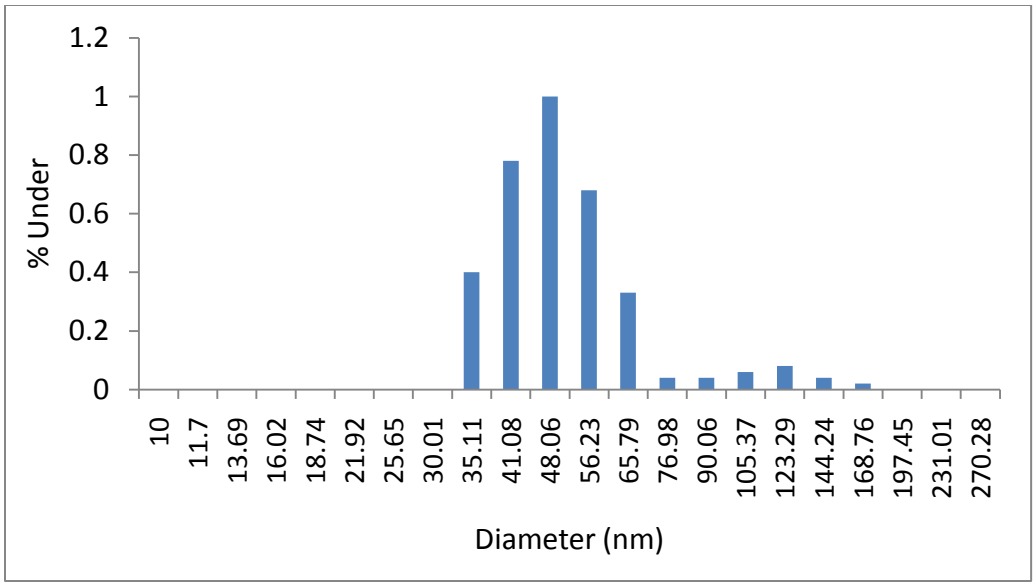

(a)

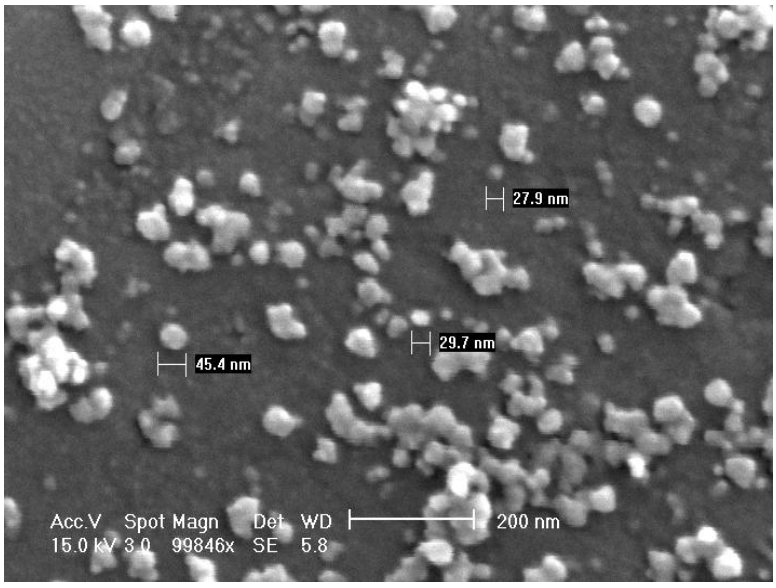

(b)

Figure 3.2 The size of the CA encapsulated silica particle was measured by (a) Dynamic Light Scattering (DSL) and (b) Scanning Electron Microscopy (SEM). The average size in aqueous solution is 48 nm determined by DSL. It is smaller, but polydispersed, in vacuum.

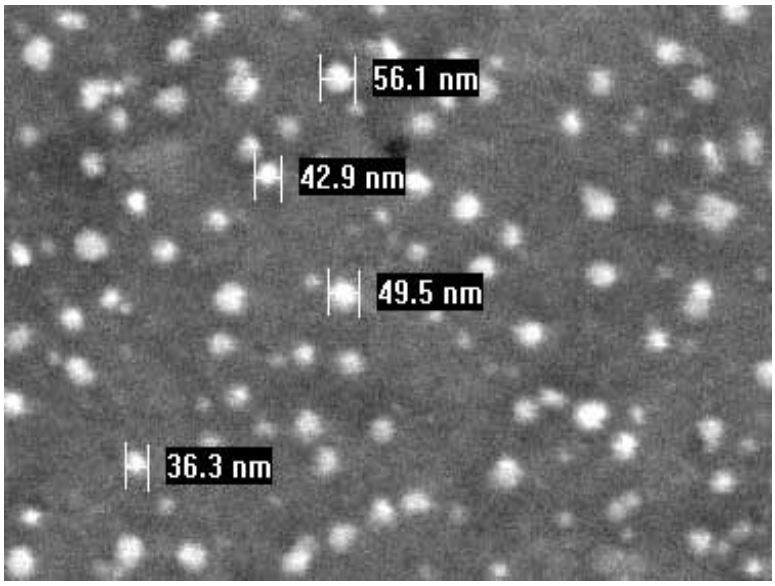

Figure 3.3 SEM image of CA encapsulated PAA PEBBLEs fabricated in AOT/Brij 30 surfactant system. The average size is about 50 nm.

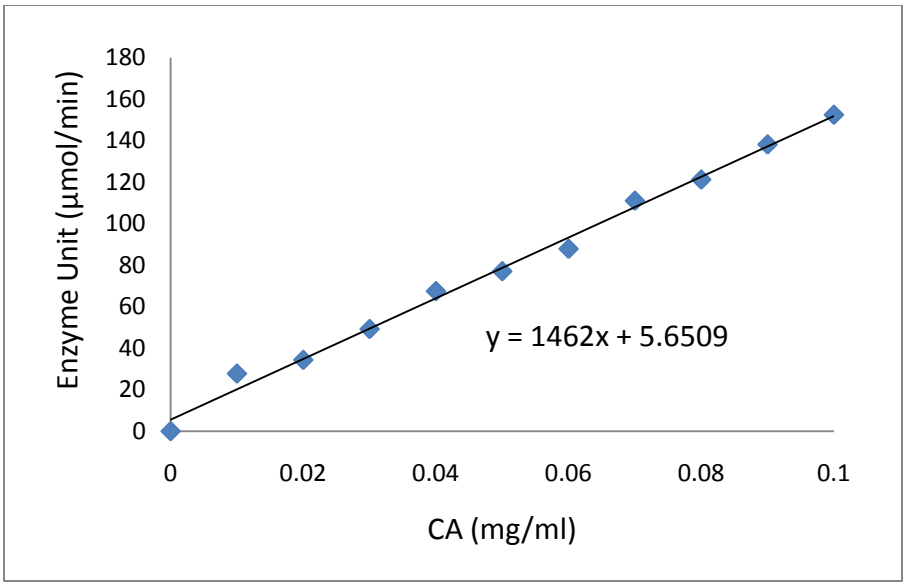

(a)

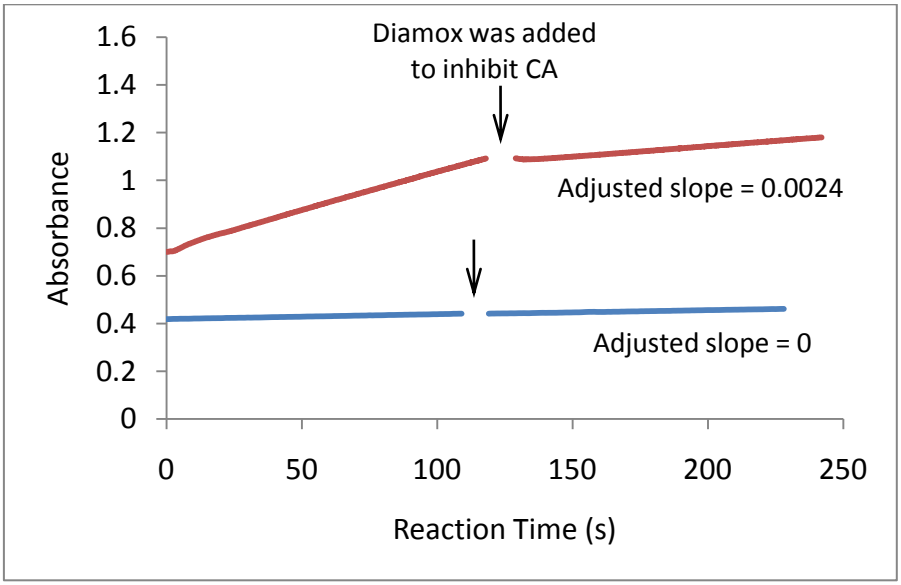

(b)

Figure 3.4 (a) Enzyme unit versus the concentration of CA. This calibration curve of the enzyme activity assay (pNPA assay) was used for quantifying the active CA inside PEBBLEs. (b). pNPA assay of CA encapsulated AOT/Brij-30 PEBBLEs (red) and blank PEBBLEs (blue). The PEBBLE concentration was 5 mg/ml.

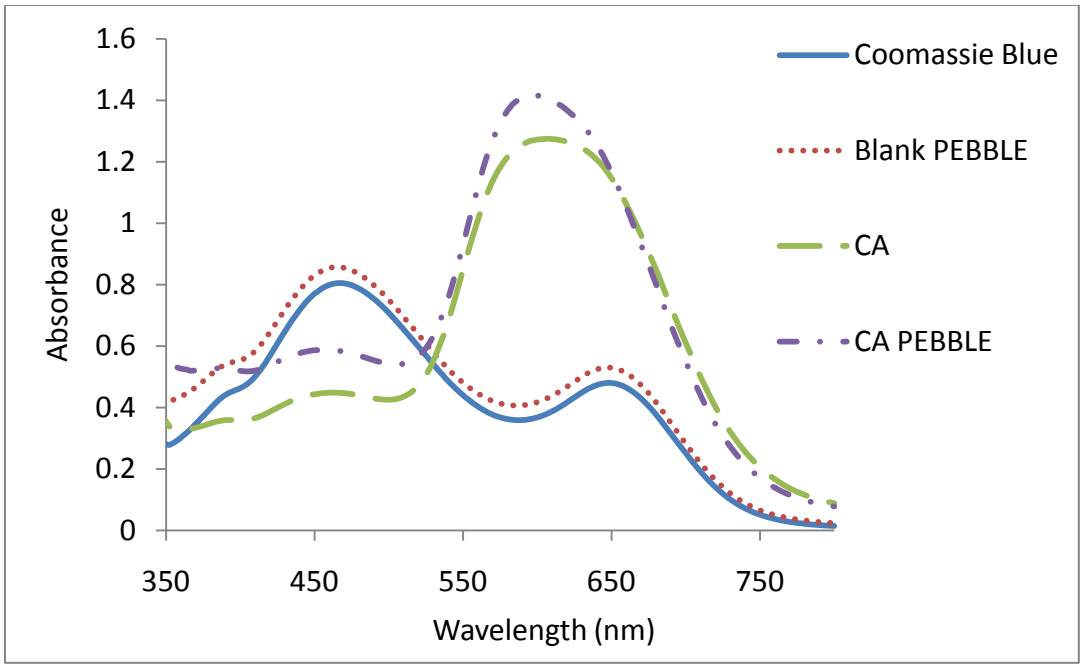
1.6
1.4
1.2
1
0.8
0.6
0.4
0.2
0
Absorbance
350
450
550
650
750
Wavelength (nm)
Coomassie Blue
Blank PEBBLE
CA
CA PEBBLE

(a)

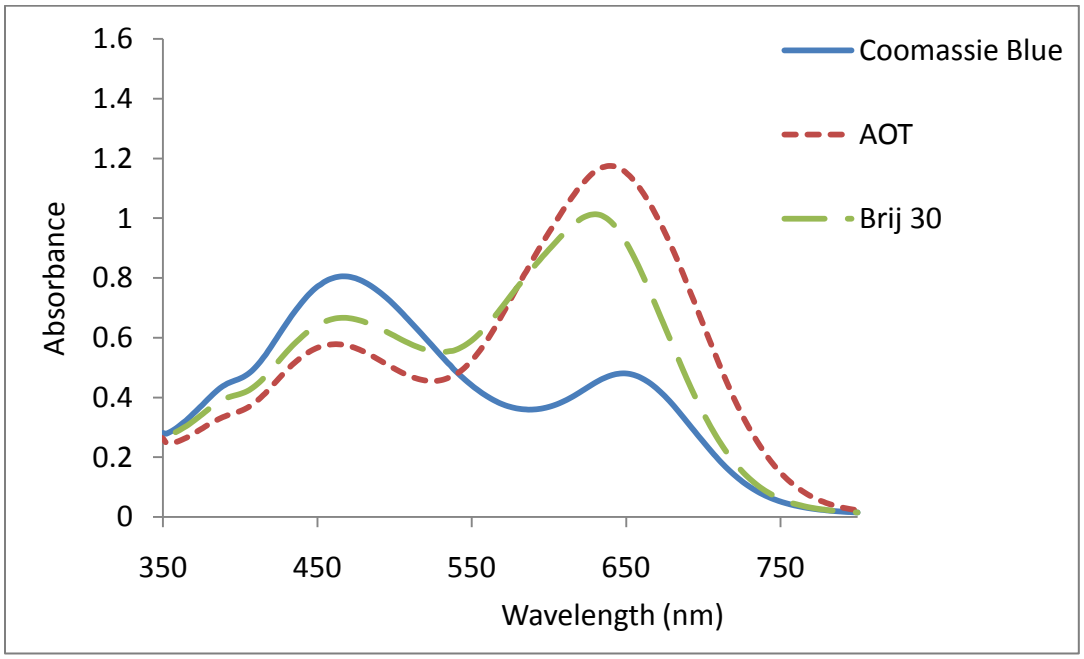
1.6
1.4
1.2
1
0.8
0.6
0.4
0.2
0
Absorbance
350
450
550
650
750
Wavelength (nm)
Coomassie Blue
AOT
Brij 30

(b)

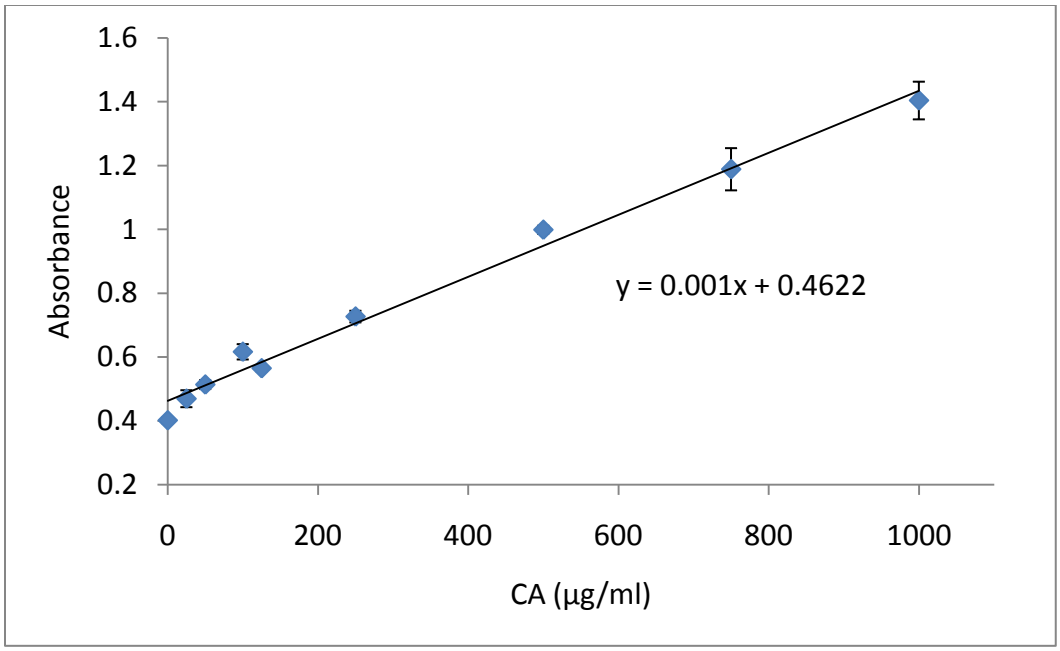

(c)

Figure 3.5 Coomassie blue protein assay. (a) Coomassie blue binds with both active and deactivated CA and its absorbance at 595 nm increases. Therefore, this assay was used for quantifying the total enzyme encapsulated in PEBBLEs. Blank PEBBLEs prepared under the same condition as the CA encapsulated PEBBLEs were tested and used as a background because AOT and brij 30 also increase the absorbance of coomassie blue (b). By subtracting the background caused by the residual surfactants in the blank PEBBLEs, the estimation of the total protein amount in CA encapsulated PEBBLEs became more accurate. (c) The absorbance of coomassie blue versus the concentration of CA. This calibration curve of the coomassie blue protein assay was used for quantifying the total CA inside PEBBLEs.

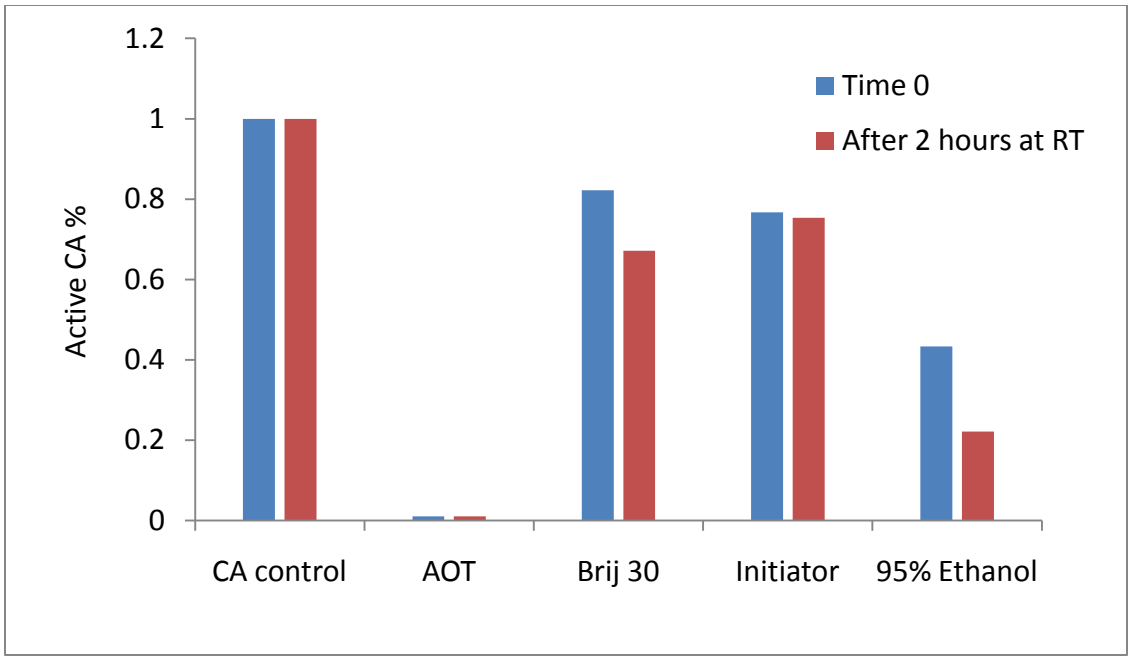

Figure 3.6 The CA activity was affected by AOT, brij 30, initiator and 95% ethanol. The concentrations of the solutions are: AOT 0.08 M, Brij 30 0.19 M, Initiator 0.1% w/w Ammonium persulfate and 1% v/v TEMED. All concentrations were the same as the concentrations used in PEBBLE preparation.

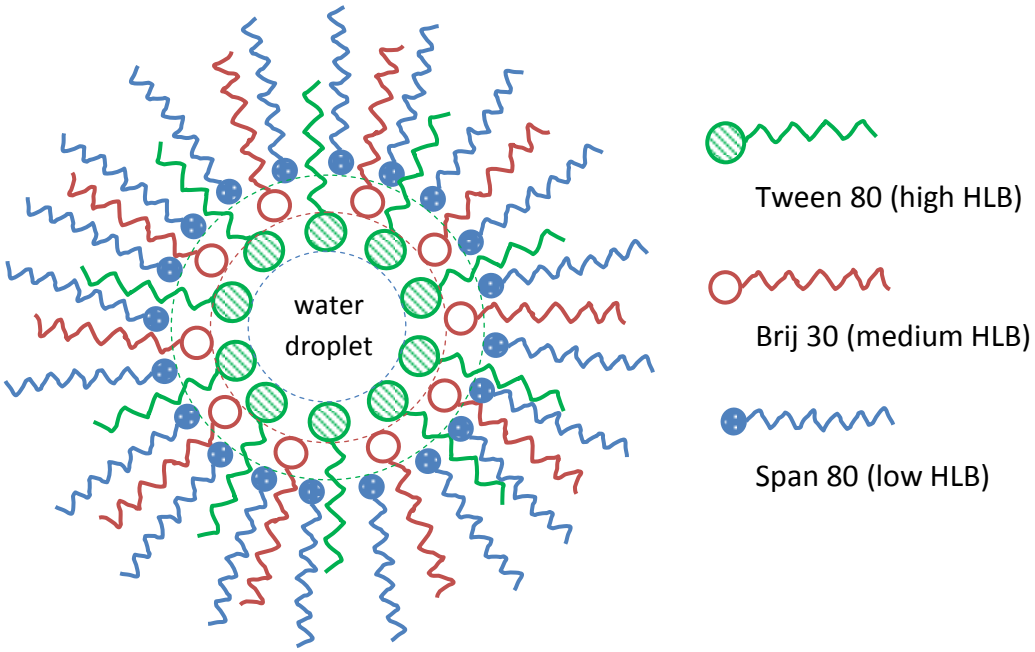

Figure 3.7 Illustration of the reverse micelles stabilized by multi-nonionic surfactant system. The hydrophilic surfactant (high HLB) tween 80 forms the inner layer surrounding the water droplet, while the lipophilic surfactant (low HLB) span 80 forms the outer layer. The layers of surfactants provide enough surface tension to stabilize the micelles.

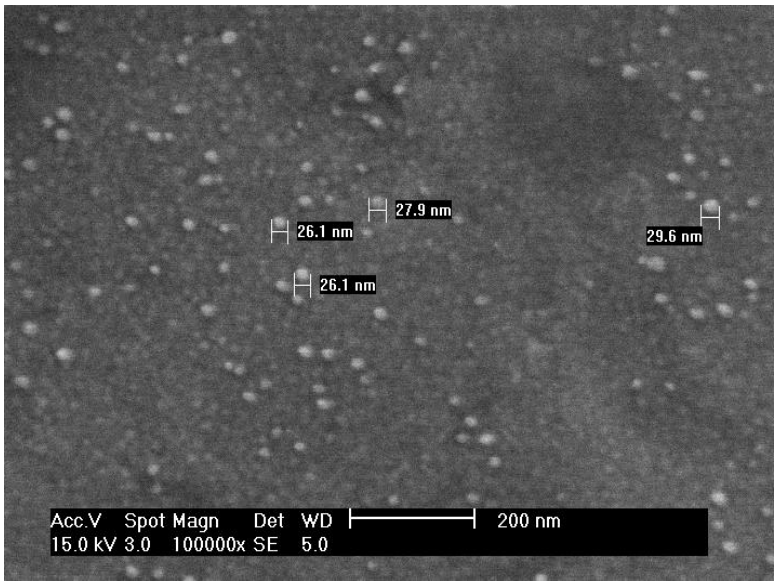

(a)

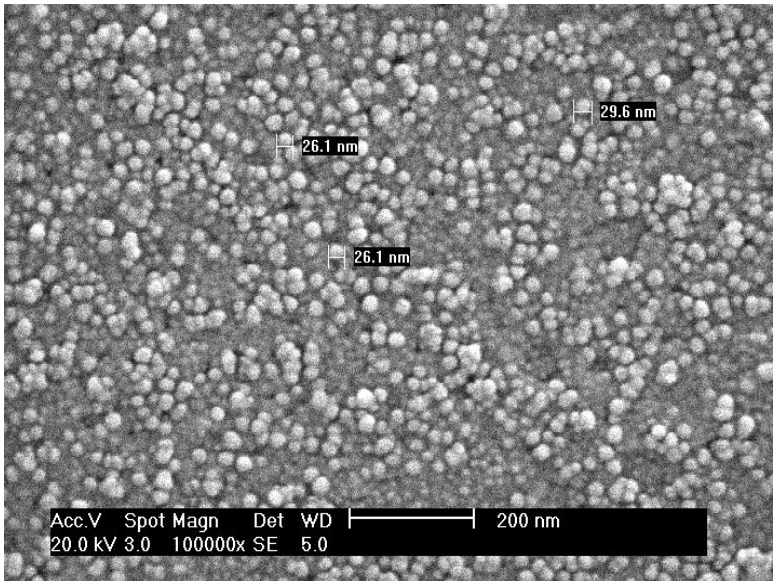

(b)

Figure 3.8 SEM images of CA encapsulated PAA PEBBLEs fabricated in (a) brij 30 system, recipe #1 in Table 3.1; and (b) span 80/tween 80/brij 30 system, recipe #2 in Table 3.1.

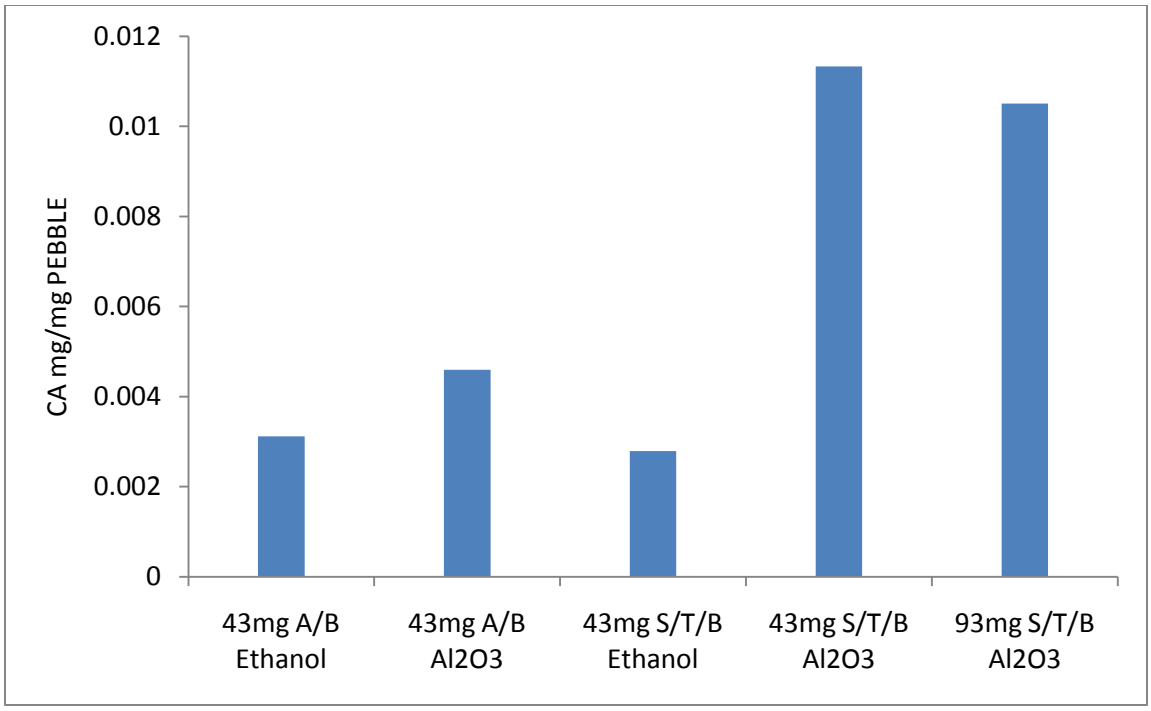

Figure 3.9 CA activity in CA encapsulated PAA PEBBLEs fabricated in A/B (AOT/Brij 30) or S/T/B (span 80/tween 80/brij 30) surfactant systems, purified by Al_2O_3 absorptive filtration (Al_2O_3) or by ethanol washing (Ethanol). CA loading amount was 43 or 93 mg.

Recipe	Surfactants	Mass	Mol %	HLB	Blank particle size (nm)	CA encapsulated particle size (nm)
1	Brij 30	8~9 g	100	9.8	40 (Brij 30 8 g)	65 (Brij 30 9 g)
2	Span 80 Tween 80 Brij 30	0.88 g 2.55 g 2.7 g	17.9 17 65.1	9.70	75	85
3	Span 80 Tween 80 Brij 30	1.3 g 1.6 g 2.6 g	26.6 10.7 62.7	8.89	75	
4	Span 80 Tween 80 1-hexanol	1.3 g 1.6 g 8.6 g	71.4 28.6	7.36	300	N/A 1-haxanol causes CA precipitation
5	Span 80 Tween 80 PEG 400	2.6 g 3.2 g 1 g	55.1 22.2 22.7	8.65	360	650 (span 80 and tween 80 were doubled)
6	Span 80 Tween 80 Tergitol	2.6 g 3.2 g 3.7 g	41.5 16.7 41.8	9.68	1400	> 2000 (span 80 and tween 80 were doubled)

Table 3.1 Multi-surfactants systems used for PEBBLE synthesis. The HLB value of each surfactant system was calculated. The particle sizes of blank PEBBLEs and CA encapsulated PEBBLEs were measured by dynamic light scattering.

References

[1] J. Kim, J. W. Grate, and P. Wang, "Nanobiocatalysis and its potential applications", *Trends in Biotechnology*, (26)11: 639-646, 2008

[2] P. Wang, "Nanoscale biocatalyst systems", *Current Opinion in Biotechnology*, (17)6: 574-579, 2006

[3] M. Vinoba, K. S. Lim, S. H. Lee, S. K. Jeong, and M. Alagar, "Immobilization of Human Carbonic Anhydrase on Gold Nanoparticles Assembled onto Amine/Thiol-Functionalized Mesoporous SBA-15 for Biomimetic Sequestration of CO_2", *Langmuir*, on-line publication, 2011

[4] K. Besteman, J. Lee, F. G. Wiertz, H. A. Heering, and C. Dekker, "Enzyme-Coated Carbon Nanotubes as Single-Molecule Biosensors", *Nano Letters*, (3)6: 727-730, 2003

[5] K. Rege, N. R. Raravikar, D. Kim, L. S. Schadler, P. M. Ajayan, and J. S. Dordick, "Enzyme−Polymer−Single Walled Carbon Nanotube Composites as Biocatalytic Films", *Nano Letters*, (3)6: 829-832, 2003

[6] V. Reukov, V. Maximov, and A. Vertegel, "Proteins Conjugated to Poly(Butyl Cyanoacrylate) Nanoparticles as Potential Neuroprotective Agents", *Biotechnology and Bioengineering*, (108)2: 243-252, 2011

[7] K. Ramanathan, B. R. Jonsson, and B. Danielsson, "Sol-gel based thermal biosensor for glucose", *Analytica Chimica Acta*, (427)1: 1-10, 2001

[8] Y. Wang, and F. Caruso, "Mesoporous Silica Spheres as Supports for Enzyme Immobilization and Encapsulation", *Chemistry of Materials*, (17)5: 953-961, 2005

[9] S. A. Grant, C. Weilbaecher, and D. Lichlyter, "Development of a protease biosensor utilizing silica nanobeads", *Sensors and Actuators B: Chemical*, (121)2: 482-489, 2007

[10] D. Avnir, S. Braun, O. Lev, and M. Ottolenghi, "Enzymes and Other Proteins Entrapped in Sol-Gel Materials", *Chemistry of Materials*, (6)10: 1605-1614, 1994

[11] U. Narang, P. N. Prasad, F. V. Bright, K. Ramanathan, N. D. Kumar, B. D. Malhotra, M. N. Kamalasanan, and S. Chandra, "Glucose Biosensor Based on a Sol-Gel-Derived Platform", *Analytical Chemistry*, (66)19: 3139-3144, 1994

[12] T. K. Jain, I. Roy, T. K. De, and A. Maitra, "Nanometer Silica Particles Encapsulating Active Compounds: A Novel Ceramic Drug Carrier", *Journal of the American Chemical Society*, (120)43: 11092-11095, 1998

[13] K. Smith, N. J. Silvernail, K. R. Rodgers, T. E. Elgren, M. Castro, and R. M. Parker, "Sol−Gel Encapsulated Horseradish Peroxidase: A Catalytic Material for Peroxidation", *Journal of the American Chemical Society*, (124)16: 4247-4252, 2002

[14] P. Billsten, U. Carlsson, B. H. Jonsson, G. Olofsson, F. Höök, and H. Elwing, "Conformation of Human Carbonic Anhydrase II Variants Adsorbed to Silica Nanoparticles", *Langmuir*, (15)19: 6395-6399, 1999

[15] M. Karlsson, L. Martensson, B. Jonsson, and U. Carlsson, "Adsorption of Human Carbonic Anhydrase II Variants to Silica Nanoparticles Occur Stepwise: Binding Is Followed by Successive Conformational Changes to a Molten-Globule-like State", *Langmuir*, (16)22: 8470-8479, 2000

[16] M. Lundqvist, I. Sethson, and B. Jonsson, "Transient Interaction with Nanoparticles “Freezes” a Protein in an Ensemble of Metastable Near-Native Conformations", *Biochemistry*, (44)30: 10093-10099, 2005

[17] A. Pollak, H. Blumenfeld, M. Wax, R. L. Baughn, and G. M. Whitesides, "Enzyme immobilization by condensation copolymerization into crosslinked polyacrylamide gels", *Journal of the American Chemical Society*, (102)20: 6324-6336, 1980

[18] C. Daubresse, C. Grandfils, R. Jerome, and P. Teyssie, "Enzyme Immobilization in Nanoparticles Produced by Inverse Microemulsion Polymerization", *Journal of Colloid and Interface Science*, (168)1: 222-229, 1994

[19] C. Daubresse, C. Grandfils, R. Jerome, and P. Teyssie, "Enzyme Immobilization in Reactive Nanoparticles Produced by Inverse Microemulsion Polymerization", *Colloid and Polymer Science*, (274)5: 482-489, 1996

[20] H. Sun, A. M. Scharff-Poulsen, H. Gu, I. Jakobsen, J. M. Kossmann, W. B. Frommer, and K. Almdal, "Phosphate Sensing by Fluorescent Reporter Proteins Embedded in Polyacrylamide Nanoparticles", *ACS Nano*, (2)1: 19-24, 2008

[21] H. Bu, S. R. Mikkelsen, and A. M. English, "NAD(P)H Sensors Based on Enzyme Entrapment in Ferrocene-Containing Polyacrylamide-Based Redox Gels", *Analytical Chemistry*, (70)20: 4320-4325, 1998

[22] N. Murthy, Y. X. Thng, S. Schuck, M. C. Xu, and J. M. Frechet, "A Novel Strategy for Encapsulation and Release of Proteins: Hydrogels and Microgels with Acid-Labile Acetal Cross-Linkers", *Journal of the American Chemical Society*, (124)42: 12398-12399, 2002

[23] K. McAllister, P. Sazani, M. Adam, M. J. Cho, M. Rubinstein, R. J. Samulski, and J. M. DeSimone, "Polymeric Nanogels Produced via Inverse Microemulsion

Polymerization as Potential Gene and Antisense Delivery Agents", *Journal of the American Chemical Society*, (124)51: 15198-15207, 2002

[24] M. Delgado, C. Spanka, L. D. Kerwin, . P. Wentworth, and K. D. Janda, "A Tunable Hydrogel for Encapsulation and Controlled Release of Bioactive Proteins", *Biomacromolecules*, (3)2: 262-271, 2002

[25] H. Xu, J. W. Aylott, and R. Kopelman, "Fluorescent Nano-PEBBLE Sensors Designed for Intracellular Glucose Imaging", *The Analyst*, (127): 1471-1477, 2002

[26] S. M. Buck, H. Xu, M. Brasuel, M. A. Philbert, and R. Kopelman, "Nanoscale probes encapsulated by biologically localized embedding (PEBBLEs) for ion sensing and imaging in live cells", *Talanta*, (63)1: 41-59, 2004

[27] H. A. Clark, R. Kopelman, R. Tjalkens, and M. A. Philbert, "Optical Nanosensors for Chemical Analysis inside Single Living Cells. 2. Sensors for pH and Calcium and the Intracellular Application of PEBBLE Sensors", *Analytical Chemistry*, (71)21: 4837-4843, 1999

[28] A. Shome, S. Roy, and P. K. Das, "Nonionic Surfactants: A Key to Enhance the Enzyme Activity at Cationic Reverse Micellar Interface", *Langmuir*, (23)8: 4130-4136, 2007

[29] C. Otero, L. Robledo, and M. I. del Val, "Two Alternatives: Lipase and/or Microcapsule Engineering to Improve the Activity and Stability of *Pseudomonas* sp. And *Candida Rugosa* Lipases in Anionic Midelles", *Progress in Colloid and Polymer Science*, (100): 296-300, 1996

[30] D. B. Wetlaufer, and Y. Xie, "Control of Aggregation in Protein Refolding: A Variety of Surfactants Promote Renaturation of Carbonic Anhydrase II", *Protein Science*, (4): 1535-1543, 1995

[31] F. Meng, Y. Park, and H. Zhou, "Role of proline, glycerol, and heparin as protein folding aids during refolding of rabbit muscle creatine kinase", *The International Journal of Biochemistry and Cell Biology*, (33)7: 701-709, 2001

[32] J. L. Cleland, C. Hedgepeth, and D. C. Wang, "Polyethylene Glycol Enhanced Refolding of Bovine Carbonic Anhydrase B", *The Journal of Biological Chemistry*, (267)19: 13327-13334, 1992

[33] H. Kunieda, and K. Shinoda, "Evaluation of the hydrophile-lipophile balance (HLB) of nonionic surfactants. I. Multisurfactant systems", *Journal of Colloid and Interface Science*, (107)1: 107-121, 1985

[34] W. C. Griffin, "Classification of Surface-Active Agents by “HLB” ", *Journal of the Society of Cosmetic Chemists*, (1): 311-326, 1949

[35] F. Harusawa, H. Nakajima, and M. Tanaka, "The Hydrophile-Lipophile Balance of Mixed Nonionic Surfactants", *Journal of the Society of Cosmetic Chemists*, (33): 115-129, 1982

[36] J. F. Krebs, J. A. Ippolito, D. W. Christianson, and C. A. Fierke, "Structural and Functional Importance of a Conserved Hydrogen Bond Network in Human Carbonic Anhydrase II", *The Journal of Biological Chemistry*, (268)36: 27458-27466, 1993

[37] Y. S. Leong, and F. Candau, "Inverse Microemulsion Polymerization", *The Journal of Physical Chemistry*, (86)13: 2269-2271, 1982

Chapter 4

Zinc Sensing Using PEBBLEs *Encapsulated* or *Conjugated* with Wild Type Bovine Carbonic Anhydrase

Introduction

As the second most abundant trace element in human body after iron, zinc is an essential cofactor in all six classes of enzymes [1-2] and several families of regulatory proteins [3-5]. Cells strictly control homeostasis of Zn^{2+}; most of the intracellular Zn^{2+} is tightly bound to metalloproteins serving as structural and catalytic components [1-2]. To that end, the cytosolic free or readily exchangeable Zn^{2+} concentration is reduced by orders of magnitude and has been determined at the picomolar level [15-16]. Despite the fact that zinc is of high physiological importance, the full purpose for the existence of zinc in biology remains unclear.

Fluorescence based chemosensors have been developed for zinc sensing, such as TSQ (N-6-methoxy-8-quinolyl)-p-toluenesulfonamide), Zinquin, ZnAF-2, FluoZin-3, FuraZin and RhodZin-3, which have been reviewed previously [6-7]. Recently more zinc chemosensors have been discovered [8-11]; these new ratiometric probes exhibit tighter zinc binding affinity than the traditional chemical probes. The detection limits of most of

these probes are at nanomolar to micromolar levels, and these probes usually have a weaker affinity for other ions such as Ca^{2+} and Mg^{2+}. Although Ca^{2+} and Mg^{2+} would not interfere with the above Zn^{2+} sensors when they are at about equal concentrations to those of Zn^{2+}, intracellular free Ca^{2+} and Mg^{2+} are orders of magnitude higher than those of free Zn^{2+}. These ions could saturate all the metal binding sites of the fluorophores and thus interfere with Zn^{2+} sensing [17].

Recently, biosensors for zinc sensing that involve the use of biologically derived molecules have become an active research area. Genetically encoded sensors based on fluorescence resonance energy transfer (FRET) have been developed [12-16]. In these sensors, binding with zinc ions induces protein conformational changes and therefore leads to changes in the energy-transfer efficiency between the fluorescent donor and acceptor [12-15]. Progress has been made by using these probes for intracellular zinc sensing as well as demonstrating their potential utility in these studies. [15-16].

Comparing with other chemo- or bio- zinc sensors, Carbonic anhydrase offers many desirable traits for zinc sensing, making it particularly useful. This has been extensively studied as a fluorescence-based biosensor by Fierke and Thompson [17-19]:

1) Wild type CA II displays a picomolar level zinc binding affinity and excellent selectivity. The zinc binding dissociation constant of wild type human CA II was determined to be 4 pM [20], which is comparable to the intracellular free Zn^{2+} concentration. Wild type CA II has very little binding affinity to Ca^{2+} and Mg^{2+}, and other transition metal divalent cations, like Mn^{2+}, Co^{2+} and Ni^{2+}, bind with CA II much less tightly than Zn [19] (see Table

4.1). The only possible binding competitor is Cu^{2+} which has a 10-fold higher binding affinity than Zn^{2+}; however, intracellular free Cu^{2+} is estimated to be a 1000-fold lower than that of Zn [17].

2) Tunable CA-zinc binding affinity, binding kinetics [20-22] and metal selectivity [23-25] has been achieved by mutagenesis. A family of CA II mutants has been developed. These mutants exhibit a femtomolar to micromolar range of zinc binding affinity, faster dissociation rate constants and altered metal selectivities. For instance, the E117A mutation displays a 5000-fold smaller dissociation rate constant and an only 40-fold decreased affinity, compared to the wild type CA II; therefore it is particularly useful for zinc sensing [20].

3) Ratiometric excitation measurement, based on FRET [16, 26], was established. A fluorophore, Alexa Fluor 594 (AF594), is covalently attached to CA II and serves as the FRET acceptor. When dapoxyl sulfonamide binds to holo CA II, it serves as a FRET donor and its excitation is transferred to AF594, which emits at a longer wavelength. The FRET intensity ratio increases with the fraction of zinc-bound CA II and thus reveals the Zn^{2+} concentration.

4) Other than fluorescence intensity or ratiometric methods, anisotropy and lifetime based methods have also been used for zinc sensing by CA II and the sulfonamide fluorophores [27-32]. All these favorable features of CA II make it an outstanding new tool to study the intracellular Zn^{2+} storage and distribution, and thus can reveal the biological functions of zinc.

Previous work accomplished in our lab has successfully embedded a commercial zinc sensing chemical probe, Newport Green, into nano-PEBBLEs [33]. This nanosensor was demonstrated to respond to zinc in a fast, reversible and reproducible manner and its dynamic sensing range has been determined to be at the micromolar level. It has also displayed many of the classical advantages of PEBBLE nanosensors, such as (1) ratiometric measurements by co-loading a reference dye, (2) reduced interference by proteins' non-specific binding, as well as other advantages detailed in Chapter 1.

In this work, bovine CA was immobilized inside, or on the surface of, nano-PEBBLEs, by encapsulation or post-conjugation. The aim was to combine the advantages of both CA II and PEBBLEs. The development of CA *encapsulated* and *conjugated* PEBBLEs for zinc sensing is described in this chapter, while the issues encountered while carrying out this work are also addressed.

Experimental and Methods

Reagents. Carbonic Anhydrase from bovine erythrocytes, acrylamide, GDMA (glycerol dimethacrylate), Brij (30polyoxyethylene (4) lauryl ether), Tween 80 (polysorbate 80), Span 80 (sorbitan monooleate), TEMED (N,N,N',N'-tetraethylmethylenediamine), ammonium persulfate, MOPS (4-morpholinepropanesulfonic acid), p-nitrophennyl acetate, Diamox (actazolamide), Sephadex G-25, aluminum oxide (neutral), bicine (N,N-Bis(2-hydroxyethyl) glycine), NTA (nitrilotriacetic acid), DPA (2,6 pyridine dicarboxylic acid), DNSA (dansyl amide or 5-(Dimethylamino)-1-naphthalenesulfonamide), ammonia solution in 1,4-dioxane, cobalt chloride and zinc chloride standard solution were purchased from Sigma-Aldrich (St. Louis, MO, USA). APMA (N-(3-aminopropyl) methacrylamide hydrochloride) was purchased from Polyscience (Warrington, PA, USA). Dapoxyl sulfonyl chloride was purchased from Invitrogen (Eugene, OR, USA). Chelex 100 resin was purchased from Bio-Rad (Hercules, CA, USA). Sulfosuccinimidyl-4-[N-maleimidomethyl]cyclohexane-1-carboxylate (Sulfo-SMCC) was purchased from Soltec Ventures (Beverly, MA). All buffer solutions were prepared from 18MΩ Milli-Q water purified by a Millipore Advantage A10 system and passed through a Chelex 100 column.

Preparation of CA *encapsulated* PEBBLE. The monomer solution was prepared by first dissolving CA in 1.2 ml MOPS buffer (pH 7.22), then dissolving 711 mg acrylamide and 55 mg APMA, and adding 240 µl GDMA at last. This monomer solution was added to an argon deoxygenated solution that contained 45 ml of hexanes, 2.6 g Brij 30, 1.6 g

Tween 80 and 1.3 g Span 80. The solution was stirred under argon throughout the duration of the preparation. To initiate the polymerization, 100 µl of 20% (w/w) ammonium persulfate solution and 100 µl TEMED were added. The solution was stirred at room temperature for two hours to assure complete polymerization.

Next step was to separate the PEBBLEs from the surfactants and unreacted monomers. First, 50 g Al_2O_3 was immersed in water-saturated hexane for 30 minutes. The w/o microemulsion was mixed with the stabilized Al_2O_3 and the mixture was stirred for 30 minutes so that the particles in aqueous phase were absorbed onto the Al_2O_3 surface, leaving most of the surfactants in the hexane phase. The mixture was then vacuum-filtered and the Al_2O_3 was washed with hexane, eight times, each time with 50 ml. After the washing step, hexane was completely evaporated by vacuum filtration or by rotary evaporation, so as to yield dry Al_2O_3 with particles absorbed on the surface. The particles were then extracted from the Al_2O_3 with water, eight times, each time with 50 ml. The resulting particle suspension was centrifuged at 5000 rpm for 10 minutes, and the precipitate and floating mass were discarded. The clear supernatant was transferred into an Amicon stir cell, and the particles were washed with 800-1000 ml water and then freeze dried.

Preparation of CA *conjugated* PEBBLE. 50 mg PEBBLEs were first suspended in 2.5 ml 10 mM MOPS pH 7.22, into which 3 mg Sulfo-SMCC was added. The mixture was kept stirring at 600 rpm for 2 hours at room temperature, then transferred to an Amicon cell and washed with 60 ml MOPS buffer. The CA solution was added into the resulting

mixture, under constant stirring at 600 rpm, and the mixture was kept stirring overnight at room temperature. 1.736 mg L-cysteine was added afterwards and the mixture was kept stirring for 2 more hours. Finally the PEBBLEs were washed in Amicon cells with 60 ml MOPS, so as to eliminate unreacted enzymes and peptides.

Synthesis of Dapoxyl Sulfonamide. Dapoxyl sulfonamide is not commercially available; therefore it was synthesized from the commercially available precursor Dapoxyl sulfonyl chloride (DSC) [32]. DSC also reacts with water and the side reaction produces a fluorescent by-product, dapoxyl sulfonyl acid. In order to reduce the side reaction, a 0.5 M ammonia solution in 1,4-dioxane was used instead of ammonium hydroxide. A 600 µl ammonia dioxane solution was added into a small vial containing 10 mg DSC and the reaction mixture was stirred at ice-cold temperature for 2 hours, in the dark, for the reaction to complete. Then the dioxane was removed by rotary evaporation.

The product was dissolved in 200 µl THF (Tetrahydrofuran), and 2-3 ml water was added. Then the pH of the solution was adjusted to about 5 by adding one drop of 1 M HCl. After sitting in room temperature for about 30 minutes, the dapoxyl sulfonamide precipitated, leaving the dapoxyl sulfonyl acid in solution. The mixture was then centrifuged at 5000 rpm for 10 minutes and the supernatant was discarded. This procedure was repeated three times and the precipitate was freeze-dried. The product was further purified by an Al_2O_3 column containing about 50 g Al_2O_3. The column was first run with 80 ml CH_2Cl_2, eluting out dapoxyl sulfonyl acid, and then the mobile phase

was changed to methanol (80 ml), eluting out dapoxyl sulfonamide. The elution was collected and the solvent was rotary-evaporated to obtain a dry yellow powder.

Product purity was assessed by Al_2O_3 TLC plates. Dapoxyl sulfonamide was identified by its yellow fluorescence when excited by a hand-held UV light while the dapoxyl sulfonyl acid exhibits a much weaker, blue fluorescence. An analysis of the product was also performed on a Micromass LCT Time-of-Flight mass spectrometer with Electrospray and APCI and the purity was estimated to be 90 % (m/Z of dapoxyl sulfonamide is 344). The concentration of dapoxyl sulfonamide was determined by its absorbance at 365 nm (ε = 22,000 $M^{-1}cm^{-1}$) [32].

Removal of Zn^{2+} from CA and PEBBLEs. The preparation of apo CA is described in the literature [34]. Basically, for free enzyme, a 20-50 μM CA solution was first prepared by dissolving CA in 10 mM MOPS (pH 7.22) containing 25 mM DPA (2,6 pyridine dicarboxylic acid). This solution was stored at 4°C overnight and the excess DPA was removed by serial dilution with 10 mM MOPS (pH 7.22), followed by concentration in an Amicon Ultra Centrifugal Filter Unit with a 10 kDa membrane cut-off size. The apo-enzyme was then further purified by running it through a 10 cm Sephadex G-25 column. For any experiments involving apo CA, all reagents were of the highest purity available and all solutions were made from 18 MΩ Milli-Q water treated by Chelex 100 resin so as to minimize the metal contamination. All plasticware used for apo CA was also pre-treated, for minimizing metal contamination. The apo CA concentration was determined by *p*NPA assay with excess Zn^{2+} added.

Regarding the PEBBLEs, a 25 mg/ml PEBBLE suspension was prepared in 10 mM MOPS pH 7.22 containing 25 mM DPA and the suspension was kept at 4°C overnight. The particles were washed with 10 mM MOPS 50~60 ml in a pre-treated low metal Amicon ultra-filtration cell to eliminate excess DPA.

Calibration of apo CA and apo CA *encapsulated* or *conjugated* PEBBLEs. A 2-5 µM apo CA solution or 2-5 mg/ml PEBBLE suspension was prepared with 10 mM MOPS pH 7.22, containing 10 mM NTA (nitrilotriacetic acid). A 4-fold molar excess of dapoxyl sulfonamide was added into the solution or suspension. The NTA was used as a chelating agent to maintain a low free Zn^{2+} concentration. Spectra were collected on a Horiba FluoroMax-3 fluorometer by exciting the sample at 365 nm and recording the resulting emission from 430 nm to 700 nm in 1 nm increments with an integration time of 0.5 sec. An aliquot of zinc chloride was added after each successive spectrum was collected. The samples were prepared and continuously stirred by a magnetic stir bar in a 4.5 ml quartz cuvette which was kept at 25°C by a water-jacketed temperature controlled cuvette holder. All experiments were repeated in triplicate.

The interference of surfactants on sulfonamide fluorescence. Solutions of 1% w/v brij 30, tween 80, span 80, triton X-100, AOT, 1-hexnaol and PEG 400 were prepared in 10 mM MOPS. Solutions of 5 µM sulfonamides were also prepared in 10 mM MOPS. The sulfonamide solutions were transferred into a 4.5 ml cuvette, and the fluorescence of dapoxyl sulfonamide (excitation 365 nm, emission 430-700 nm) or dansylamide (excitation 330 nm, emission 400-650 nm) was recorded on the fluorometer. Then, 20 µl

of each surfactant solution was added to the sulfonamides solutions, and the fluorescence changes induced by the surfactants were measured at 535 nm for dapoxyl sulfonamide and at 450 nm for dansylamide, respectively.

Results and Discussion

In this chapter, both CA *encapsulated* PEBBLE and CA *conjugated* PEBBLE were tested for zinc sensing. As stated in Chapter 3, bovine CA was used as a substrate because of its robust nature and the affordable price. The bovine CA (Sigma-Aldrich) is a mixture of isoforms, and no purity claim is made by the vendor. The zinc binding dissociation constant K_d of this commercial product was measured in our study and was determined to be 29±7 pM. As a reference, the reported K_d of pure wild type human CA II is 4 pM [20].

The zinc sensing scheme is shown in Figure 4.1. Briefly, holo CA was first incubated with the zinc chelator DPA, to remove Zn^{2+} from its active site and thus produce apo CA. The sulfonamide fluorophores bind to zinc-bound CA and the fluorescence change of the fluorophores was measured. A non-fluorescent sulfonamide inhibitor, diamox, which has a much tighter binding affinity with CA than the fluorescent inhibitors, was added into the solution so as to replace the fluorescent inhibitors, and the background fluorescence was subsequently measured. The excitation, emission, quantum yield and CA binding affinity of the fluorescent inhibitors used in this work, dapoxyl sulfonamide and dansylamide, are listed in Table 4.2.

Figure 4.2 shows the fluorescence change of dapoxyl sulfonamide while binding to the blank PEBBLE and CA encapsulated PEBBLE. The blank PEBBLE was purified by washing the particles in Amicon stirred cells with 500 ml ethanol and 500 ml water. The residual surfactants interacted with the fluorophore, resulting in a background

fluorescence that showed little change when 0.5 mM diamox was added. On the other hand, although CA inside the CA encapsulated PEBBLEs did bind with dapoxyl sulfonamide, therefore inducing a fluorescence increase, it also showed a higher background than the blank PEBBLEs when diamox was added. This is because the Al_2O_3 absorptive filtration purification method did not eliminate the surfactants as effectively as ethanol washing. The interference of the surfactants with sulfonamide fluorophores was tested by monitoring the spectra of the fluorophores, in the presence and absence of the surfactants, as shown in Figure 4.3. Almost all the nonionic surfactants used in PEBBLE preparation enhanced the fluorescence of both the dapoxyl sulfonamide and the dansylamide. While AOT and 1-hexanol did not interact with the fluorophores, they deactivated CA.

The CA encapsulated PEBBLEs were incubated with DPA at 4°C for 48 hour, then washed with 10 mM MOPS pH 7.22 in pre-treated, low metal, Amicon stirred cells so as to remove the Zn-DPA complex and excess DPA. Finally, the zinc binding affinity of the PEBBLEs was tested. However, these tests showed no fluorescence change at different free Zn^{2+} levels, as shown in Figure 4.4. Therefore, the zinc sensing was not successful.

A possible reason for the above failure is that Zn^{2+} is difficult to remove from the CA after the CA was encapsulated by the PEBBLEs. It has also been reported that Zn^{2+} is difficult to remove from some CA fluorescence conjugates, and that it is necessary to replace the zinc with cobalt (II) before conjugation, then conjugate the cobalt bound enzyme and remove the cobalt last, because CA binds with cobalt much less tightly than

with zinc [18]. For that reason, Co-bound CA was prepared and the removal rate of Co^{2+} or Zn^{2+} from CA was tested, based on the enzyme activity. As shown in Figure 4.5, by incubating with DPA at room temperature for one hour, 80% Co^{2+} and 25% Zn^{2+} were removed, confirming that Co^{2+} binds with CA much less tightly than Zn^{2+}. However, possibly the enzyme became less stable when the Zn^{2+} was replaced by Co^{2+}, because it is much easier for CA to lose Co^{2+} and become deactivated. So the attempt of overcoming the above problem by encapsulating Co-bound CA in PEBBLEs, while maintaining its enzyme activity, has failed. So far, zinc sensing using CA encapsulated PEBBLEs has encountered many difficulties; most likely it is not a promising method.

Another enzyme immobilization approach was performed. This time, the enzyme was post-conjugated onto blank PEBBLEs, after the PEBBLEs were washed with plenty of ethanol and water to completely eliminate the surfactants. The amine groups on the PEBBLEs were first reacted with Sulfo-SMCC and then the maleimide-activated PEBBLEs were linked with the thiol groups of the enzyme. The detailed reaction mechanism is available at the vendor website, (http://www.piercenet.com/). The activity of the Co-bound CA conjugated PEBBLEs was determined to be 2-fold higher than the activity of the CA encapsulated PEBBLE prepared by the new method, detailed in Chapter 3, and has almost 7-fold the activity of the CA encapsulated PEBBLEs prepared by the traditional method (see Figure 4.6).

In Figure 4.7, the binding of CA conjugated PEBBLEs and dapoxyl sulfonamide was verified by the fluorescence change of dapoxyl sulfonamide. After adding diamox,

the PEBBLEs showed almost no surfactants interference. The zinc binding affinity of the conjugated CA on the PEBBLE's surface was also tested, and the dissociation constant K_d was determined to be 7.50±2.34 pM (see Figure 4.8). Therefore, the post-conjugation method has demonstrated many advantages and the zinc sensing by CA conjugated PEBBLEs has been successful.

Conclusions

Two enzyme immobilization methods were described in this chapter. Free zinc sensing by CA encapsulated PEBBLEs was not successful because of the listed issues: 1) The enzyme is very delicate; therefore we had to use a much milder recipe and purification methods for the CA to remain active in the PEBBLEs. However, higher amounts of residual surfactants were thus left in the PEBBLEs. 2) The residual nonionic surfactants enhance the fluorescence of the sulfonamide probes and thus result in a significant background. 3) Zn^{2+} is difficult to remove from the CA after its encapsulation in PEBBLEs. 4) Although Co^{2+} is easier to remove from CA than Zn^{2+}, after encapsulation in PEBBLEs the Co-bound CA became deactivated. For all these reasons, the CA encapsulated PEBBLEs are not a promising avenue for zinc sensing.

Meanwhile, the post conjugation of CA on the PEBBLE surface showed many advantages over the encapsulation method. The preparation is quite straightforward and the surfactants can be eliminated almost completely. Since the enzyme was post-conjugated, after the PEBBLEs were washed with plenty of ethanol, the interference of surfactants with the sulfonamide probes is minimal, and, at the same time, the CA activity can be preserved. However, it is noted that the CA is immobilized onto the surface of the PEBBLEs; therefore, in intracellular measurements, the enzyme will be exposed directly to the cellular environment and thus a few of the classic PEBBLE advantages will no longer be available. The cellular environment and the CA are not protected from each other; the interaction between CA and cellular biomicromolecules,

such as protease attack, cannot be reduced or eliminated. However, very important advantages, like targeted delivery and reduced sequestration, should still be present. In summary, the CA conjugated PEBBLEs are a very promising tool for intracellular free zinc sensing.

pK_d	Zn (II)	Cu (II)	Ni (II)	Co (II)	Mn (II)	Ca (II)	Mg (II)
Wild Type Human CA II	12	13	7.8	6.8	<3.4	<2	<1.3

Table 4.1 Binding affinity to wild type human CA II of divalent cations [17].

	Free/Bound	λ_{EX} (nm)	λ_{EM} (nm)	Quantum Yield	K_d (μM)
Dansylamide	Free	330	560	0.08	
	Bound		450	0.55	0.8
Dapoxyl sulfonamide	Free	365	615	0.01	
	Bound		535	1.00	0.13

Table 4.2 CA fluorescence inhibitors used as Zn^{2+} sensing probes [19].

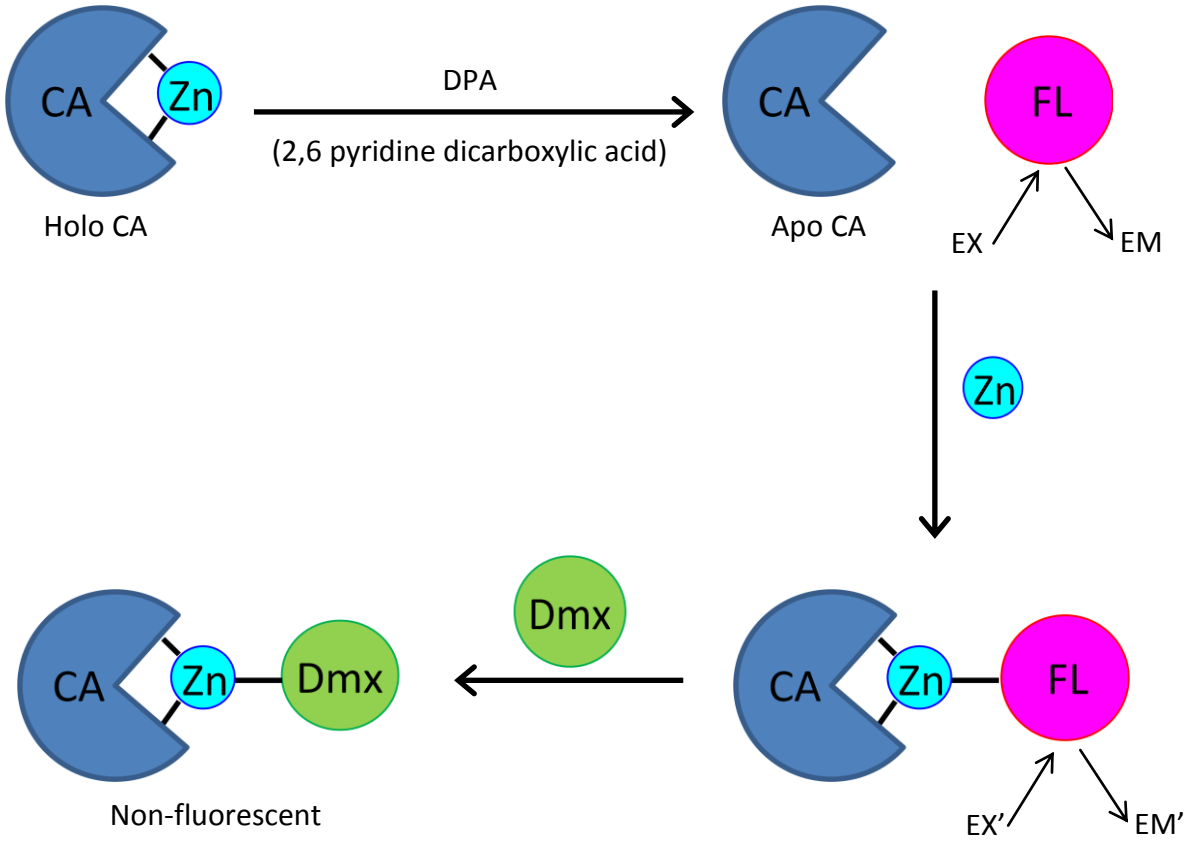

Figure 4.1 The CA sensing scheme for Zn^{2+}. After the Zn^{2+} is removed from holo CA, it forms apo CA, which binds with the sulfonamide fluorophore (FL) in the presence of Zn^{2+} and induces a fluorescence change on the fluorophore. Then the fluorophore is exchanged to diamox which binds with CA, with a tighter affinity, and forms a non-fluorescent complex for measuring the background.

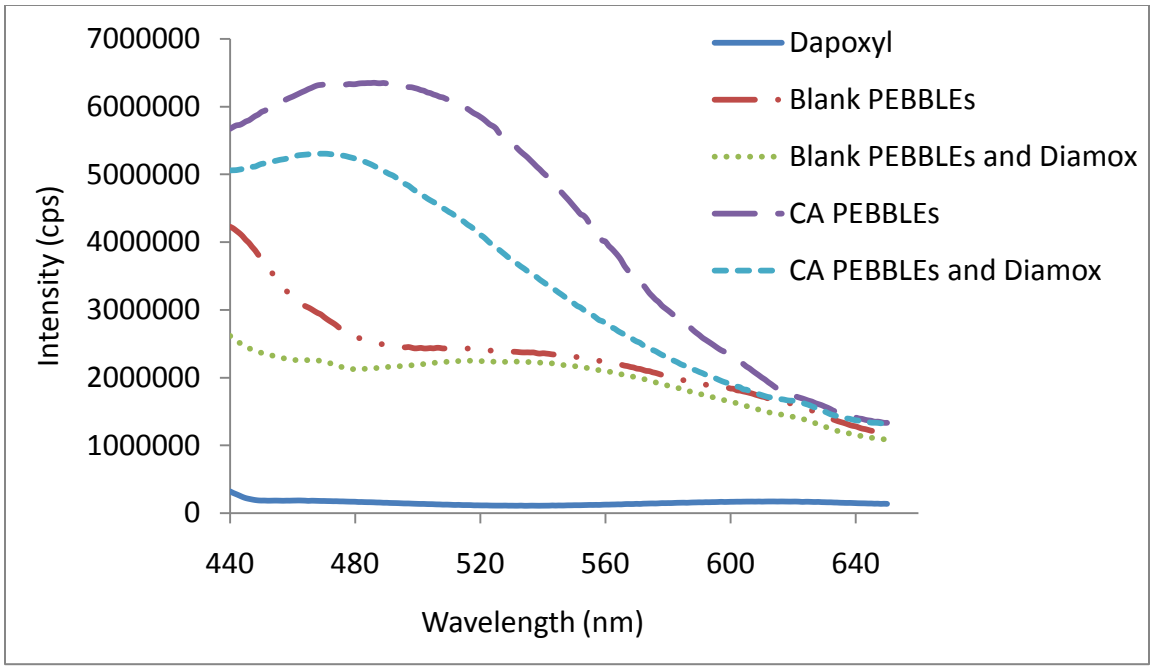

Figure 4.2 The fluorescence of dapoxyl sulfonamide binding with either blank or CA encapsulated PEBBLEs. Blank PEBBLEs were purified by ethanol washing and the CA encapsulated PEBBLEs were purified by Al_2O_3 absorptive filtration. After recording the spectra of dapoxyl sulfonamide binding with the PEBBLEs, diamox was added to replace dapoxyl sulfonamide and the background was recorded.

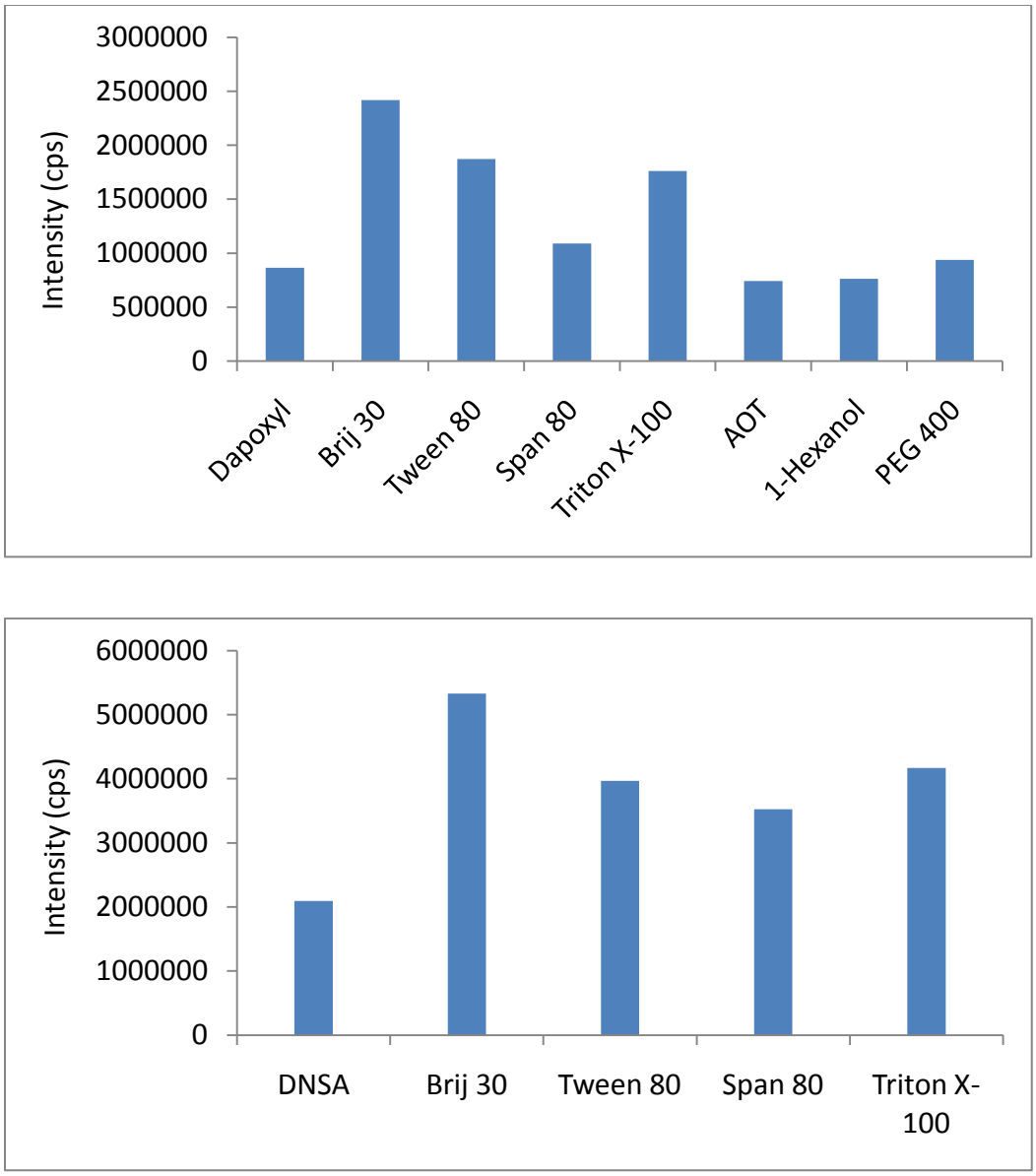

Figure 4.3 The interference of surfactants on the fluorescence of the sulfonamide fluorophores. All of the surfactants used in PEBBLE synthesis (brij 30, tween 80 and span 80) enhance the fluorescence of the sulfonamides, dapoxyl sulfonamide (DPS) and dansylamide (DNSA). Excitation: DPS 365 nm, DNSA 330 nm; emission DPS 535 nm, DNSA 450 nm.

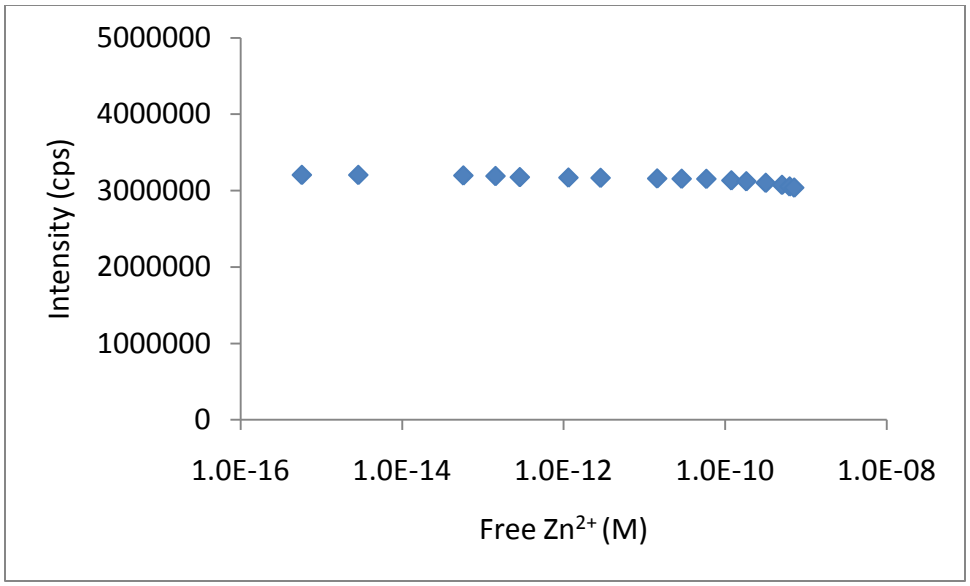

Figure 4.4 Calibration of the CA encapsulated PEBBLEs. This graph shows no fluorescence change as Zn^{2+} is added, indicating that this sensing scheme is not successful for CA encapsulated PEBBLEs. Calibration was performed in 10 mM MOPS (pH 7.22) containing 10 mM NTA at 25°C.

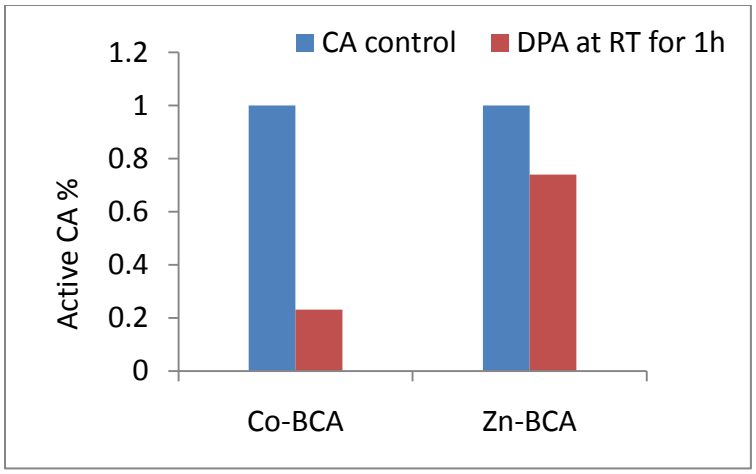

Figure 4.5 The removal of Co^{2+} and Zn^{2+} from bovine CA. After incubating with the Zn chelator DPA (2,6 pyridine dicarboxylic acid) for one hour at room temperature, 80% Co^{2+} and 25% Zn^{2+} are removed, assuring that Co^{2+} binds with CA much less tightly than Zn^{2+}.

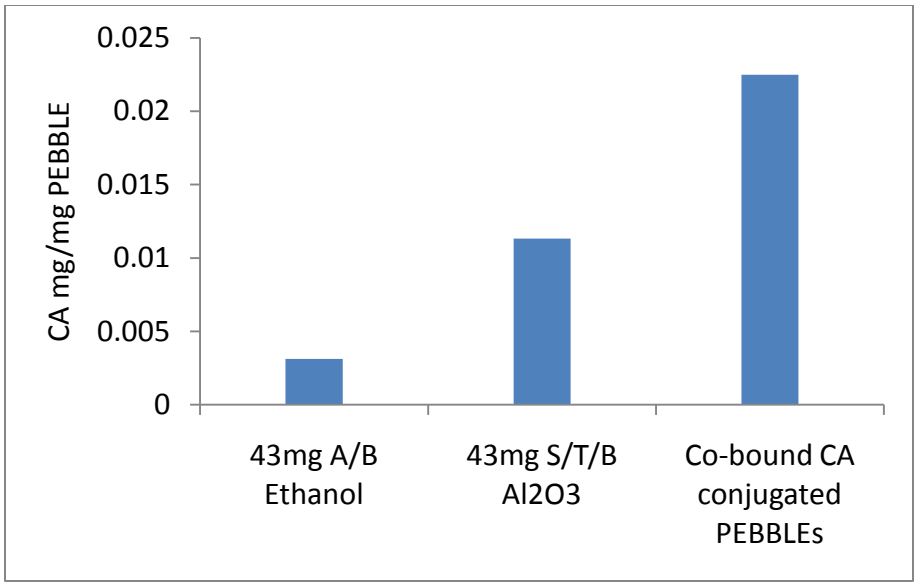

Figure 4.6 The activity of the CA conjugated PEBBLEs (Co-bound CA conjugated PEBBLEs) is 2-fold than the activity of the CA encapsulated PEBBLEs, prepared by the nonionic surfactant system S/T/B (span 80/tween 80/brij 30) and purified by Al_2O_3 absorptive filtration; almost 7-fold than the activity of CA encapsulated PEBBLEs prepared by the A/B (AOT/Brij 30) surfactant system and ethanol washing.

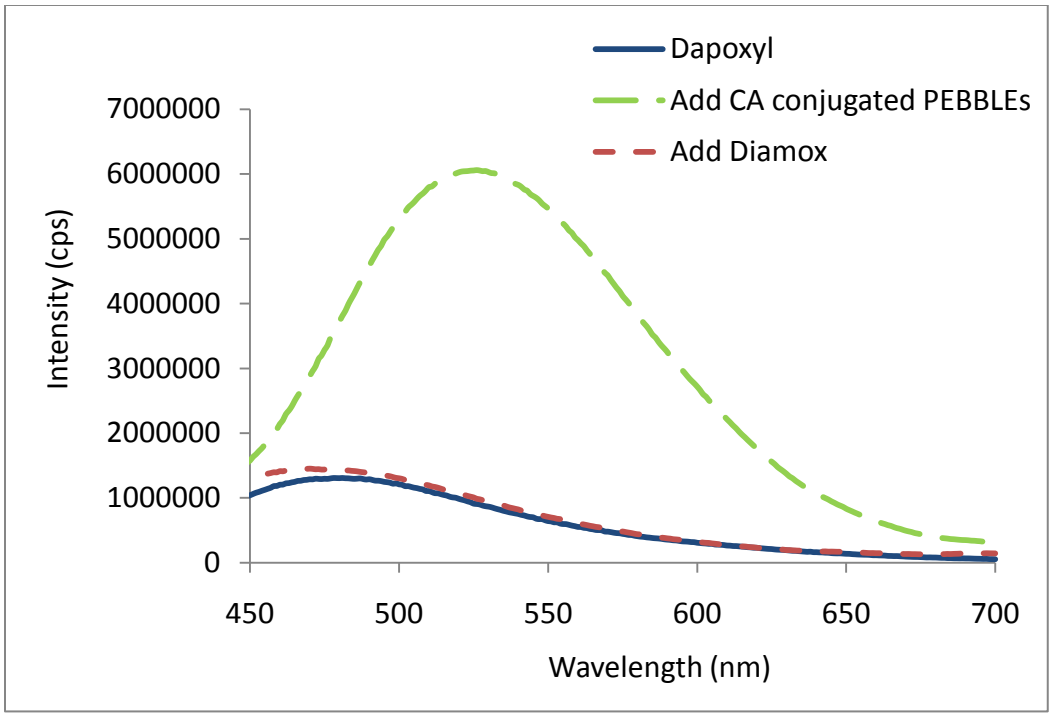

Figure 4.7 The fluorescence of dapoxyl sulfonamide binding with CA conjugated PEBBLEs. The PEBBLEs are washed with plenty of ethanol and water before CA is conjugated onto the PEBBLEs. Therefore, the interference of the residual surfactants is minimal and the enzyme structural integrity is well preserved.

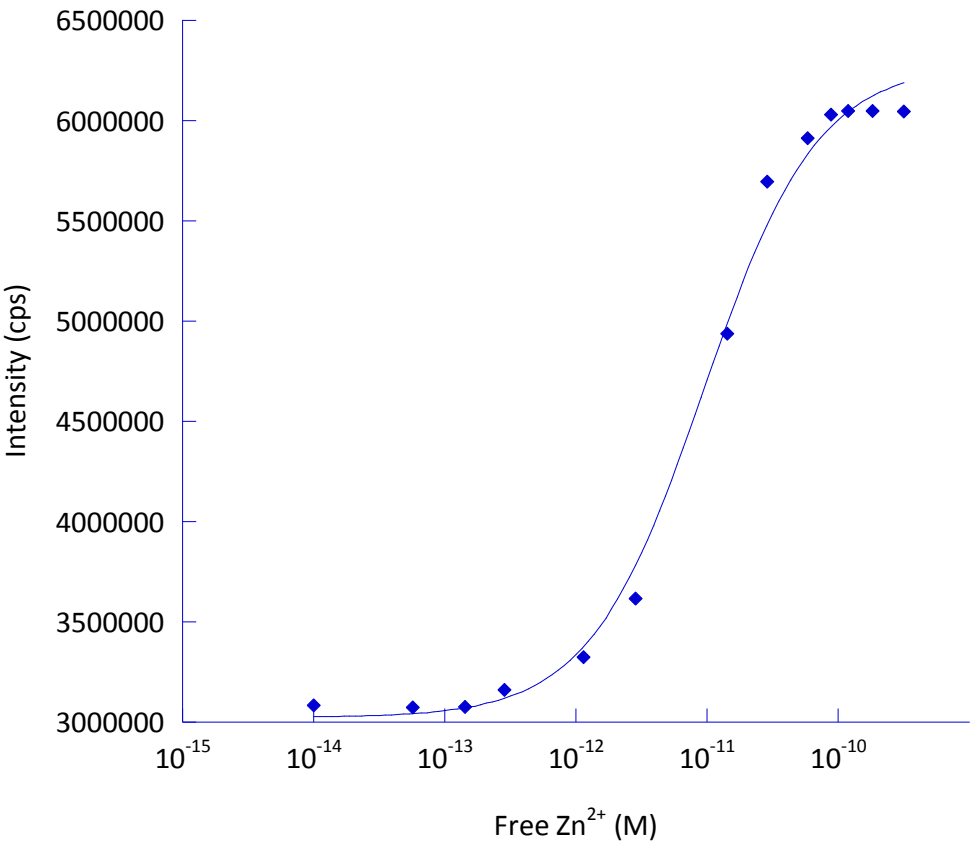

Figure 4.8 Free Zn^{2+} sensing calibration with the CA conjugated PEBBLEs. The Zn dissociation constant K_d is determined to be 9.4±1.2 pM. Calibration was performed in 10 mM MOPS (pH 7.22) containing 10 mM NTA at 25°C.

References

[1] J. E. Coleman, "Zinc Proteins: Enzymes, Storage Proteins, Transcription Factors, and Replication Proteins", *Annual Review of Biochemistry*, (61)1: 897-946, 1992

[2] B. L. Vallee, and D. S. Auld, "Zinc coordination, function, and structure of zinc enzymes and other proteins", *Biochemistry*, (29)24: 5647-5659, 1990

[3] J. M. Berg, and Y. Shi, "The galvanization of biology: a growing appreciation for the roles of zinc", *Science*, (271): 1081-1085, 1996

[4] T. V. O'Halloran, "Transition metals in control of gene expression", *Science*, (261): 5122, 1993

[5] J. M. Matthews, and M. Sunde, "Zinc fingers − folds for many occasions", *IUBMB Life*, (54): 351-355, 2002

[6] K. Kikuchi, K. Komatsu, and T. Nagano, "Zinc sensing for cellular application", *Current Opinion in Chemical Biology*, (8)2: 182-191, 2004

[7] R. B. Thompson, "Studying zinc biology with fluorescence: ain't we got fun?", *Current Opinion in Chemical Biology*, (9)5: 526-532, 2005

[8] H. M. Kim, and B. R. Cho, "Two-Photon Probes for Intracellular Free Metal Ions, Acidic Vesicles, And Lipid Rafts in Live Tissues", *Accounts of Chemical Research*, (42)7: 863-872, 2009

[9] S. Mizukami, S. Okada, S. Kimura, and K. Kikuchi, "Design and Synthesis of Coumarin-Based Zn^{2+} Probes for Ratiometric Fluorescence Imaging", *Inorganic Chemistry*, (48)16: 7630-7638, 2009

[10] Z. Liu, C. Zhang, Y. Li, Z. Wu, F. Qian, X. Yang, W. He, X. Gao, and Z. Guo, "A Zn2+ Fluorescent Sensor Derived from 2-(Pyridin-2-yl)benzoimidazole with Ratiometric Sensing Potential", *Organic Letters*, (11)4: 795-798, 2009

[11] A. Helal, S. H. Kim, and H. Kim, "Thiazole sulfonamide based ratiometric fluorescent chemosensor with a large spectral shift for zinc sensing", *Tetrahedron*, (66)52: 9925-9932, 2010

[12] W. Qiao, M. Mooney, A. J. Bird, D. R. Winge, and D. J. Eide, "Zinc binding to a regulatory zinc-sensing domain monitored *in vivo* by using FRET", *Proceedings of the National Academy of Science*, (103)23: 8674-9679, 2006

[13] E. M. van Dongen, T. H. Evers, L. M. Dekkers, E. W. Meijer, L. W. Klomp, and M. Merkx, "Variation of Linker Length in Ratiometric Fluorescent Sensor Proteins Allows Rational Tuning of Zn(II) Affinity in the Picomolar to Femtomolar Range", *Journal of the American Chemical Society*, (129)12: 3494-3495, 2007

[14] P. J. Dittmer, J. G. Miranda, J. A. Gorski, and A. E. Palmer, "Genetically encoded sensors to elucidate spatial distribution of cellular zinc", *The Journal of Biological Chemistry*, (284)24: 16289-16297, 2009

[15] J. L. Vinkenborg, T. J. Nicolson, E. A. Bellomo, M. S. Koay, G. A. Rutter, and M. Merkx, "Genetically encoded FRET sensors to monitor intracellular Zn^{2+} homeostasis", *Nature Methods*, (6)10: 737-740, 2009

[16] R. A. Bozym, R. B. Thompson, A. K. Stoddard, and C. A. Fierke, "Measuring Picomolar Intracellular Exchangeable Zinc in PC-12 Cells Using a Ratiometric Fluorescence Biosensor", *ACS Chemical Biology*, (1)2: 103-111, 2006

[17] T. K. Hurst, D. Wang, R. B. Thompson, and C. A. Fierke, "Carbonic anhydrase II-based metal ion sensing: Advances and new perspectives", *Biochimica et Biophysica Acta (BBA) - Proteins & Proteomics*, (1804)2: 393-403, 2010

[18] R. Bozym, T. K. Hurst, N. Westerberg, A. Stoddard, C. A. Fierke, C. J. Frederickson, and R. B. Thompson, "Determination of zinc using carbonic anhydrase-based fluorescence biosensors", *Methods in Enzymology*, (450): 287-309, 2008

[19] C. A. Fierke, and R. B. Thompson, "Fluorescence-based biosensing of zinc using carbonic anhydrase", *BioMetals*, (14)3: 205-222, 2001

[20] L. L. Kiefer, S. A. Paterno, and C. A. Fierke, "Hydrogen bond network in the metal binding site of carbonic anhydrase enhances zinc affinity and catalytic efficiency", *Journal of the American Chemical Society*, (117): 6831-6837, 1995

[21] D. W. Christianson, and C. A. Fierke, "Carbonic Anhydrase: Evolution of the Zinc Binding Site by Nature and by Design", *Accounts of Chemical Research*, (29)7: 331-339, 1996

[22] J. A. Hunt, and C. A. Fierke, "Selection of carbonic anhydrase variants displayed on phage", *The Journal of Biological Chemistry*, (272)33: 20364-20372, 1997

[23] J. A. Hunt, M. Ahmed, and C. A. Fierke, "Metal Binding Specificity in Carbonic Anhydrase Is Influenced by Conserved Hydrophobic Core Residues†", *Biochemistry*, (38)28: 9054-9062, 1999

[24] J. D. Cox, J. A. Hunt, K. M. Compher, C. A. Fierke, and D. W. Christianson, "Structural Influence of Hydrophobic Core Residues on Metal Binding and Specificity in Carbonic Anhydrase II", *Biochemistry*, (39)45: 13687-13694, 2000

[25] K. A. McCall, and C. A. Fierke, "Probing Determinants of the Metal Ion Selectivity in Carbonic Anhydrase Using Mutagenesis†", *Biochemistry*, (43)13: 3979-3986, 2004

[26] R. B. Thompson, M. L. Cramer, R. Bozym and C. A. Fierke, "Excitation ratiometric fluorescent biosensor for zinc ion at picomolar levels", *Journal of Biomedical Optics*, (7)4: 555-560, 2002

[27] R. B. Thompson, and M. W. Patchan, "Lifetime-Based Fluorescence Energy Transfer Biosensing of Zinc", *Analytical Biochemistry*, (227)1: 123-128, 1995

[28] D. Elbaum, S. K. Nair, M. W. Patchan, R. B. Thompson, and D. W. Christianson, "Structure-Based Design of a Sulfonamide Probe for Fluorescence Anisotropy Detection of Zinc with a Carbonic Anhydrase-Based Biosensor", *Journal of the American Chemical Society*, (118)35: 8381-8387, 1996

[29] R. B. Thompson, B. P. Maliwal, and C. A Fierke, "Expanded dynamics range of free zinc ion determination by fluorescence anisotropy", *Analytical Chemistry*, (70): 1749-1754, 1998

[30] R. B. Thompson, B. P. Maliwal, V. L. Feliccia, C. A. Fierke, and K. McCall, "Determination of picomolar concentrations of metal ions using fluorescence anisotropy: biosensing with a “reagentless” enzyme transducer", *Analytical Chemistry*, (70): 4717-4723, 1998

[31] R. B. Thompson, B. P. Maliwal, and C. A. Fierke, "Selectivity and Sensitivity of Fluorescence Lifetime-Based Metal Ion Biosensing Using a Carbonic Anhydrase Transducer", *Analytical Biochemistry*, (267)1: 185-195, 1999

[32] R. B. Thompson, B. P. Maliwal, and H. Zeng, "Zinc biosensing with multiphoton excitation using carbonic anhydrase and improved fluorophores", *Journal of Biomedical Optics*, (5)1: 17-22, 2000

[33] J. P. Sumner, J. W. Aylott, E. Monson, and R. Kopelman, "A fluorescent PEBBLE nanosensor for intracellular free zinc", *The Analyst*, (127): 11-16, 2002

[34] J. B. Hunt, M. Rhee, and C. B. Storm, "A rapid and convenient preparation of apocarbonic anhydrase", *Analytical Biochemistry*, (79)1-2: 614-617, 1977

Chapter 5

Conclusions and Future Directions

As discussed in Chapter 1, the remarkable engineer-ability of the PEBBLE nanosensors makes them more advantageous for intracellular sensing than the free indicators. These advantages are summarized as follows: 1) Minimal physical and chemical perturbations to the cells due to the small size and the chemically inert matrix. 2) Protection of the cellular environment from the potential toxicity of the indicator and vice versa. 3) Elimination of the interference to the indicator caused by the nonspecific binding of the indicator to proteins or membranes. 4) Reducing the unwanted sequestration of the indicator by cellular organelles. 5) Enabling ratiometric measurements by co-loading a reference dye and a non-ratiometric indicator in the same PEBBLE. 6) Fast response time enabled by the high surface-to-volume ratio. 7) Targeted delivery to a specific location of interest and/or to avoid unwanted compartmentalization, such as into endosomes. 8) Synergistic detection schemes, e.g. the combination of an enzyme (glucose oxidase) and a fluorescent indicator (for oxygen) to measure an analyte (glucose).

The first six advantages listed above were well demonstrated by the Rhod-2 PEBBLEs for intracellular Ca^{2+} sensing, as detailed in Chapter 2. It was verified by our results that nonspecific binding of Rhod-2 to BSA was eliminated due to the protection of the PEBBLE matrix, because the fluorescence and the binding affinity of the Rhod-2 PEBBLEs did not change in the presence, or absence, of BSA. The Rhod-2 PEBBLEs were designed to be ratiometric by co-loading a reference dye (Hilyte fluor 647), while the Rhod-2 free dye is not ratiometric by itself.

One limitation of this work is that the PEBBLEs were delivered into cells by nonspecific endocytosis; therefore the nanoparticles may stay in endosomes which usually have acidic pH. This may affect the accuracy of the Ca^{2+} detection, since acidic pH interferes with Ca^{2+} sensing by Rhod-2 PEBBLEs. In order to solve this issue, in our future experiments, PEBBLEs will be delivered through receptor-mediated endocytosis with surface-conjugated translocating proteins or peptides (such as F3 peptide), or through the cell-penetrating TAT peptide. By these means, PEBBLEs can be directly delivered into the cytosol and thus unwanted compartmentalization in endosomes can be avoided.

Another PEBBLE design, for our future research, is to monitor multiple signals using single-nanoparticle platforms, and, in this case, monitor intracellular local pH and Ca^{2+} at the same time. We name it “multi-channel detection” which has become one of our research interests in the past few years [1]. To date, the new technologies in confocal fluorescence microscopy that allow the simultaneous detection of multiple emission

channels, have made the “multi-channel detection” possible. As shown in our results in Chapter 2, the calibration of the Ca^{2+} nanosensor was skewed when the pH was below 6, indicating that the Ca^{2+} sensing was not accurate or that corrections to the calibration were required at low pH. Therefore, by monitoring intracellular local pH and Ca^{2+} simultaneously, we will be able to differentiate any spots with pH lower than 6 and thus make corrections to the Ca^{2+} levels of those spots, so that the accuracy of the intracellular Ca^{2+} sensing will be improved. Additionally, the concept of “multi-channel detection” would enable a diversity of simultaneous experiments, which would be highly useful for studying biological processes. For example, it has been reported that mitochondrial Ca^{2+} signaling is affected by cytosolic Mg^{2+} level, and previous studies have shown that mitochondrial Ca^{2+} uptake increases with the increase of cytosolic Mg^{2+} concentration [2]. By monitoring the Ca^{2+} and Mg^{2+} levels at the same time, this biological process can be further clarified by using PEBBLE nanosensors. We also note that a combination of two calcium indicators, e.g. Rhod-5N and Fluo-3 or Fluo-4, if spectrally resolved, could provide a wider dynamic range (from nanomolar to millimolar) for the analyte.

The development of enzyme based sensors is also a research field of interest due to the improved sensitivity and selectivity of the enzyme based biosensors. For example, carbonic anhydrase (CA) II exhibits a picomolar Zn^{2+} sensing affinity and also excellent selectivity to Zn^{2+} over other cations [3]. Chapter 3 focused on the fabrication and purification of enzyme encapsulated nanoparticles, using bovine CA as a substrate. Due to the delicate structure of the enzymes, the entire preparation procedure of the

enzyme based PEBBLEs must be highly biocompatible and biofriendly. Any harsh condition, such as very high or very low pH, use of ethanol or toxic reagents, may cause the deactivation or denaturization of the enzyme. Our study has established a biofriendly PEBBLE preparation method, by using a nonionic surfactant system and by avoiding using ethanol to wash the PEBBLEs. Comparing with the traditional PEBBLE preparation procedure, this new method has improved the CA survival rate almost four times as demonstrated in Chapter 3.

In Chapter 4, the study of zinc sensing, using CA encapsulated or conjugated PEBBLEs, was discussed. Unfortunately, the zinc sensing using CA encapsulated PEBBLEs was not successful because of the following reasons: 1) Nonionic surfactants interfere with zinc sensing by enhancing the fluorescence of the zinc sensing probes. 2) Zinc is difficult to remove from the holo CA after encapsulation. 3) The cobalt bound CA, from which cobalt is easier to remove than zinc, is not robust enough to survive the PEBBLE preparation procedure. Although the zinc sensing using CA encapsulated PEBBLEs was not successful, the encapsulation method developed in Chapter 3 can be used for other enzymes, proteins, or biomacromolecule sensors, which of course must be more robust, and with a simpler sensing scheme than CA.

As so many difficulties were encountered when using the CA encapsulated PEBBLEs for zinc sensing, we experimented with using CA conjugated PEBBLEs and successfully demonstrated their ability to monitor the zinc concentrations in solution tests. Comparing with the encapsulation method, the preparation of the CA conjugated

PEBBLEs is very straightforward. The enzyme was post conjugated onto the particle surface after the particles were washed with plenty of ethanol and water, so as to completely remove residual surfactants; therefore the interference by surfactants was minimal. Since CA is covalently linked onto the particle surface, the structural integrity of CA was preserved and the zinc (or cobalt) was able to be easily removed from the holo CA. As demonstrated by our study in Chapter 4, the zinc binding affinity of CA conjugated PEBBLEs was found to be at the picomolar level, which is comparable to the free CA.

Since CA was conjugated onto the particle surface, and therefore it will be in direct contact with cellular environment for intracellular sensing, a few advantages of PEBBLE nanosensors (such as protecting the cellular environment from the potential cytotoxicity of the indicator, and protecting the indicator from protease attack or nonspecific binding caused by proteins) will no longer be available. However, other advantages such as minimal physical perturbation, fast response, ratiometric measurement, reduced sequestration and targeted delivery, still remain.

In our future studies, the CA conjugated PEBBLEs will be designed for ratiometric measurement by co-loading a reference dye, and targeted delivery will be achieved by surface-conjugating F3 or TAT peptide. Intracellular zinc sensing through confocal fluorescence microscopy will be performed. Moreover, FRET based CA conjugates and CA mutants, developed with altered zinc binding affinity, binding kinetics and metal

selectivity by Fierke and colleagues [3], will be conjugated onto PEBBLEs and utilized for intracellular zinc sensing.

In summary, this work has lead to several developments and significant progress concerning PEBBLE nanosensors, and it will contribute to improvements and optimization of sensing platforms in future research.

References

[1] Y. Koo Lee, R. Smith, and R. Kopelman, "Nanoparticle PEBBLE Sensors in Live Cells and In Vivo", *Annual Review of Analytical Chemistry*, (2)1: 57-76, 2009

[2] G. Szanda, A. Rajki, S. Gallego-Sandín, J. Garcia-Sancho, and A. Spät, "Effect of cytosolic Mg^{2+} on mitochondrial Ca^{2+} signaling", *Pflügers Archiv-European Journal of Physiology*, (457)4: 941-954, 2009

[3] T. K. Hurst, D. Wang, R. B. Thompson, and C. A. Fierke, "Carbonic anhydrase II-based metal ion sensing: Advances and new perspectives", *Biochimica et Biophysica Acta (BBA) - Proteins & Proteomics*, (1804)2: 393-403, 2010